RESILIENT AND RAPID REPAIR MEASURES FOR SEISMICALLY VULNERABLE BRIDGES FOLLOWING MAJOR EARTHQUAKES

Final Report

PROJECT SPR 816

Oregon Department of Transportation

RESILIENT AND RAPID REPAIR MEASURES FOR SEISMICALLY VULNERABLE BRIDGES FOLLOWING MAJOR EARTHQUAKES

Type of Report

PROJECT SPR 816

By

A K M Golam Murtuz, Graduate Research Assistant
Peter Dusicka, Professor
Ilya Palnikov, former Research Engineer
Gregory Norton, former Graduate Research Assistant

Department of Civil and Environmental Engineering
Portland State University

for

Oregon Department of Transportation
Research Section
555 13th Street NE, Suite 1
Salem OR 97301

and

Federal Highway Administration
1200 New Jersey Avenue SE
Washington, DC 20590

September 2021

Technical Report Documentation Page

1. Report No. FHWA-OR-RD-22-07	2. Government Accession No.	3. Recipient's Catalog No.
4. Title and Subtitle Resilient and Rapid Repair Measures for Seismically Vulnerable Bridges Following Major Earthquakes		5. Report Date September 2021 6. Performing Organization Code
7. Author(s) A K M Golam Murtuz, Grad Research Asst 0000-0002-5058-4409 Peter Dusicka, Professor 0000-0003-2199-1619 Ilya Palnikov, Project Engineer 0000-0001-6119-3246 Gregory Norton, Structural Engineer 0000-0002-5132-326X		8. Performing Organization Report No.
9. Performing Organization Name and Address Oregon Department of Transportation Research Section 555 13th Street NE, Suite 1 Salem, OR 97301		10. Work Unit No. (TRAIS) 11. Contract or Grant No.
12. Sponsoring Agency Name and Address Oregon Dept. of Transportation Research Section 555 13th Street NE, Suite 1 Salem, OR 97301 Federal Highway Admin. 1200 New Jersey Avenue SE Washington, DC 20590		13. Type of Report and Period Covered Final Report 14. Sponsoring Agency Code
15. Supplementary Notes		

16. Abstract: The Cascadia Subduction Zone (CSZ) earthquake threatens bridges across the Pacific Northwest. Damage is expected to be geographically spread throughout the region and will have a nearly simultaneous impact on transportation through several important corridors. While bridge repair and replacement will ultimately be needed, priority will be placed on resuming mobility such that repairs will need to be implemented quickly. To anticipate this need, a repair method is being developed for rapid repair with the goal of achieving semi-permanent installation that also considers the different bridge damage states for future earthquakes. The proposed repair involves encasing the damaged column in a steel jacket, which is then anchored to the foundation through replaceable ductile fuse hold-downs. The design objective is to isolate all inelastic strains to the hold-downs thus creating a low-damage solution for the repaired columns.

Full-scale cyclic tests were conducted to investigate the cyclic performance on substandard column-to-foundation specimens. The proposed repair was applied to the damaged column and the specimen was then re-tested using the cyclic loading that is representative of CSZ demands. The experiments validated the design goal of achieving restored or controlled strength, while also exhibiting no additional damage and self-centering behavior. The proof-of-concept experiments have shown the potential of this methodology to rapidly repair earthquake-damaged columns with a relatively generic approach.

17. Key Words	18. Distribution Statement
Resilient and Rapid Repair, Dissipative Controlled Rocking, Earthquake-Damaged Bridges, Accelerated Bridge Construction	Copies available from NTIS, and online at www.oregon.gov/ODOT/TD/TP_RES/

19. Security Classification (of this report): Unclassified	20. Security Classification(of this page): Unclassified	21. No. of Pages 114	22. Price

SI* (MODERN METRIC) CONVERSION FACTORS

APPROXIMATE CONVERSIONS TO SI UNITS

Symbol	When You Know	Multiply By	To Find	Symbol
		LENGTH		
in	inches	25.4	millimeters	mm
ft	feet	0.305	meters	m
yd	yards	0.914	meters	m
mi	miles	1.61	kilometers	km
		AREA		
in^2	square inches	645.2	millimeters squared	mm^2
ft^2	square feet	0.093	meters squared	m^2
yd^2	square yards	0.836	meters squared	m^2
ac	acres	0.405	hectares	ha
mi^2	square miles	2.59	kilometers squared	km^2
		VOLUME		
fl oz	fluid ounces	29.57	milliliters	ml
gal	gallons	3.785	liters	L
ft^3	cubic feet	0.028	meters cubed	m^3
yd^3	cubic yards	0.765	meters cubed	m^3
~NOTE: Volumes greater than 1000 L shall be shown in m^3.				
		MASS		
oz	ounces	28.35	grams	g
lb	pounds	0.454	kilograms	kg
T	short tons (2000 lb)	0.907	megagrams	Mg
		TEMPERATURE (exact)		
°F	Fahrenheit	(F-32)/1.8	Celsius	°C

APPROXIMATE CONVERSIONS FROM SI UNITS

Symbol	When You Know	Multiply By	To Find	Symbol
		LENGTH		
mm	millimeters	0.039	inches	in
m	meters	3.28	feet	ft
m	meters	1.09	yards	yd
km	kilometers	0.621	miles	mi
		AREA		
mm^2	millimeters squared	0.0016	square inches	in^2
m^2	meters squared	10.764	square feet	ft^2
m^2	meters squared	1.196	square yards	yd^2
ha	hectares	2.47	acres	ac
km^2	kilometers squared	0.386	square miles	mi^2
		VOLUME		
ml	milliliters	0.034	fluid ounces	fl oz
L	liters	0.264	gallons	gal
m^3	meters cubed	35.315	cubic feet	ft^3
m^3	meters cubed	1.308	cubic yards	yd^3
		MASS		
g	grams	0.035	ounces	oz
kg	kilograms	2.205	pounds	lb
Mg	megagrams	1.102	short tons (2000 lb)	T
		TEMPERATURE (exact)		
°C	Celsius	1.8C+32	Fahrenheit	°F

*SI is the symbol for the International System of Measurement

ACKNOWLEDGEMENTS

The authors would like to thank the members of ODOT's Technical Advisory Committee as well as the Research Section for their support, advice and assistance in the preparation of this report.

DISCLAIMER

TABLE OF CONTENTS

LIST OF TABLES

LIST OF FIGURES

1.0 INTRODUCTION

1.1 GENERAL

Seismic retrofit or replacement of the entire ODOT vulnerable bridge inventory is unlikely in the foreseeable future, leaving Oregon with a large bridge inventory of seismically vulnerable bridges. Simultaneously, the Cascadia Subduction Zone (CSZ) earthquake has a significant probability of occurrence in our lifetime (Goldfinger et al, 2012). One of the major issues facing the transportation infrastructure during and following CSZ earthquake is not necessarily the strength of shaking at any site alone, but the vast and varied damage that will be distributed throughout the state. Damage is expected to be geographically spread and to affect the transportation system west of I-5, up and down the state. Significant aftershocks are expected for months to possibly years. Variability in intensity across the state, combined with the actual individual bridge responses, will mean that the extent of damage throughout the inventory will vary from minor to significant.

Bridge repair, in lieu of replacement, will be needed following the CSZ earthquake. Priority will be placed on resuming mobility such that repairs will need to be implemented quickly and in many cases expected to remain for the useful life of the bridge, as not all damaged bridges would be slated for replacement. In an effort to anticipate this need, a strategy is required for having a rapid repair methodology in place prior to the CSZ earthquake hitting our region. Ideally, this would be a strategy that will allow for rapid repair. The goal would be achieving semi-permanent installation that also considers resiliency in future earthquakes, including aftershocks.

1.1 BACKGROUND AND SIGNIFICANCE OF WORK

Seismically substandard bridges in Oregon are typically characterized by multicolumn bridge bents, which can develop damage in the columns, in the foundations and in the bent beams. The damage can range from rebar yielding and concrete cracks to more severe lap-splice pull-out or longitudinal rebar buckling and fracture. Yet, the collapse mechanism continues to depend on the component's ability to carry gravity loads. Numerous bent and column experiments and observations from post-earthquake reconnaissance have shown that collapse is not inevitable just because the lateral system is damaged. Despite severe degradation of the lateral strength in specific areas, bridges can continue to carry design level gravity loads because the gravity structure retains sufficient capacity.

Conventional repair methods aim to restore strength to the damage zones, such as repairing of cracked concrete and encasing the column in a concrete jacket, steel jacket, or FRP wrap. This may be appropriate for cases of low damage, whereby the steel reinforcement cage remains largely intact. However, more involved procedures are needed for cases of loss of lap splice, buckled or fractured rebar, or merely loss of confidence at the remaining low cycle fatigue capacity for subsequent earthquakes. Most past research focused on coupling the rebar in

various ways for continuity prior to the encasement or wrap. While effective at restoring the column, there are three significant issues with these approaches:

1. Restoring rebar continuity is labor intensive resulting in lengthy and potentially costly repairs,

2. The affected area can be damaged again in an aftershock requiring new significant repairs, and

3. Encasing results in higher stiffness and strength that would likely shift failures to other parts of the bridge under future earthquake demands.

An alternative post-earthquake repair method is proposed that can be rapidly implemented and that has the potential for increasing the resilience for future shaking. The method utilizes externally mounted brackets, which are secured to the non-damaged parts of the bent. The brackets can be fabricated quickly following the earthquake from standard drawings or prefabricated and stockpiled for common geometries. Researchers at PSU have developed a similar concept for retrofit of slender equipment support structures (Palnikov, 2017) and a similar approach has also been proposed for new precast ABC bridge construction in New Zealand (Mashal et al., 2014). The proposed repair measure would be best suited for bents that had significant damage, but not lost gravity capacity. This is expected to encompass a majority of bridges statewide.

Damage outside of the columns is possible for vulnerable bridge types in Oregon and repairing for strength in those components can be relatively conventional. The difficulty is in repairing for ductility and providing future resiliency, which this rapid approach would offer. The proposed methodology incorporates externally attached ductile fuses to bypass the damaged zone and restore the lateral capacity. The advantage of this approach is bypassing the internal rebar continuity within the damaged zone. This in turn significantly simplifies the repair, which is made in part by saw cutting cover depth around the perimeter and removing loose debris. The number of replaceable fuses and their individual capacity then control the lateral behavior, leaving the rest of the repair to be relatively generic and conventional. Following capacity design, subsequent earthquake damage would be forced into the replaceable fuses and thereby provide significant resilience in the future.

1.2 OBJECTIVE AND SCOPE

The proposed research aims to develop, design, and validate a practical post-earthquake repair methodology that can be rapidly implemented and that incorporates low damage earthquake resilience for future shaking. The effectiveness of existing repair methods will be reviewed whilst considering rapid installation and susceptibility to future earthquake damage. These will be contrasted to the proposed concept that utilizes the external collar with ductile fuses. In order to evaluate the proposed repair method, damaged components of a typical bent will be repaired and tested in the laboratory.

1.3 BENEFITS

Restoring mobility following a CSZ earthquake is an important consideration for ODOT in order to restore not just lifeline routes following a CSZ earthquake, but the full highway network in order to achieve disaster recovery for all communities. While the damage can be vast, the need to repair and restore the network functionality quickly will be high. The benefit to ODOT also relates directly to cost. The anticipated research product introduces a new tool in the repair toolbox, a tool that has the potential to be simpler to implement and significantly more resilient than conventional methods alone.

2.0 LITERATURE REVIEW

To develop a suitable repair methodology, it is necessary to understand the damage that a typical reinforced concrete (RC) bridge column experiences during an earthquake. The first subsection of this literature review describes common failure modes of reinforced concrete bridge columns and provides observations from past earthquakes and previous experimental research. Furthermore, this literature review covers previous research and findings relevant to the repair of earthquake-damaged columns, dissipative controlled rocking, and energy dissipating ductile fuses. Applicable sources relating to column retrofit are also mentioned, as there are many similarities between column repair methods and column retrofit methods.

2.1 EARTHQUAKE DAMAGE TO RC BRIDGE COLUMNS

Priestley et al. (1996) describes the most common failure modes and deficiencies of reinforced concrete bridge columns as a direct result of an inadequate design philosophy, called the elastic design philosophy, that was widely accepted and used prior to the 1970s. Failures are classified as either flexural strength and ductility failures or shear failures. Figure 2.1(a) and (b) are examples of a flexural failure and a shear failure, respectively. Both examples are from the 1994 Northridge earthquake.

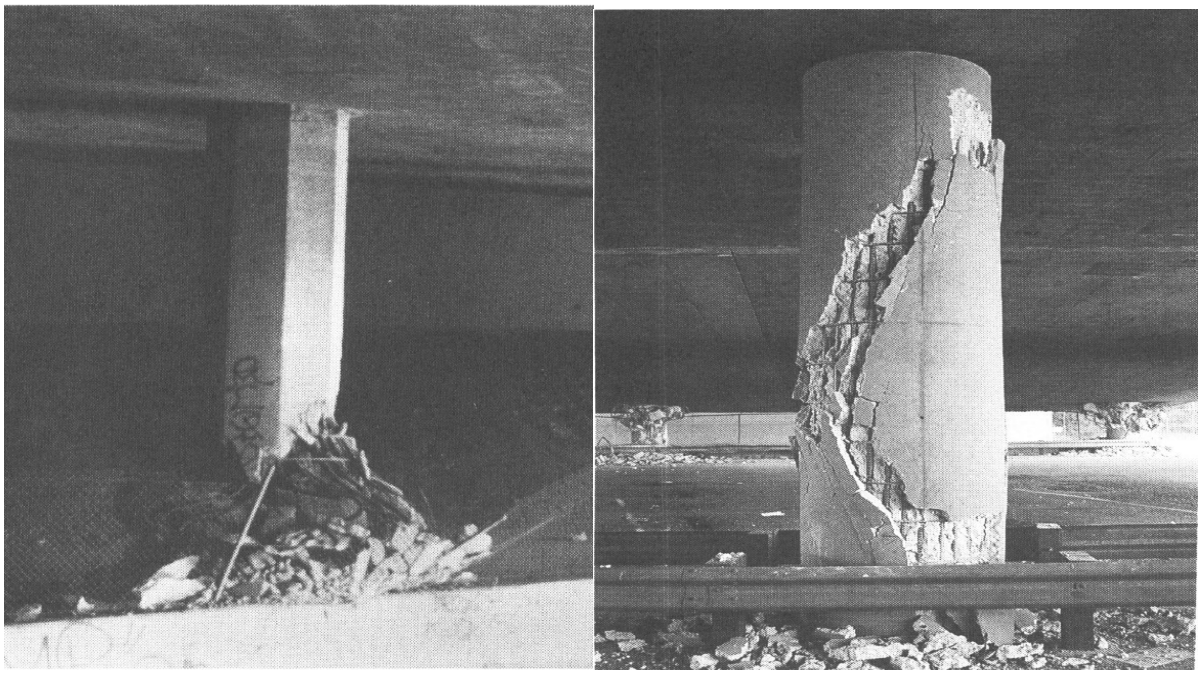

a) **b)**

Figure 2.1: (a) Column flexural failure (Bull Creek Canyon Channel Bridge), (b) Column shear failure and collapse (I-10 Freeway at Fairfax/Washington Undercrossing), 1994 Northridge earthquake (Priestley et al. 1996)

Flexural and ductility failures can generally be attributed to four common deficiencies: (1) inadequate flexural strength, (2) undependable column flexural strength, (3) inadequate flexural ductility, and (4) premature termination of column reinforcement.

1. Inadequate Flexural Strength – Historically, bridge designers drastically underestimated the seismic forces that are expected in reinforced concrete bridge columns. Priestley et al. (1996) claims that it was common for bridges in California to be designed for seismic lateral loads of around 6% of the typical gravity loads. Now it is thought that these loads are greater than 100% of the gravity load.

2. Undependable Column Flexural Strength – Inadequate development length of lap splices is commonly found in reinforced concrete bridge columns. Furthermore, these lap splices often reside at the top and bottom of the column, where seismic loading produces large flexural forces. Priestley et al. (1996) found lap splice lengths as short as 20 bar diameters to be common in California. Inadequate development length prevents reinforcing bars from reaching their design levels, causing the column flexural design strength to be undependable. An example of lap splice failure from the 1989 Loma Prieta earthquake is shown in Figure 2.2(a).

3. Inadequate Flexural Ductility – Reinforced concrete bridges often have inadequate flexural ductility. Again, this is a result of the elastic design philosophy in which the idea of plastic hinging did not exist. The current design philosophy is to allow reinforced concrete bridge columns to undergo inelastic deformation, dissipating energy through plastic hinging action. Columns that are not well confined (i.e. columns with large transverse reinforcement spacing) often suffer from inadequate flexural ductility because as they experience inelastic flexural deformations. The crushing and degradation of concrete quickly infiltrates the core concrete of the column.

4. Premature Termination of Column Reinforcement – Mid-height flexural failures have been attributed to premature termination of the longitudinal reinforcing bars. Priestley et al. (1996) found that a series of columns that failed in the 1995 Kobe earthquake had 33% of the longitudinal rebar terminate at 20% of the column height. The plastic hinge formed above this termination, where the flexural strength was less, causing a flexural-shear failure at mid-height. The failed column is shown in Figure 2.2(b).

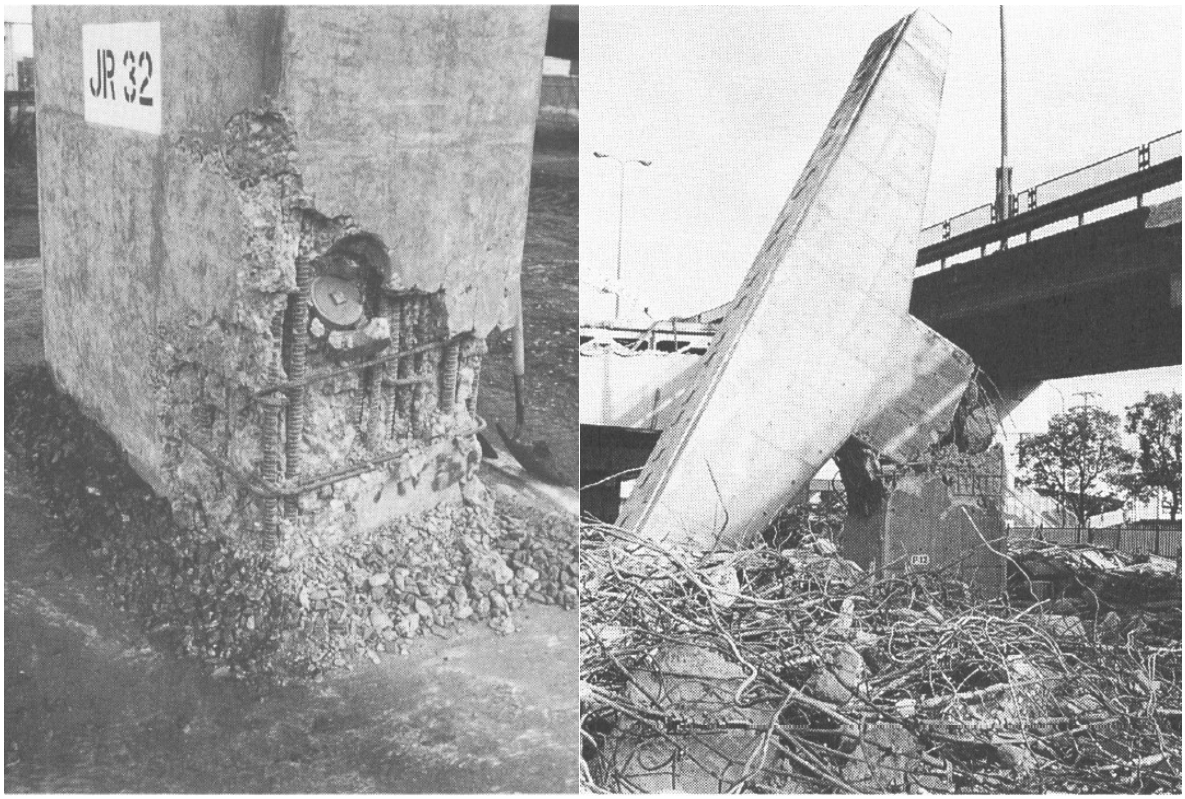

a) **b)**

Figure 2.2: (a) Lap splice failure, 1989 Loma Prieta earthquake, (b) Mid-height failure, 1995 Kobe earthquake (Priestley et al. 1996)

Priestley et al. (1996) also found shear failures to be common in reinforced concrete columns. The 1971 San Fernando earthquake, the 1994 Northridge earthquake and the 1995 Kobe earthquake all provided examples of reinforced concrete bridge columns that failed in shear. Shear reinforcement in older columns often consists of No. 4 bars spaced at 12 inches. This size and spacing is found in columns with a large range of demand requirements causing the authors to speculate that shear strength considerations were often neglected by bridge designers.

2.2 CONVENTIONAL REPAIR METHODS

Conventional repair approaches aim to restore a damaged column to some degree of its original strength and stiffness. Repair methods have been the focus of numerous research projects for many decades. For reinforced concrete bridge columns, the most common repair methods involve the application of a reinforced concrete jacket, a steel jacket, or a fiber-reinforced polymer (FRP) jacket (Lehman et al. 2001). He et al. (2015) compiled the research findings from over 20 studies on the repair of reinforced concrete bridge columns. The following subsection will summarize the findings of this article

He et al. (2015) state the major challenge with repair of damaged columns is estimating the residual capacity of the damaged structure. Bridge columns are designed as the primary source of

energy dissipation during seismic activity for bridges. Many bridges built in the 70s are inadequately detailed and are expected to require significant repair after major seismic events.

The researchers summarize repair techniques for various damage types including flexural and shear cracking, longitudinal reinforcement yielding, cover spalling, crushing of the diagonal compression strut, yielding of the transverse reinforcement, longitudinal bar buckling, spiral fracture, and longitudinal bar fracture. Repair of RC bridge columns without fractured longitudinal bars generally could be accomplished by injecting cracks with epoxy, replacing damaged concrete, and strengthening column. Another method is reinforced concrete jackets that require enlarging the column cross section. Steel Jackets have also been used to repair bridge columns without longitudinal bar fractures. Steel jacket installation includes casting new concrete to restore the cross section, installing steel jacket, and filling the gap between the jacket and column with non-shrink grout. The authors state that research has shown that steel jacketing repair enhances strength and ductility compared to the as-built structure.

FRP jackets could also be used to repair damaged bridge columns where the fibers could be oriented in different orientations to achieve different responses from the FRP. Fibers oriented in the hoop direction improve shear performance while fibers oriented along the length of the column mainly improve flexural strength of the column. The authors state that tests have been performed with scaled columns that were repaired with epoxy injections and FRP jackets, test results indicated restoration of initial stiffness and increase in ductility compared to the as-built column.

Similarly, the authors also summarized research conducted on repairing reinforced bridge columns with fractured longitudinal bars. Longitudinal bar fracture occurs due to high ductility demands in flexural-dominant RC columns. Repair techniques include connecting fractured bars with couplers, placing new longitudinal bars anchored in footing with enlarged cross section, and applying externally bonded longitudinal reinforcement.

Based on the compilation of studies, the authors draw conclusions for the repair methods. For reinforced concrete columns without longitudinal bar fracture, the academics determined that the repair methods are able to restore, or even enhance, performance compared to as-built columns. The repair methods included passive confinement though RC, steel, or FRP jacketing. Active confinement included shape memory alloy (SMA), steel jacketing, and FRP jacketing. The authors state that jackets may alter the stiffness of the column resulting in a change in dynamic response. According to the researchers, RC jackets are time consuming and required specialty equipment for construction.

For RC columns with fractured longitudinal bars, the authors state that mechanical coupler repairs show successful strength and ductility recovery. In addition, increasing the RC column section with well-anchored bars showed successful column response. The researchers state that the larger cross section may result in changes in structural behavior. Other repair methods shift the location of the plastic hinge zone from the region previously damaged, but the results indicate that this decreases ductility because the new region must undergo large rotations to achieve the same ductility. The authors state that most of the methods require a lot of time and are not suited for rapid repair. The researchers state that external FRP bars have been attempted as a rapid repair method and some repair methods may result in a lower limit state performance.

2.3 DISSIPATIVE CONTROLLED ROCKING WITH SELF-CENTERING

Conventional structures depend on inelastic deformation of primary structural members to dissipate energy in seismic events leaving structural damage at critical locations. Even structures that are compliant with modern building codes are expected to have structural damage to primary elements such as columns, beams, and shear walls (Chancellor et al. 2014). The seismic design philosophy of reinforced concrete bridge columns relies on the inelastic response of the structure to occur within plastic hinge regions that are expected to form at the top and/or bottom of reinforced concrete columns leading to significant structural damage which will require repair after an earthquake (Palermo & Pampanin 2005).

Dissipative controlled rocking (DCR) is a concept that eliminates inelastic deformations in primary structural elements during seismic events. Instead, inelastic deformations are isolated to energy dissipating ductile fuses. The result is a low-damage structure that will require minimal repairs after an earthquake. The concept has been proposed and experimentally implemented on steel braced frames (Eatherton et al. 2014), cross-laminated timber shear walls (Smith, A. D. 2019), and pre-cast concrete bridge bents (Staton et al. 2014, Mashal et al. 2014).

Mashal et al. (2014) experimentally investigated the concept of DCR for accelerated bridge construction. The results from quasi-static cyclic testing of half-scale precast column-to-footing specimens with external energy dissipaters showed that DCR is a viable option for creating low damage bridge columns. The following subsection is a summary of this research.

2.4 QUASI-STATIC CYCLIC TESTS OF HALF-SCALE FULLY PRECAST BRIDGE BENTS INCORPORATIVE EMULATIVE AND POST-TENSIONED LOW DAMAGE SOLUTIONS

Mashal et al. (2014) outlined the prototype development, design detailing, construction, assembly, and experimental testing of two half-scale, fully-precast, bridge bents incorporative emulative and post-installed low damage solutions. Figure 2.3 shows the prototype bridge used for the detailing of the specimen components. The first specimen is an “Accelerated Bridge Construction (ABC) High-Damage” specimen with grouted ducts and member socket connections (MSC). The ABC High-Damage solution is expected to have plastic hinge formation, residual displacement, and require repair or replacement after an earthquake. The grouted ducts and member socket connections have a similar concept to “Highways for Life” bents, which have not been experimentally tested. While testing the ABC High-Damage emulative specimen, spalling occurred in the four expected plastic hinge regions. The specimen emulated behavior of cast-in-place bridge construction.

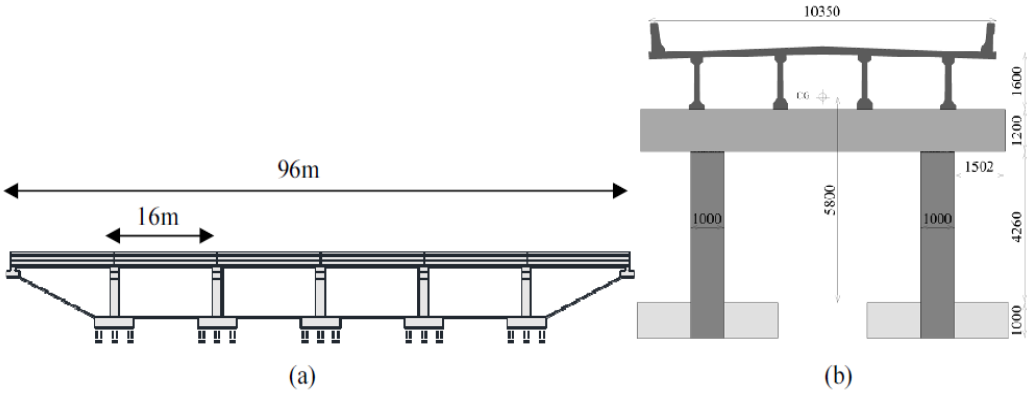

Figure 2.3: Prototype bridge: (a) longitudinal profile, (b) transverse section (Mashal et al. 2014)

The second specimen referred to as "ABC Low-Damage" is a dissipative controlled rocking (DCR) bent with self-centering and external dissipaters. The connections are designed to be low-damage and have replaceable energy dissipaters. The proposed configuration and system response are shown in Figure 2.4. The selected dimensions and properties reflected typical highway bridge-pier support-structures for low to medium span bridges in New Zealand.

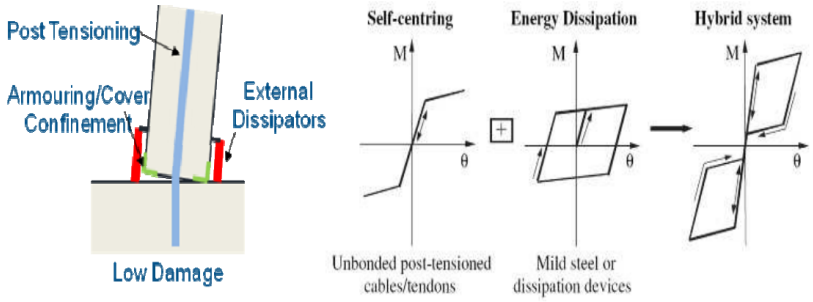

Figure 2.4: Low damage system configuration and expected response (Mashal et al. 2014)

The ABC Low-Damage specimen was identical to the High-Damage specimen construction, but the connection was replaced with a hybrid connection. The hybrid connection consisted of a combination of post-tensioning with external replaceable dissipaters. The system provides self-centering with minimal permanent deformation and damping through the hysteretic devices. The expected ABC Low-Damage bent hysteresis curve is flag shaped with no permanent structure drift. The ABC Low-Damage bent was designed using the outline procedures in PRESSS Design Handbook (Pampanin et al. 2001). To prevent concrete spalling at the ends of the precast columns, 10mm steel jackets were installed as shown in Figure 2.5. The steel shells connected to the concrete column core through welded studs. For the low-damage system, the steel shell length was determined based on the MSC column plastic hinge length and a length of 500 mm was used.

Figure 2.5: Precast Bridge Columns with 10mm steel jackets (Mashal et al. 2014)

Plates were installed on the rocking interfaces of the footing and under the cap beam. In addition, a shear key was used to transfer shear force and prevent excessive sliding at the base interface. Tapped holes in the steel plate allow for attaching the hysteretic devices to the foundation plate. The plate was bolted into the existing foundation, which allows high stresses due to rocking to be distributed on the footing. The plate design included tapped holes for installation of the base plate. Brackets on the steel shell allowed for attaching the hysteretic devices to the column. The hysteretic device designed by the researchers is a steel bar with a reduced cross-section, the reduced section is incased in a steel tube to prevent buckling while maintaining similar tensile and compressive capacity. The proposed hysteretic device is shown in Figure 2.6(a). Figure 2.6(b) shows the installed base plate and column shear key.

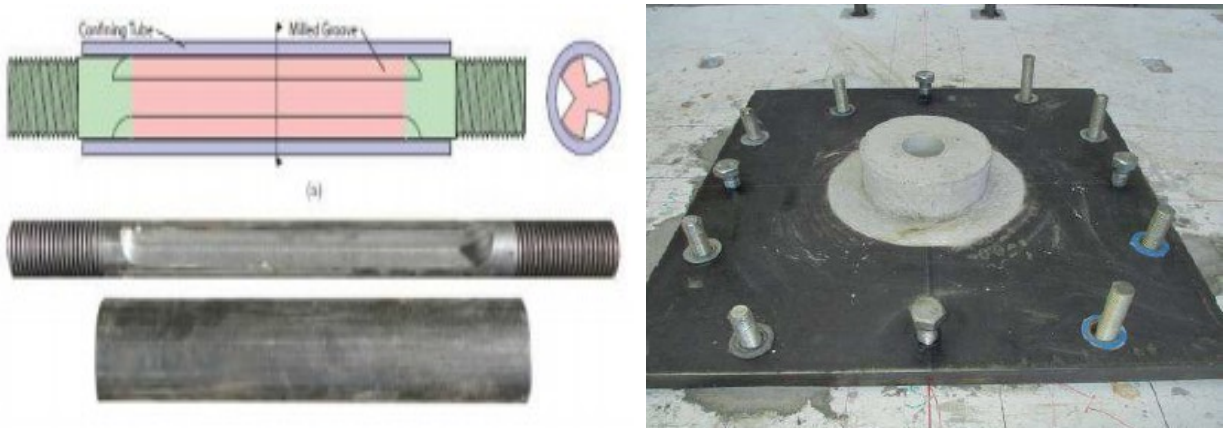

a) **b)**

Figure 2.6: (a) Energy dissipating reduced bar, (b) Column base plate (Mashal et al. 2014)

The assembled bridge bent is shown in Figure 2.7 where the footing, column and bent cap are post-tensioned using Macalloy bars running through the center of the precast columns. Two hydraulic actuators were used to control lateral and gravity forces during the experiment. The foundation base plate, steel column shell, device brackets, and hysteretic energy dissipaters are shown for the bottom and top column interface in Figure 2.8.

Figure 2.7: Test configuration (Mashal et al. 2014)

a) **b)**

Figure 2.8: (a) Lower rocking interface, (b) Upper rocking face (Mashal et al. 2014)

Three quasi-static unidirectional tests were performed at three levels of post-tensioning (PT). The protocol was repeated for the three PT levels: 15%, 30%, 45% of yielding strength of Macalloy bars. As the PT force increased, less slipping at the rocking interface was observed. The authors conclude that the capacity of the connection, size of gap opening, and re-centering ratio were directly related to the PT load. Each of the three tests were taken up to 2.2% drift and no damage or cracks in the columns were observed. For the lower PT levels, 15% and 30%, slight sliding at the interfaces was observed.

Phase 1 of the ABC Low-Damage system essentially tested a rocking system without supplemental damping. The system showed true re-centering with no damage to the columns, footings, and cap beams. The columns remained intact with not even hairline cracks visible. High re-centering ratios were observed, ranging from 1.2-1.5, and none of the tests presented residual displacement.

2.5 ENERGY DISSIPATING DUCTILE FUSE HOLD-DOWNS

In 1972, a novel approach was developed by Kelly et al. (1972) to increase the energy absorption capacity of structural connections using special devices as mechanisms of energy absorption. The special devices, called U-shaped Flexural Plates (UFPs), utilize the plastic deformation of

mild steel to dissipate energy. Through testing, it was shown that the UFPs are an extremely efficient mechanism for the dissipation of energy (Kelly et al. 1972).

Figure 2.9(a) is an illustration of a UFP dissipater located between flexibly based shear walls in a composite building. Figure 2.9(a) is just one of many possible scenarios where UFPs could be implemented to dissipate energy. This device can be implemented between any adjacent surfaces whose relative displacement is parallel. Recent research has shown successful implementation of UFPs for energy dissipating hold-downs in a rocking cross-laminated-timber shear wall (Smith, 2019). A view of the UFPs inside of the hold-down is illustrated in Figure 2.9(b). The outer angle of the hold-down is rigidly anchored to the foundation and connected to the wall through an alternating arrangement of UFPs. When the wall undergoes rocking, the adjacent surfaces of the UFPs are displaced in a parallel direction to one another, and energy is dissipated through plastic deformation.

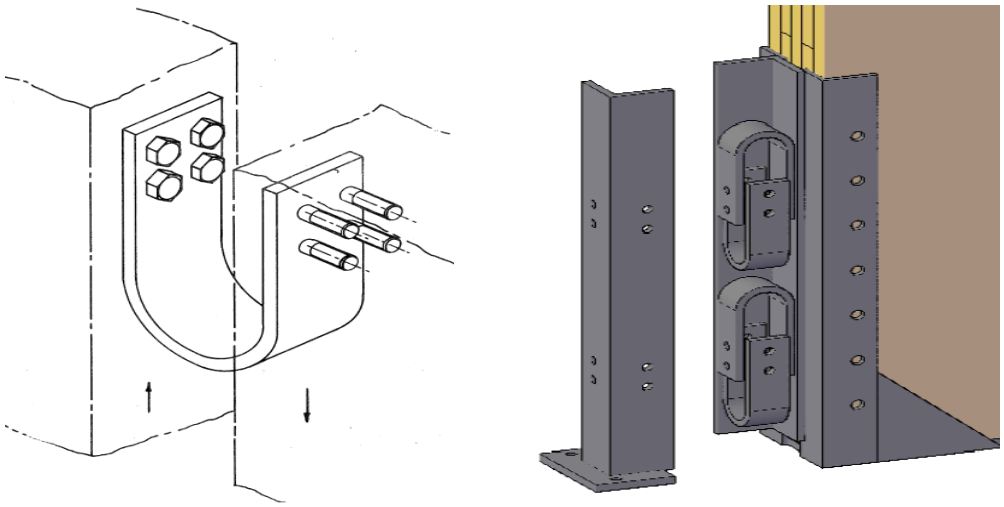

a) **b)**

Figure 2.9: (a) UFP dissipater located between flexibly based shear walls in a composite building (Kelly et al. 1972), (b) UFPs in an energy dissipating hold-down on a rocking CLT shear wall (Smith, A. D. 2019)

Another compelling reason to utilize UFPs in energy dissipating hold-downs is that their strength is easily controllable. The maximum force they are able to resist is a function of their geometry and steel strength. Kelly et al. (1972) was the first to analytically derive the force provided by relating the plastic moment to the shear couple. The plastic moment occurs when the entire cross section has exceeded the yield strain and is given by equation (2-1). In this equation, the UFP width and thickness are b_u and t_u while σ_y is the yield stress of the steel. Equation (2-2) relates the plastic moment to the shear couple to give the maximum force provided by the UFP where D_u is the bend diameter of the UFP.

$$M_p = \sigma_y Z_{UFP} = \frac{\sigma_y b_u {t_u}^2}{4} \quad \textbf{(2-1)}$$

$$F_p = \frac{2M_p}{D_u} = \frac{\sigma_y b_u {t_u}^2}{2D_u}$$

(2-2)

Figure 2.10(a) shows the geometry of a UFP with the controlling dimensions and Figure 2.10(b) shows a free body diagram of the forces and moments on the UFP.

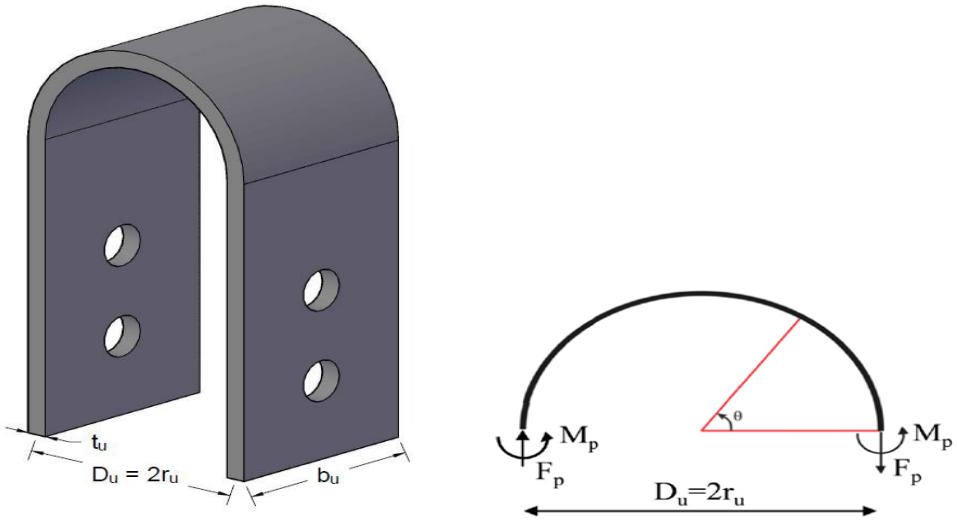

a) **b)**

Figure 2.10: (a) UFP Geometry (Palnikov 2017), (b) UFP shear couple (Baird et al. 2014)

3.0 METHODOLOGY

3.1 DESIGN APPROACH AND CONSIDERATIONS

Conventional repair approaches aim to restore strength, stiffness, or both strength and stiffness in a damaged column using concrete jacketing, steel jacketing, FRP jacketing, and/or bar replacement. Most conventional bridge-column repair-methods do not eliminate or prevent damage in the columns in future events and require subsequent repairs. The research methodology presented aims to limit, or eliminate, damage due to lateral loading.

Many gap-opening systems have been explored and implemented for various types of structures including CLT shear walls, bridge piers, and steel frame structures. The proposed methodology utilizes external energy dissipaters rather than the formation of plastic hinges to dissipate energy.

The design approach considered the following design objectives:

- Primary structure remains elastic without bar yielding
- Eliminate or limit damage in bridge columns
- Rapid repair approach
- Economically competitive with conventional repair methods
- Ability to sustain aftershocks and future seismic events
- Accessible external energy dissipaters

Conditions and implementation:

- Cover requirements due to contact with soil
- Galvanization and other requirements for exposed steel components
- Deterioration due to weather and exposure
- Toe concrete crushing
- Bridge deck loaded upward

Above mentioned conditions and implementation issues can play significant role in deciding the effectiveness of the repair system. Hence, all the conditions should be further investigated. The scope of the current research undertaking is limited in developing the appropriate design methodology and validating the principle through laboratory application on full-scale specimens.

The readers can also raise a question about the applicability of the proposed repair method for columns under deep fill due to the issue of accessibility of the column base. However, any post-earthquake reconnaissance to examine the extent of damage in the plastic hinge region of the column will require the removal of soil. Hence, the applicability of the proposed repair system does not warrant separate excavation work to expose the bottom of the column rather it can be quickly implemented following the post-earthquake reconnaissance.

A reinforced concrete collar-jacket confining the original column and allowing force to transfer to the energy dissipating devices through shear friction is to be implemented. All gravity loads are to be transferred through the original column and an intentional gap will be provided at the base of the new jacket to eliminate contact of the collar-jacket with the foundation when gap opening occurs. By not transferring the gravity load through the collar-jacket column interface, a smaller normal force is required to eliminate jacket slipping.

The adopted repair concept is to utilize a short external steel collar that is used to encase the damaged parts of the column. The collar utilizes externally attached ductile fuses to bypass the damaged zone and connect to the rest of the bridge to restore the lateral capacity. The advantage of this approach is bypassing the internal rebar continuity within the damaged zone, which can significantly simplify the repair, and provides control over the strength of the hinging by selecting appropriately sized ductile fuses. The number of fuses and their individual capacity then controls the behavior, leaving the rest of the repair to be relatively generic. Figure 3.1 is an illustration of the proposed repair methodology. In this illustration, the hold-down on the left is pulled away from the jacket, exposing the arrangement of ductile fuses.

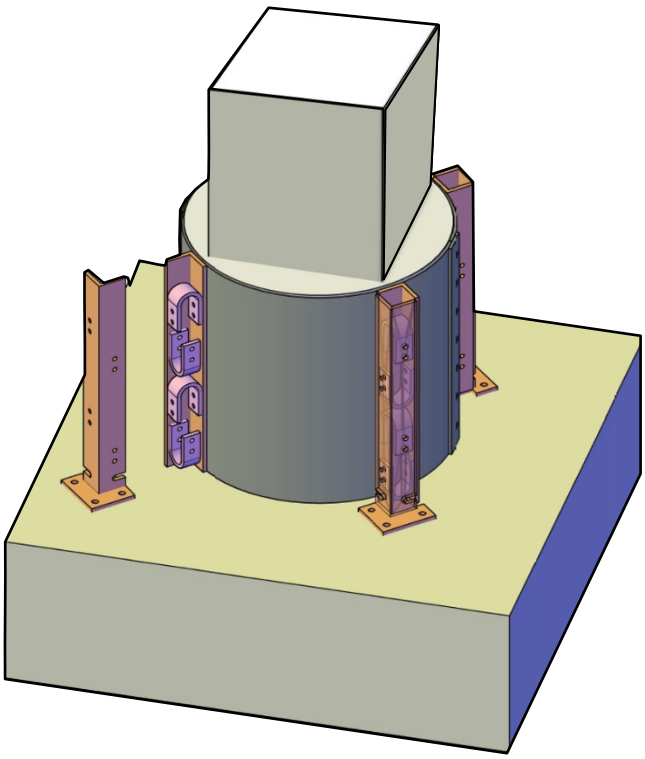

Figure 3.1: Proposed repair methodology.

The steel jacketing method has been used for both repair and retrofit of reinforced concrete bridge columns. The Seismic Retrofitting Manual for Highway Structures (Buckle et al. 2006), provides design guidelines for the steel jacketing method. It states that the steel jacketing method is the preferred method by the California Department of Transportation. This manual was used in the design of the proposed repair methodology. The following subsections will address individual considerations in the design of the proposed methodology.

3.1.1 Design Moment and Base Forces

The proposed design approach aims to eliminate column yielding when subjected to lateral loading. The objective of the repair method is to eliminate damage in the column due to subsequent events and protecting the column is the primary objective while reestablishing flexural capacity in the column. The columns cracking moment, M_{crack}, yield moment, M_y, and the plastic moment, M_p are dependent on the axial load and the critical loading must be considered in design. After the cross-section M_{crack}, M_y, and M_p is determined, the maximum allowable base moment could be determined such that the column does not exceed the yield moment at the top of jacket-column interface. The jacket height should consider plastic hinge length, height of column damage, and shear forces required to eliminate slipping at the jacket-column interface. To keep the column elastic, the maximum moment in the original column should not exceed M_y at the top of the jacket as shown in Figure 3.2. The base moment could be determined based on the jacket height and the column length.

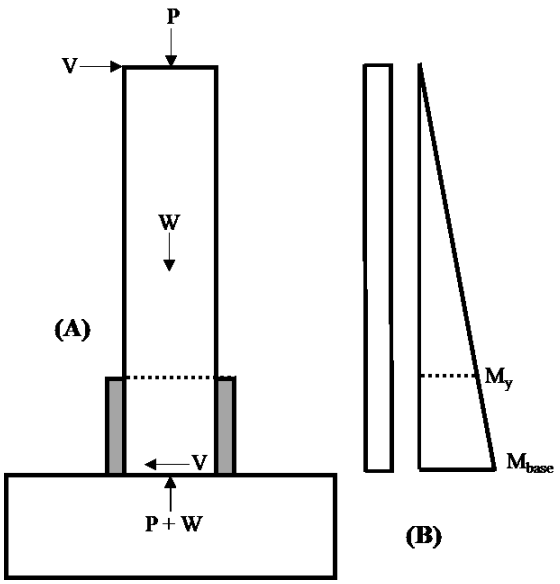

Figure 3.2: (a) System free body diagram (FBD), (b) System shear and moment Diagram

Next, using the location of the dissipaters, the maximum device force could be determined such that the allowable base moment is not exceeded. The calculated force is the absolute maximum force in the device, including all overstrength and material uncertainties. Figure 3.3 shows the forces acting on the system when undergoing rocking. The rocking point is intentionally kept at the edge of the existing column such that the axial load is not transferred to the new jacket. Transferring the axial force through the new jacket would significantly increase the required

shear friction to eliminate slipping at the collar-column interface. Summing the moments around the rocking point "O" with V= M_{base}/L and assuming F1=F2, the maximum device force could be calculated.

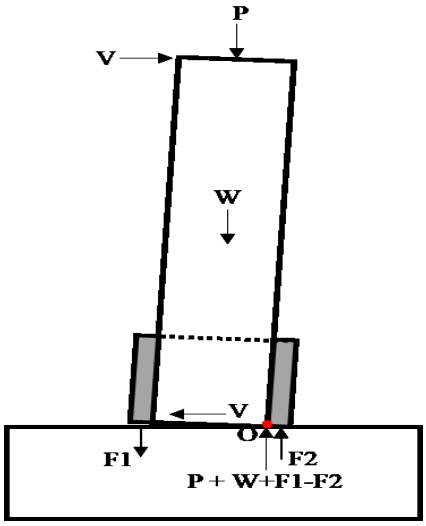

Figure 3.3: Rocking system forces.

When the inertial forces are no longer present on the system, the lateral force (V) is no longer present on the system and the moment produced by self-weight (W) and axial force (P) must exceed the moment resisting F1 and F2. An additional force will be present on the system when analyzed with a deck, as gap opening occurs, the column will push up on the deck. Assuming the deck remains elastic, an additional elastic spring will be introduced.

The design forces were primarily determined considering the low-cycle fatigue (i.e., earthquake) loads and the high-cycle fatigue is not considered an issue for this repair system. The hold-down components only engage when there is a significant amount of moment in the connection to overcome the 'decompression point', i.e., overcome the self-centering effect of gravity loads on the column. The decompression point can be defined as the onset of gap opening at the column-footing interface and this is not expected to occur under fatigue vehicular loading. The gravity load will dictate the behavior of the repair system until this decompression point and any load before this point will not engage the UFPs, hold-downs or the anchor rods.

3.1.2 Device Sizing

Various types of devices could be utilized to dissipate the energy, but the maximum force capacity of the device must be governed to eliminate yielding in the repaired column. If the devices are not properly sized, yielding above the repair jacket or large system drifts may occur. UFPs are the proposed device for the ease of fabrication, and their stable hysteretic behavior. UFPs are non-axial hysteretic energy dissipating devices where the strain of the device is not dependent on length of the device.

Based on the maximum allowable base moment, the maximum device force is determined where the maximum device force is considered the greater of F_u and $1.5F_p$. Where the overstrength of

the device is taken from the UFP plastic force, and determined to be 1.5 based on component testing of various UFP geometries at Portland State University.

Other energy dissipating devices could be used if found to be easier to implement but overstrength, dependence on core length, velocity dependence, and other parameters must be considered to properly size and accommodate the required stroke and allowable base couple force.

3.1.2.1 Cross-Sectional Shape

The adopted repair concept utilizes a jacket with a circular cross section. A rectangular jacket was considered in the design, but the circular jacket was selected for two reasons: (1) superior strength, and (2) easier to construct and assemble. The manual (Buckle et al. 2006) suggests the use of circular jackets rather than rectangular jackets, even if the column is rectangular. Attempts to retrofit rectangular columns with rectangular jackets have been less successful, even when the jackets have been extensively stiffened. This is because the confining action of the rectangular jackets can only be developed through lateral bending of the jacket sides, which is a very flexible action, compared to the membrane action developed in an oval or circular jacket.

3.1.2.2 Jacket Height

It is necessary for the steel jacket to entomb areas with extensive damage. Previous research has been conducted regarding the flexural behavior of reinforced concrete columns. It has been found that extensive damage such as cover concrete spalling and rebar buckling will occur within the plastic hinge zone (Murtuz et al. 2020, Zhao et al. 2011). The length of the plastic hinge can be estimated using Equation (3-1) developed by (Priestley and Park 1987). In this equation, the distance from the critical section to the point of contraflexure is z, and the diameter of longitudinal bar is d_b. For the specimens in this study, z = 102.675 inches, and d_b = 1.00 inches. The resulting plastic hinge length, L_p, is estimated to be 14.2 inches.

$$L_p = 0.08z + 6d_b \tag{3-1}$$

For the proposed repair methodology, a jacket height of 36 inches was selected. This was a conservative decision to ensure that all serious damage would be entombed within the steel jacket.

The proposed jacket height was determined based on plastic hinge length. For a flexural dominated column, it is expected that all the damages will be within the plastic hinge region. Hence, a jacket height covering the plastic hinge region should provide enough confinement against any damage in the column section after repair. However, the plastic hinge length depends on the shear span of the column and the longitudinal bar diameter. So, any changes in the column geometry and reinforcing detail should be considered while calculating the jacket height. It should also be noted that the jacket height is

proportioned so that the bending moment at the top of the steel shell is below the yield moment.

3.1.2.3 Jacket Diameter

The Seismic Retrofitting Manual for Highway Structures (Buckle et al. 2006) suggests that the steel jacket be comprised of two steel-plate half-shells that are rolled to a diameter large enough to leave 1 inch of clearance at the corner of the column. Figure 3.4 illustrates the clearance space required at the column corners. The purpose of this clearance space is to allow the flow of grout around the corner of the column. However, the manual also suggests for grout to be poured from all four openings as to not rely on the flow of grout around the corners. For repair of the 24-inch square test specimen, a shell diameter of 36 inches was selected, leaving a clearance space of approximately 1 inch at each corner.

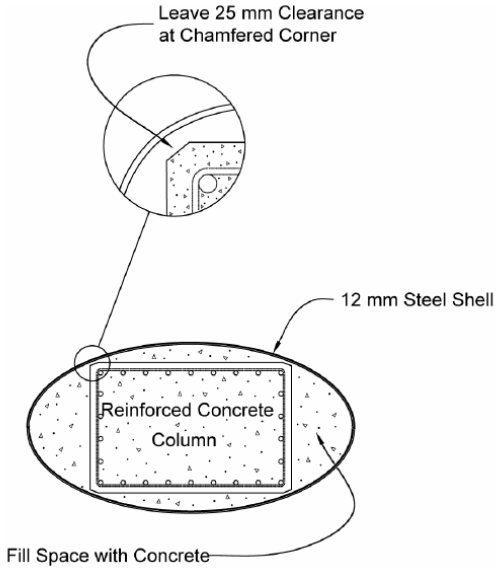

Figure 3.4: FHWA steel shell recommendations (Buckle et al. 2006).

3.1.2.4 Jacket Thickness

A jacket thickness of 0.375 inches was selected for the proposed repair methodology. The Seismic Retrofitting Manual for Highway Structures (Buckle et al. 2006) suggests a minimum jacket thickness of 0.375 inch. This limitation is based on handling the required strength from flexural forces in the column. The manual also places a limit on the maximum thickness of the plate due to restrictions on the construction and fabrication procedures typically used for bending thick plates. The maximum plate thickness is suggested to be 1 inch.

3.1.2.5 Axial Load Path

The axial load is designed to be transferred to the footing through the as-built column. This means the attached steel collar and ductile fuses are not intended to transfer axial load. The Seismic Retrofitting Manual for Highway Structures (Buckle et al. 2006) suggests a vertical space of 2 inches be provided between the jacket and the footing. This space is necessary to allow the column to rotate at its base without bearing on the steel collar at large drift angles. Even at large angles, the jacket will not contact the footing, and axial load will be transferred through the concrete of the as-built column and not through the jacket.

3.1.2.6 Hold-down Orientation

Figure 3.5 illustrates two possible orientations of the hold-downs around the column. In Figure 3.5(a), the hold-downs are positioned at the column corners and will be referred to as corner orientation. Figure 3.5(b) has the hold-downs positioned at the column faces and will be referred to as face orientation. Hold-down orientation has performance implications because it alters the lever arm distance for each hold-down. Both corner and face orientation were tested as part of this study and the performance implications were explored.

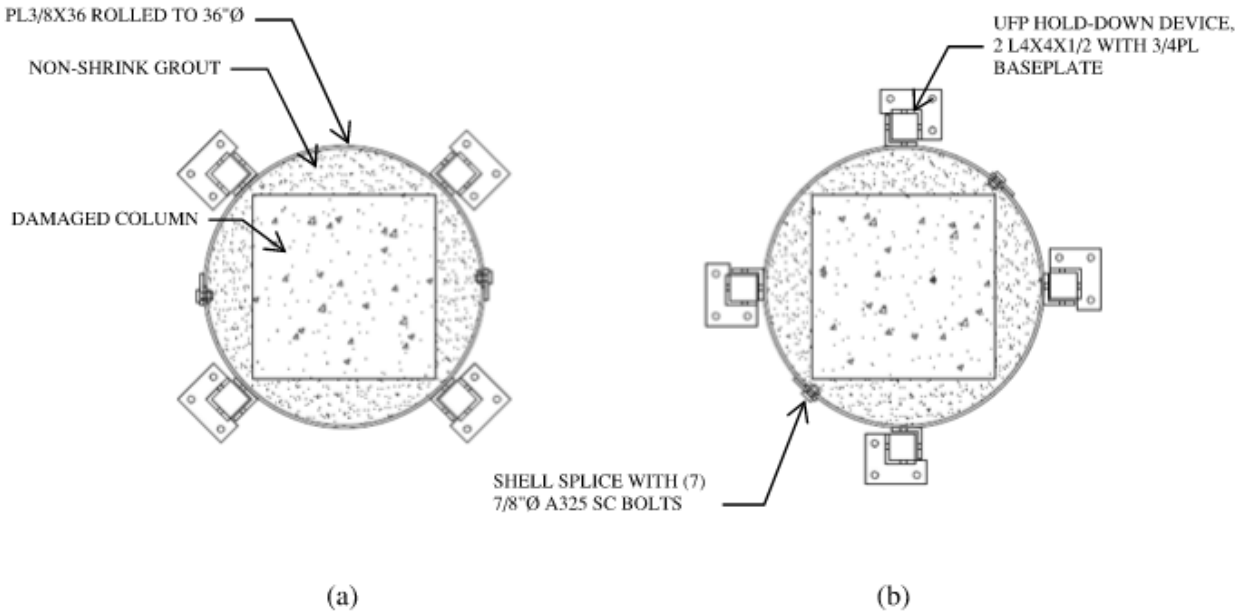

Figure 3.5: Hold-down orientations (a) corner orientation (b) face orientation.

3.2 ANALYTICAL PREDICTIONS AND INITIAL DESIGN PHILOSOPHY

This section provides an analytical approach to estimate the strength and behavior of the proposed repair methodology. The analytical approach outlined in section 3.2.1 was used to select the appropriate UFP geometry for the initial test. Analytical predictions are also necessary

prior to testing to determine the force and displacement capabilities of the instrumentation and equipment (ACI 374.1 2013).

The following analytical procedures are expected to overestimate the strength of the repair for two reasons. First, the following procedures are based on rigid body deformation of the column where the horizontal displacement of the column is due to the rotation between the repaired column and its footing, and the curvature of the column is assumed to be negligible. Second, the following procedures assume that the rocking point, or neutral axis, will be on the outer edge of the column. The actual rocking point will not be directly at the edge of the column, it will be at some distance inside of the column cross section. Through testing, the actual rocking point of the column will be found and used to refine the analytical predictions.

3.2.1 Static Analysis

For initial design considerations and selection of the UFPs, the static analysis was developed. This simple analysis characterizes the horizontal force on the column as a function of the hold-down force and the axial load. For this analysis, the following assumptions are made:

1. The rocking point is at the edge of the column
2. Column curvature is negligible
3. The force in each hold-down is equal to its theoretical maximum

The forces acting around the assumed rocking point are illustrated in Figure 3.6 (a) for corner hold-down orientation and Figure 3.6 (b) for face hold-down orientation. It is important to note that the hold-down orientation affects the distance from each hold-down to the assumed rocking point and will thus affect the overall performance of the repair.

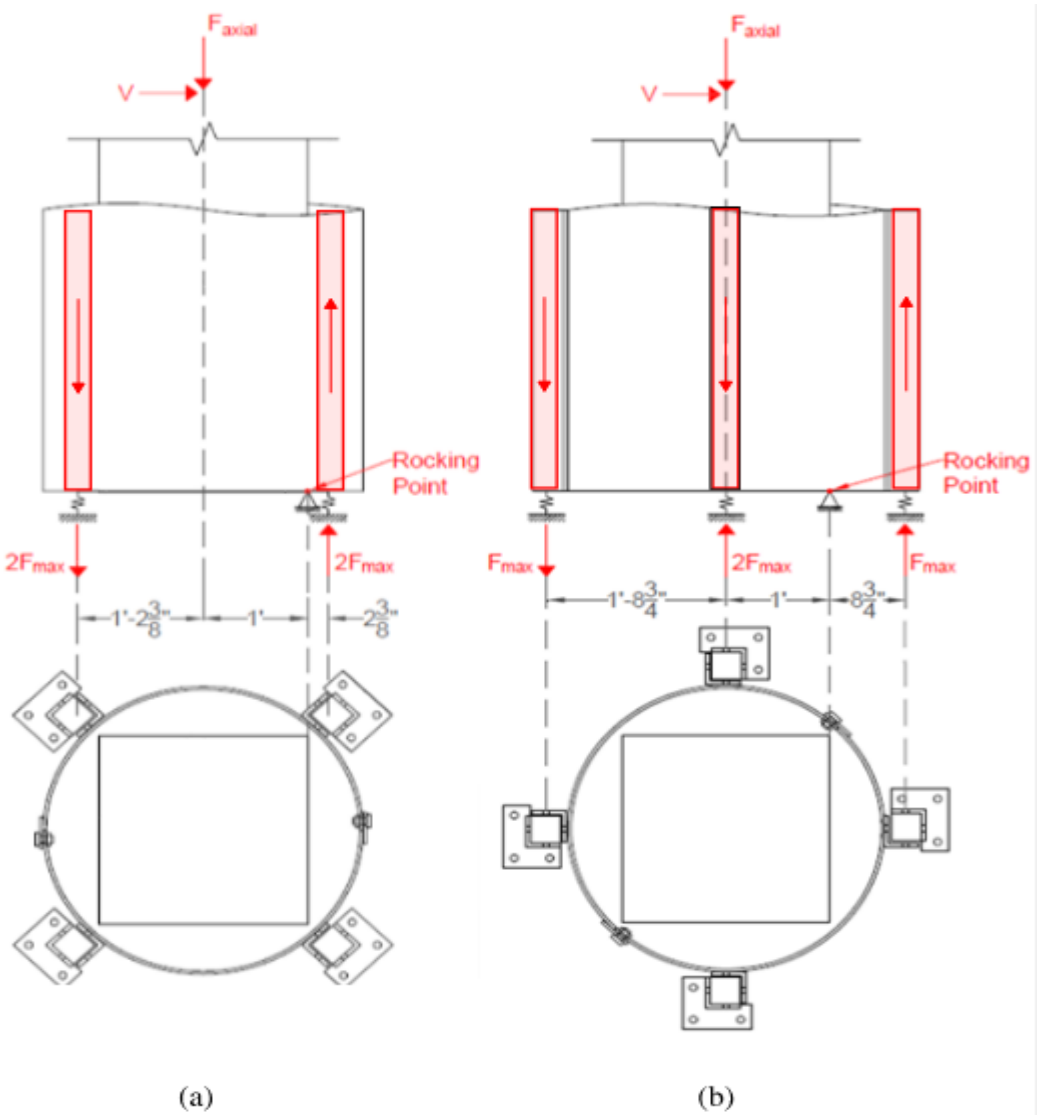

Figure 3.6: Forces about the rocking edge (a) corner orientation (b) face orientation.

By taking the sum of the moments around the rocking point, equations (3-2) and (3-3) can be derived. Equation (3-2) gives the maximum horizontal force expected for the corner hold-down configuration and equation (3-3) gives the maximum horizontal force expected for the face hold-down configuration.

$$V_{max} = \frac{12F_{axial} + 57.5F_{HD}}{h_c} \quad \textbf{(3-2)}$$

$$V_{max} = \frac{12F_{axial} + 65.5F_{HD}}{h_c} \quad \textbf{(3-3)}$$

This analysis fails to address the complete force-displacement relationship of the hold-downs. In the undeformed state, the hold-down force is assumed to be zero under the current analysis. The following section provides a more in-depth analysis that accounts for the force-displacement relationship of the hold-downs.

3.2.2 Pushover Analysis

This analysis method was developed to refine the static analysis method by addressing the assumption that the hold-down force is equal to its theoretical maximum. However, the first two assumptions from the static analysis are still applied to the pushover analysis. The assumptions are:

1. The rocking point is at the edge of the column
2. Column curvature is negligible

In this analysis, the hold-down force is no longer assumed to be its theoretical maximum. The hold-down force is now considered to be a function of total horizontal displacement. When the column is undeformed, the hold-downs are at rest and the force is zero. As the column is displaced horizontally, the hold-downs engage and develop force resistance. The relationship between hold-down deformation and horizontal column displacement is based on ridged body deformation and is given by equation (3-4) where Δ_{HD} is the hold-down deformation, Δ_{column} is the horizontal deformation at the top of the column, d_{HD} is the horizontal distance between the hold-down and the assumed rocking point and h_{column} is the height of the column.

$$\Delta_{HD} = \Delta_{Column}\left(\frac{d_{HD}}{h_{column}}\right) \tag{3-4}$$

The force in each hold down is given by equation (3-5) where F_{HD} is the force provided by the hold-down, K_{HD} is the initial stiffness of the hold down and F_p is the plastic moment force of the hold-down. K_{HD} and F_p are described in more detail in section 2.5. Based on previous studies, the maximum force in each hold-down is limited to $1.5F_p$.

$$F_{HD} = \Delta_{HD} K_{HD} \leq 1.5 F_p \tag{3-5}$$

This analysis also accounts for the varying position of the axial load. In the static analysis, the moment arm for the axial load was taken to be half of the column width. In the pushover analysis, the moment arm of the axial load is reduced by the horizontal displacement at the top of the column and is given by equation (3-6) where d_{axial} is the length of the moment arm of the axial load about the assumed rocking point.

$$d_{axial} = 12" - \Delta_{column} \tag{3-6}$$

Figure 3.7 shows a comparison of the static analysis and the pushover analysis. This figure is for a column that was repaired with hold-downs in the face orientation and with UFPs that have a plastic moment force of 5.4 kips.

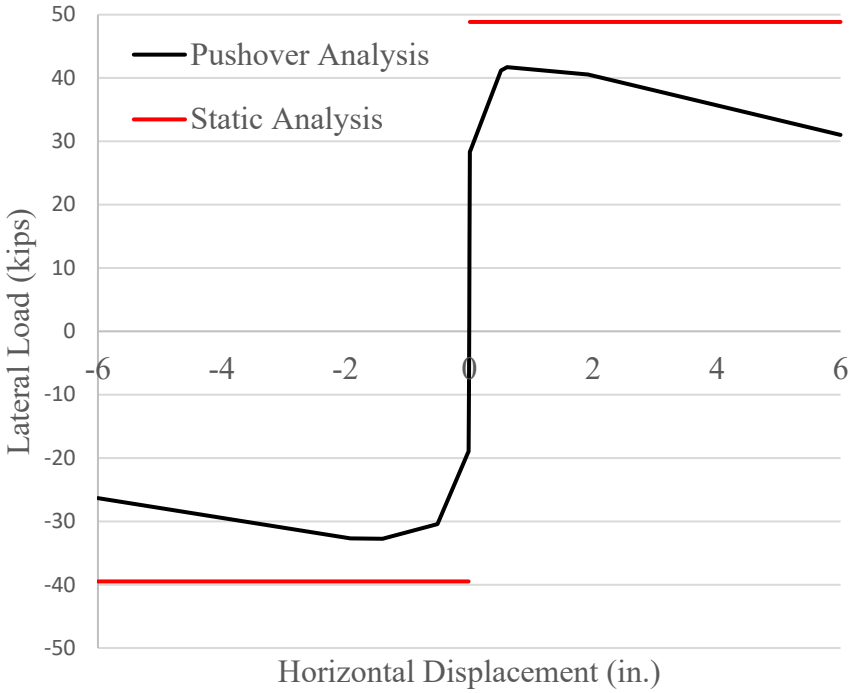

Figure 3.7: Pushover analysis vs. static analysis

3.3 SHEAR AND LOAD TRANSFER TO DEVICES

Two approaches were investigated to determine if the friction between the original column and the collar-jacket would produce a shear friction greater than the shear load produced by the energy dissipating devices. Method 1 referred to as "Moment Couple Approach" treats the reinforced-concrete collar as a sleeve that must transfer the load to the UFP devices through a moment couple, which produces a normal force on the mating surfaces. Method 2 referred to as "Hoop Yielding Approach" assumes yielding of the hoops/confining bars and determines the required spacing to transfer the bar/device tension force through shear friction between the mating surfaces.

Method 1, Moment Couple Approach utilizes moment couple within the repair sleeve to produce a normal force between the column surface and the interior sleeve surface to transfer load to the energy-dissipating device. The loading in the sleeve will likely be a distributed force but the forces will be heavily concentrated on the top and bottom of the sleeve. Figure 3.8(a) shows the expected forces acting on the column. The friction force between the collar column increases proportionally with the increase of the base shear. The friction forces denoted G and K in Figure 3.8 (a) and (b) are functions of the moment couple R and the friction coefficient of concrete-to-concrete surfaces. According to section 22.9.4.2 of ACI 318-14 (2014) the coefficient of friction for normal weight concrete placed against clean, laitance free, non-intentionally roughed

concrete is μ = 0.6. The shear force between the jacket and the column is G = K = μR. Based on the base shear, V, the jacket reaction R is determined, and the jacket shear reinforcing is designed such that the jacket has the required shear strength. The required shear transfer (G and K) must exceed the greater of F_u and $1.5F_p$ for the device (sum of the UFPs) to transfer the load into the energy dissipating devices.

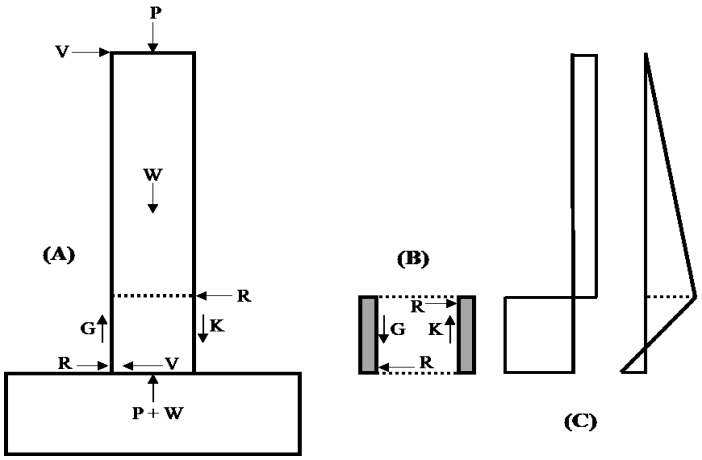

Figure 3.8: Method 1-Collar-Moment Couple Approach; (a) Column FBD, (b) Collar FBD, (c) Column shear force and bending moment Diagram.

Method 2, Hoop Yielding Approach uses a similar approach to that summarized in Lehman et al. (2001) where the stress distribution in the ties is related to the total clamping force per bar and the spacing of the ties is determined as outlined in Figure 3.9.

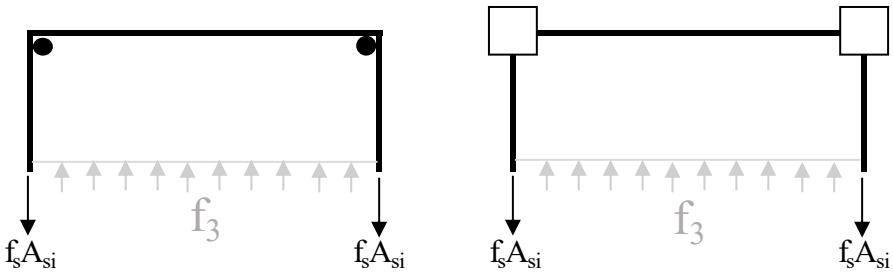

Figure 3.9: Stress distribution in Method 2-Hoop Yielding Approach.

$A_s = \sum A_{si}$ (Total steel area)

b= outside to outside of ties (b1=b2 for square columns)

$f_3(b \cdot s) = f_s A_s$ (Equalibrium of concrete compression to steel tension)

$$\boldsymbol{f_3 = \left(\frac{f_s \cdot A_s}{b \cdot s}\right)} \qquad \textbf{(3-7)}$$

4.0 EXPERIMENTAL VALIDATION

4.1 TEST SETUP

To validate the repair methodology, an experimental test setup was constructed in Portland State University's infraStructure Testing and Applied Research (iSTAR) Laboratory. A layout of the test setup is illustrated in Figure 4.1. The test setup was designed to subject a full-scale column-to-foundation assembly to the forces and deformations expected in an earthquake. In order to impose the expected forces and deformations, it was necessary for the test setup to be designed with three considerations. First, the test setup must be capable of imposing cyclic lateral deformations. Second, the test setup must be capable of imposing a variable axial load. Third, the variation in axial load must be synchronized with the lateral deformations to simulate the frame action of a multi-column bridge bent.

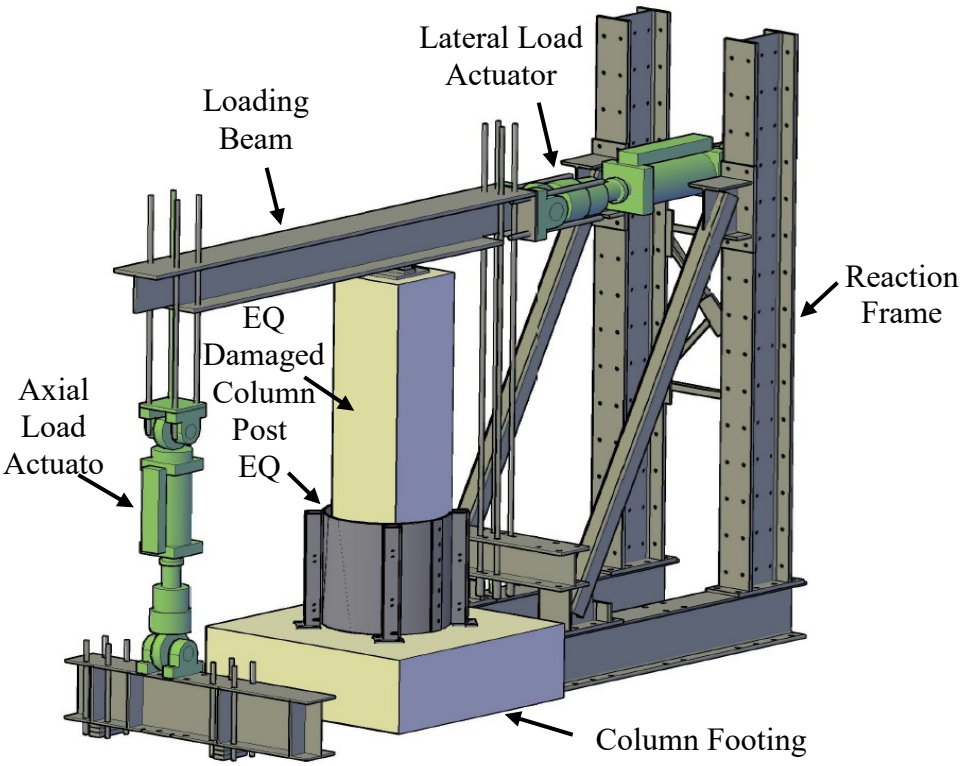

Figure 4.1: Experimental Test Setup Layout

To impose both lateral deformation as well as axial load, the test setup includes two hydraulic actuators. The lateral load actuator is a Shore Western 92 Series Actuator with a stroke of ±10 inches. This actuator can produce 220 kips in tension and 335 kips in compression which greatly exceeds the expected maximum lateral load. The axial load is applied by a ±100-kip MTS actuator with a stroke of ±6 inches. The loading beam is proportioned such that the column axial

load is applied at one third of its overall length, creating a lever capable of imposing an axial load of up to 300 kips.

4.2 TEST MATRIX

Two columns from ODOT SPR#802 were repaired and four experimental tests were conducted. Table 4.1 summarizes the experimental program. The column designation is adopted from ODOT SPR#802 (Murtuz et al. 2020).

Table 4.1: Experimental Test Matrix

Test	SPR#802 Column Designation	Hold-down Orientation	Lateral Loading Protocol	UFP F_p (kips)	Expected Hold-down Force, F_{max} (kips)*	Expected Lateral Load V_{max} (kips)**
1	SVF#8	Corner	Subduction	5.45	32.73	46.4
2	LVF#8	Face	Conventional	5.43	32.60	48.9
3	LVF#8	Face	Subduction	5.43	32.60	48.9
4	LVF#8	Face	Subduction	8.83	52.97	61.9

*The maximum expected hold-down force was calculated as $F_{max} = (1.5F_p)$ * (4 UFPs per hold-down)

**Expected lateral load as calculated in section 3.2

4.3 REPAIR IMPLEMENTATION PROCESS

To apply the proposed repair concept, the existing longitudinal rebar between the column and the foundation needs to be disconnected so as not to participate in the load path. The disconnected rebar can be seen in Figure 4.2(a). In this study, the damaged columns had four #8 rebar dowels, one at each corner of the column. At the time of the repair, these sections of rebar were mostly exposed due to spalling in the damaged zone of the column. The remaining concrete around the rebar was removed and the rebar was cut with an oxy-acetylene torch. Figure 4.3(a) is a picture of the column after the longitudinal rebar was exposed and cut. If this repair methodology were to be applied to a column with less damage (i.e., no spalling), the longitudinal rebar does not necessarily need to be exposed. The rebar could be disconnected by plunge cutting with a circular saw blade.

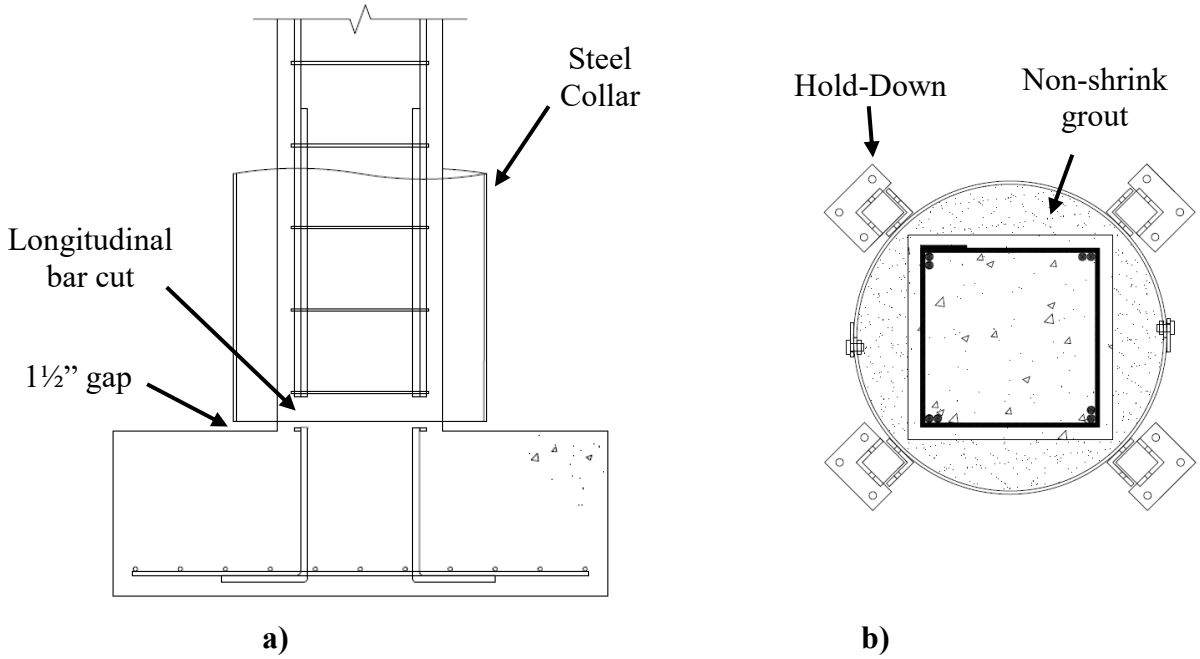

Figure 4.2: Repair methodology (a) elevation view (b) section view.

The next step of the repair process is to place the prefabricated steel collar around the column with the necessary 1.5-inch space above the foundation. The recommended gap height for the steel jacket was 2.0 inch (Buckle et al. 2006) but it was determined that the 1.5 inch space should be sufficient to accommodate the ultimate drift angle considering the existing substandard RC bridge column detail. Furthermore, the gap height was also reduced to cover the maximum possible area confined within the plastic hinge region. In order to place the jacket for attachment, the jacket was set on top of two layers of ¾" plywood that act as temporary spacers to create the necessary gap. Figure 4.3(b) is a picture of the steel jacket sitting on top of the temporary spacers. The collar is then filled with non-shrink grout to secure it to the column. The placement of the steel collar around the column can be seen in Figure 4.2(b) in a top section view. After the grout has cured, the temporary spacers can be removed.

The final step of the repair is to attach the ductile fuse hold-downs. Inside of the hold-down, there are four UFPs that act as ductile fuses. One side of the hold down is welded to the steel jacket while the other side is anchored to the foundation via conventional threaded rods with Hilti epoxy. Figure 4.4 shows the ductile fuse hold-down before the outer leg is installed. The UFPs are bolted with two 5/8-inch diameter slip-critical A325 bolts on each leg. Nuts are welded to the inside of the UFP such that the bolts can be secured without access to the inside of the UFP. Upon installation of the hold-downs, there is a gap between the hold-down base plate and the foundation. This gap is to be filled with self-leveling grout before the anchor rod nuts are tightened. Figure 4.3(c) shows a picture of temporary forms that were installed for the base plate grout. Figure 4.5 shows the base plate with anchor rods after the forms have been removed.

a) b) c)

Figure 4.3: Prototype Repair Sequence

Figure 4.4: UFPs inside hold-down

Figure 4.5: Hold-down base plate

4.4 INSTRUMENTATION

The actuators in the test setup are equipped with load cells that were used to measure the horizontal and axial load that were applied to the column. The global displacement at the top of the column was instrumented with a string potentiometer and is labeled in Figure 4.6. The repaired column was instrumented with linear variable displacement transducers (LVDT) to measure local deformations and global displacements. Figure 4.6 illustrates the layout of LVDT's on a repaired column.

Each hold-down was equipped with one vertical LVDT to measure local displacement of the hold-down. These LVDT's are labeled on plan in Figure 4.6 and an example of how it was installed is pictured in Figure 4.7. Five LVDT's on each side of the column were used to measure the curvature of the column above the repaired zone. One LVDT on each side was used to measure vertical slippage between the steel collar and the grout as shown in Figure 4.8. Three LVDT's were equipped at each shell splice to monitor slip at the bolted connection of the steel collar (Figure 4.8). Two LVDT's were attached via a string tangent to the circumference of the shell to monitor rotation that could result from undesired non-symmetric behavior. The foundation was equipped with two vertical LVDT's to monitor uplift/rocking and two horizontal LVDT's to measure sliding.

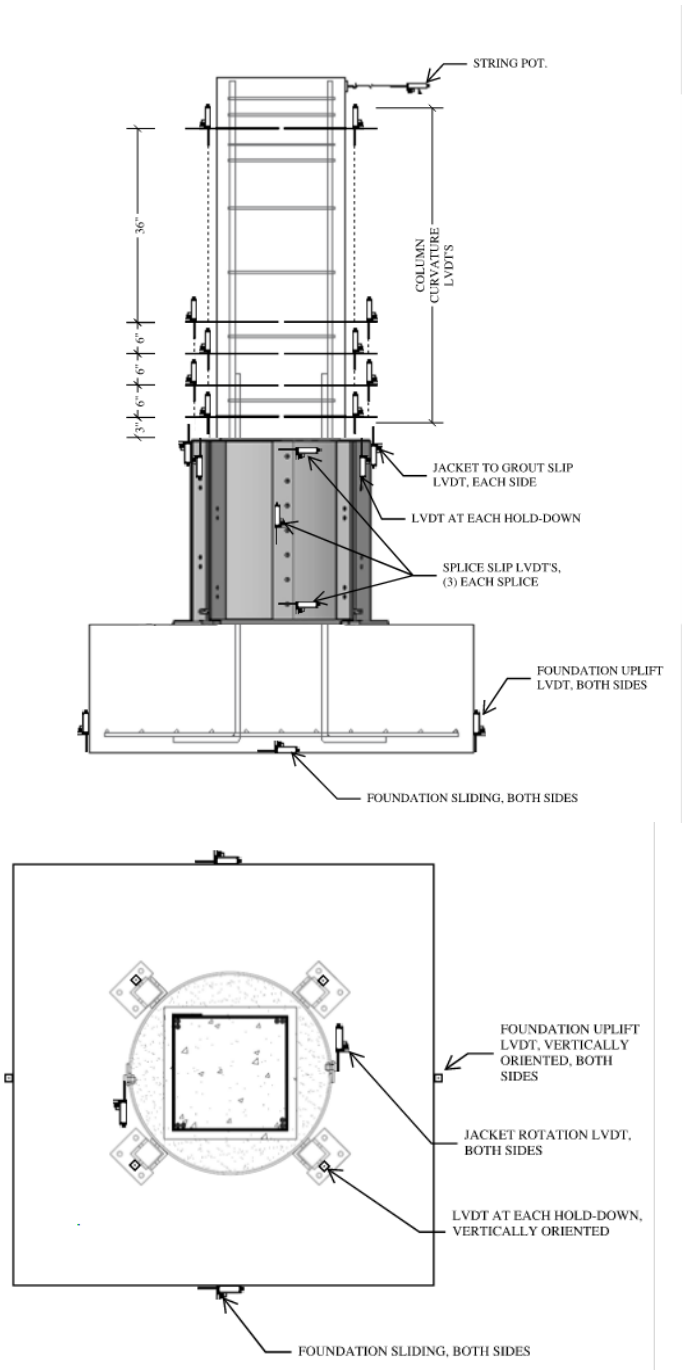

Figure 4.6: Instrumentation Plan

Figure 4.7: Hold-down instrumentation

Figure 4.8: Shell splice instrumentation

5.0 EXPERIMENTAL RESULTS

This section presents the observations and data from each of the four tests. Qualitative observations and inter-test design modifications are presented in section 5.1. Quantitative data from instrumentation is presented in section 5.2. The observations and data from all four tests are then discussed in subsequent sections to evaluate the success of the design objectives.

5.1 OBSERVATIONS

5.1.1 Test 1

The first test was conducted on specimen SVF#8. The subduction zone lateral loading protocol was used for both the as-built test, and the repaired test. The maximum lateral load from the as-built column was 45 kips. The repair was implemented using the corner orientation. The repair was designed with the intention of matching the as-built behavior by selecting UFPs to yield a similar expected lateral load based on the procedure outlined in section 4.3. The chosen UFPs were PL1/2X2-1/2 grade A36 steel with a bend diameter of 3.25 inches. With four UFPs per hold-down, the expected maximum hold-down force was 32.7 kips, and the expected maximum lateral load was 46.4 kips. The repaired column can be seen with the test set-up in Figure 5.1.

The repair implementation functioned as expected. The column was rocking along the compression edge and the hold-downs were engaging to resist overturning forces. Figure 5.2 shows the column at a displacement of 2.5 inches. Vertical displacement can be seen at each hold-down along with rotation of the individual hold-down legs. In this picture, there is visible separation between the legs of the tension hold-down. The outer hold-down legs appeared to undergo plastic rotation causing residual deformation during compression cycles, which was not restored upon the opposite tension cycle. The residual deformation is pictured in Figure 5.3.

At the final target displacement of 5.4 inches, the axial load actuator stroked out and axial load on the column was lost. The column was returned to its unloaded state while the test set-up was adjusted. The test was resumed, but after three more cycles at the same target displacement of 5.4 inches, the test was terminated when the southeast hold-down failed while in tension. The weld between the L4X4X1/2 and the base plate ruptured. The ruptured weld is pictured in Figure 5.4. The weld was a 5/16-inch fillet weld around the perimeter of the angle. While the weld was sufficient to resist the axial capacity of the hold down, it was not designed for combination axial plus flexural forces.

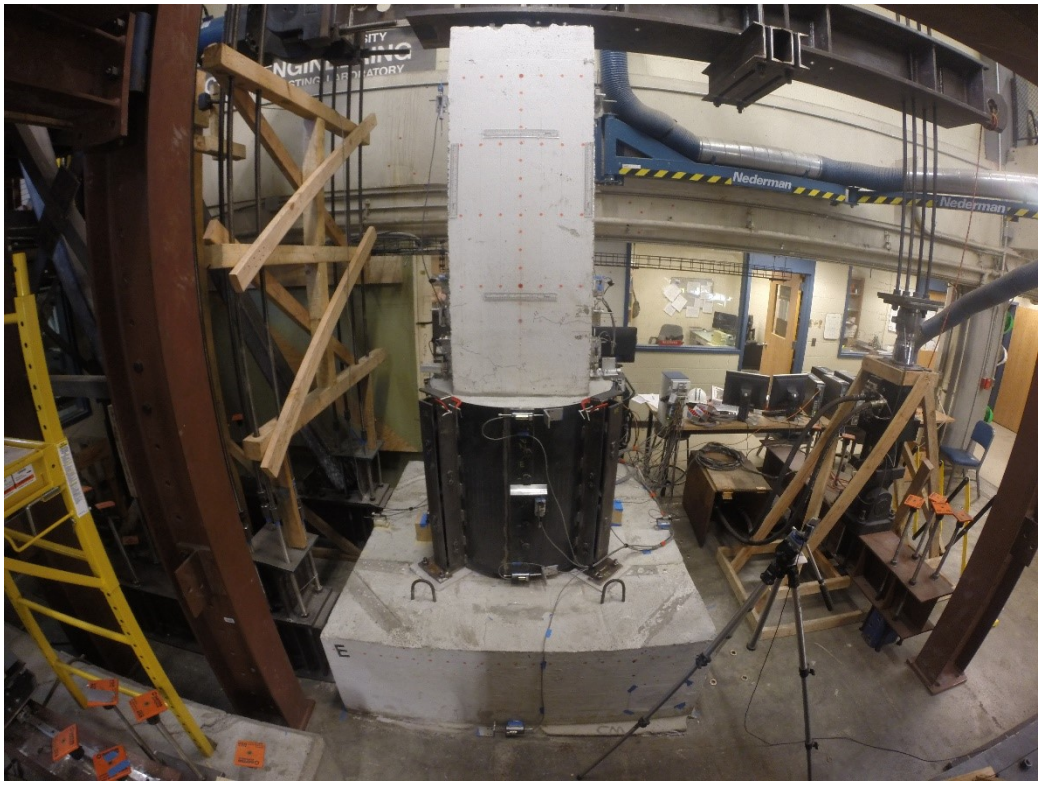

Figure 5.1: Test 1 @ initial state

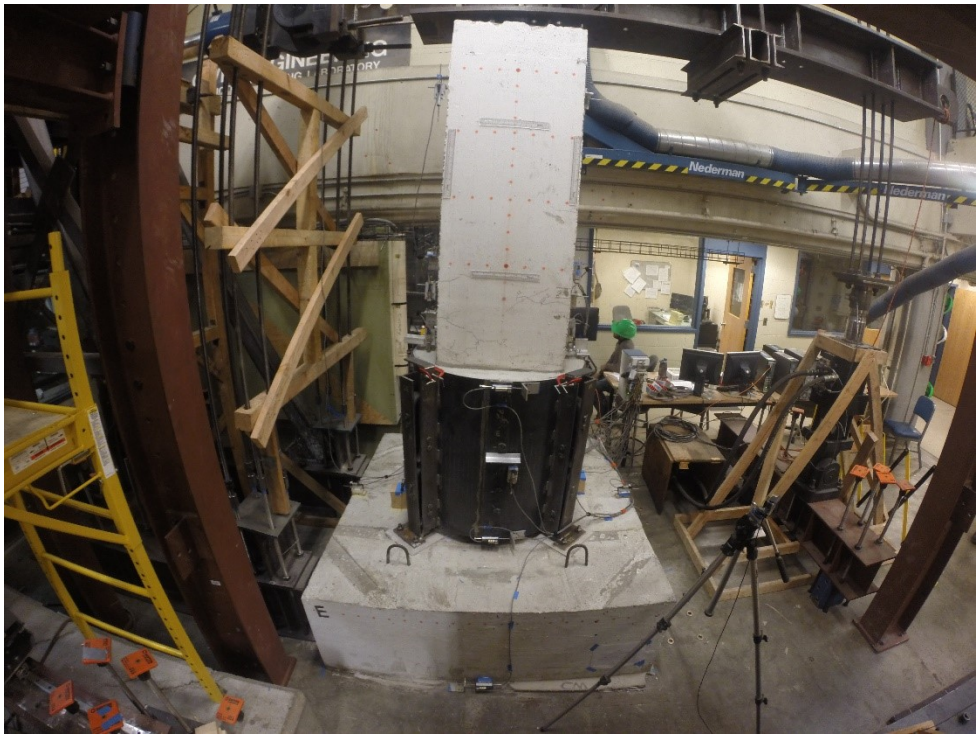

Figure 5.2: Test 1 @ 2.5 inches lateral displacement

Figure 5.3: Residual hold-down deformation

Figure 5.4: Hold-down weld failure

5.1.2 Test 2

Lessons of the previous test provoked three design modifications, which are shown in Figure 5.5 and are visible in Figure 5.6. The three design modifications are:

1. Oversized holes and plate washers - the first repair revealed constructability issues due to bolt hole alignment tolerances. It was found that imperfections in UFP bend geometry and zero tolerance from welded nuts created misalignments between bolt holes. Installation was difficult and time consuming. To improve constructability and reduce assembly time, oversized holes and plate washers were added to the exterior leg of the hold-down. This resulted in a much easier and faster installation.

2. Reduced section plastic hinge – A reduced section was introduced at the base of the exterior hold-down legs. 1.5-inch slots with a ½-inch radius were cut into the legs of the L4X4X1/2, reducing its cross-sectional properties to that of a L2-1/2X2-1/2X1/2. This hinge allows the hold-down to rotate with the column and shell, while limiting flexural forces to the previously failed weld.

3. Hold-down caps – Each hold-down was equipped with a cap. The cap was attached via an angle bracket that was welded to the interior hold-down on the inside of the hold-down. This cap serves two purposes. First, it prevents separation of the exterior leg while allowing the leg to slide within, displacing vertically. Secondly, the cap serves as an encapsulation for subgrade applications.

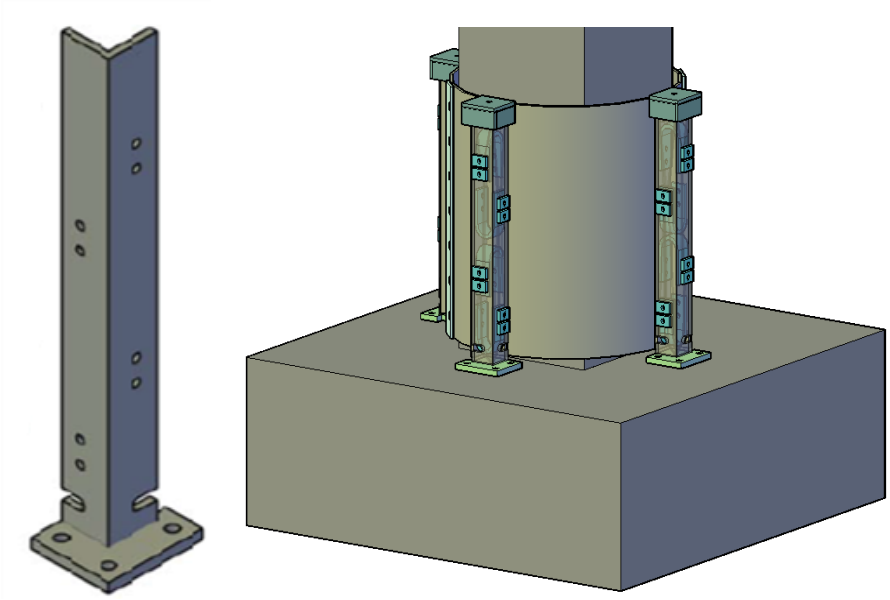

Figure 5.5: Test 2 design modifications

For the second test, specimen LVF#8 was repaired using the face orientation and the three design modifications were implemented. The standard laboratory lateral loading protocol was used for both the as-built test, and the repaired test. The hold-down UFPs were the same as test 1, PL1/2X2-1/2 grade A36 steel with a bend diameter of 3.25 inches. The expected maximum

hold-down force was also the same as test 1, 32.7 kips. However, the expected maximum lateral load was 48.9 kips which is an increase due to the hold-down orientation. The repaired specimen and test setup are pictured in Figure 5.6 in its initial state before testing.

The hold-down caps did not function as intended. With each cycle, the cap was slowly pushed up as the angle bracket yielded. Figure 5.7 show the final state of the test specimen. The cap bracket has yielded and no longer engages the exterior leg of the hold-down. Following this test, the hold-down cap was abandoned and replaced by hold-down rollers that are discussed in the following section.

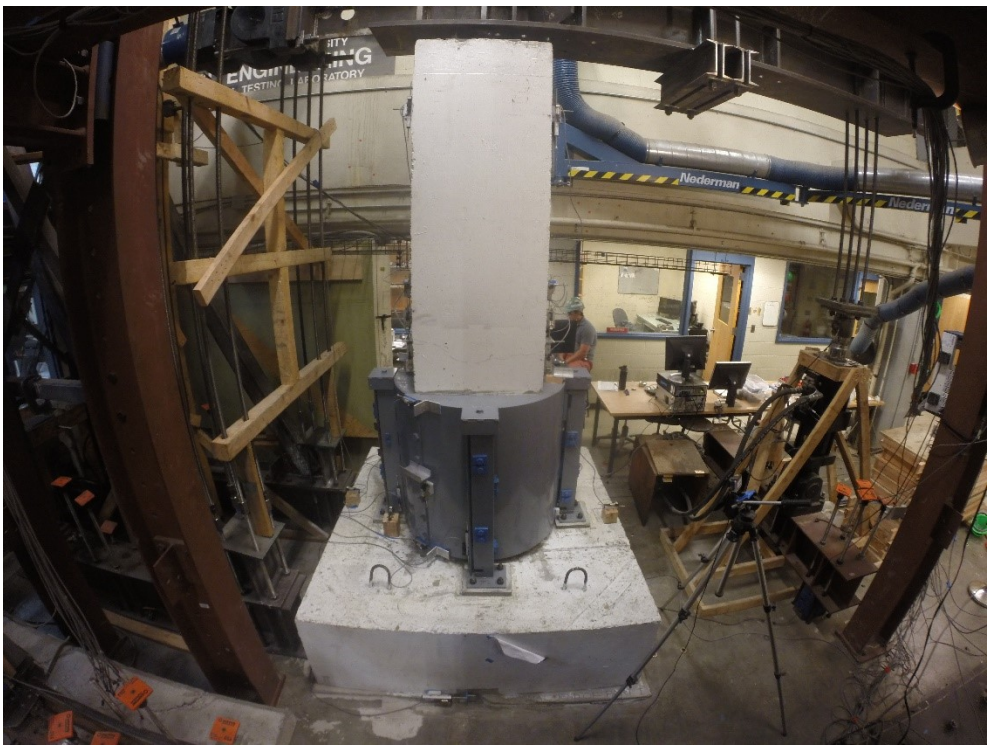

Figure 5.6: Test 2 @ initial state

Figure 5.7: Test 2 @ final state

5.1.3 Test 3

For the third test, the hold-down caps were removed, and new hold-down rollers were installed. The hold down roller is shown in Figure 5.8. The roller was made from a ½-inch threaded rod and a hollow pipe that were mounted using ¼-inch plate welded to the shell. The rollers prevent hold-down separation while allowing vertical displacement.

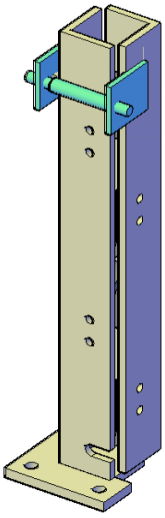

Figure 5.8: Test 3 modification - hold-down roller

The third test was a repeated repair on specimen LVF#8. The shell remained attached to the column in face orientation. Only the hold-downs were replaced. The hold-down UFPs were the same test geometry as tests 1 and 2, PL1/2X2-1/2 grade A36 steel with a bend diameter of 3.25 inches. The subduction zone loading protocol was used. The repaired specimen and test setup are pictured in Figure 5.9 in its initial state before testing. The hold-down rollers functioned as intended, preventing separation of the hold-down legs. Figure 5.10 shows the hold down rollers before and after the test. They were designed and installed with a ¼" gap between the roller and the hold-down leg. During the test, the gap opened and closed on push and pull cycles.

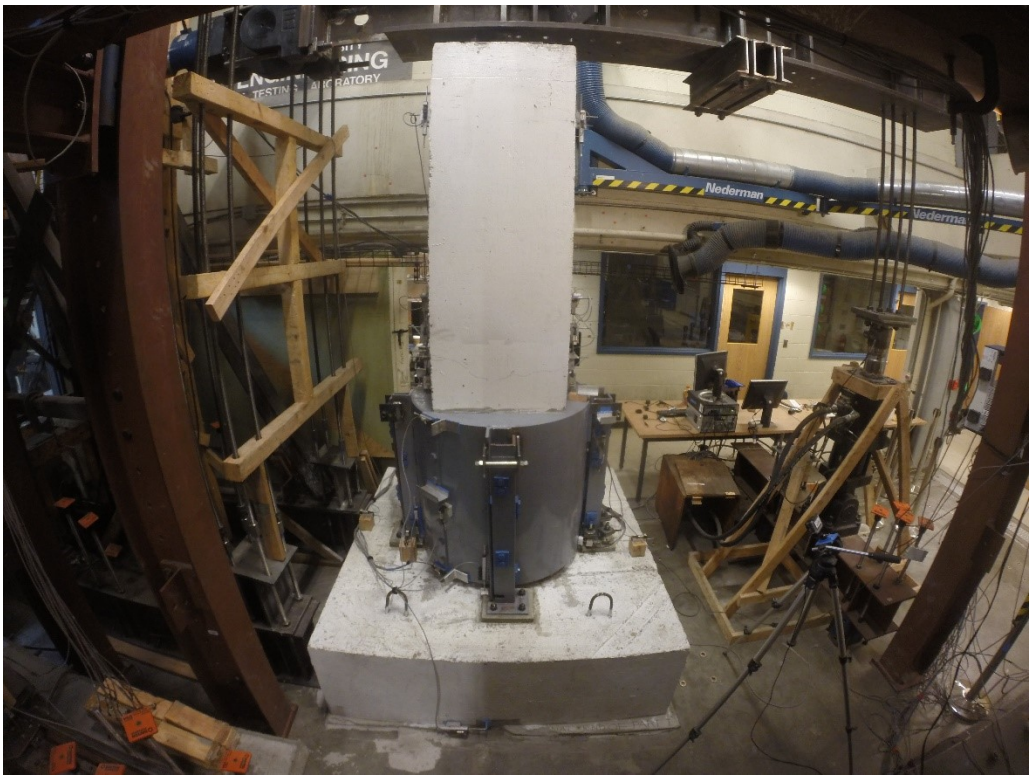

Figure 5.9: Test 3 @ initial state

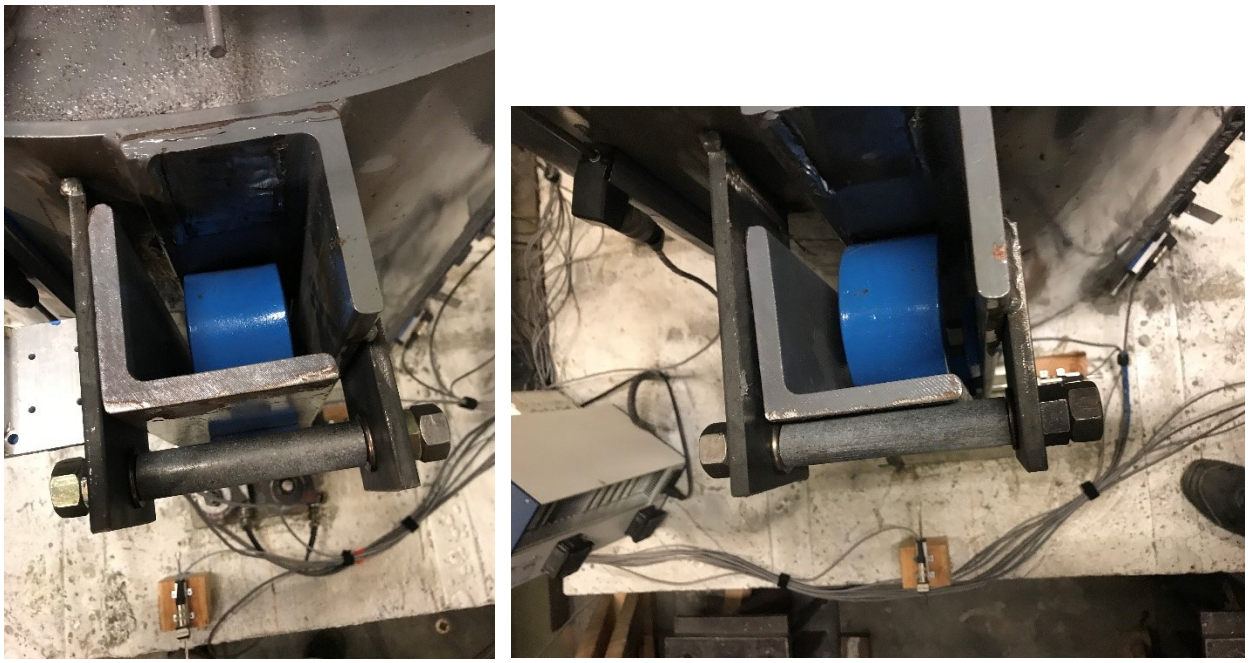

Figure 5.10: Hold-down rollers (a) before and (b) after test

5.1.4 Test 4

The fourth test was also a repeated repair on specimen LVF#8. New exterior legs were installed. The previous legs were permanently distorted and fatigued from cyclic loading over the first three tests. For this test, the objective was to design the hold-downs such that the lateral capacity of the repaired column would be greater than the as-built column. To increase capacity, the UFP thickness was increased by 1/8 inch and the bend diameter was decreased such that the outside diameter remained constant. This results in a 63% increase in maximum hold-down force and a 27% increase in expected lateral load. The fourth test is shown in its initial state in Figure 5.11.

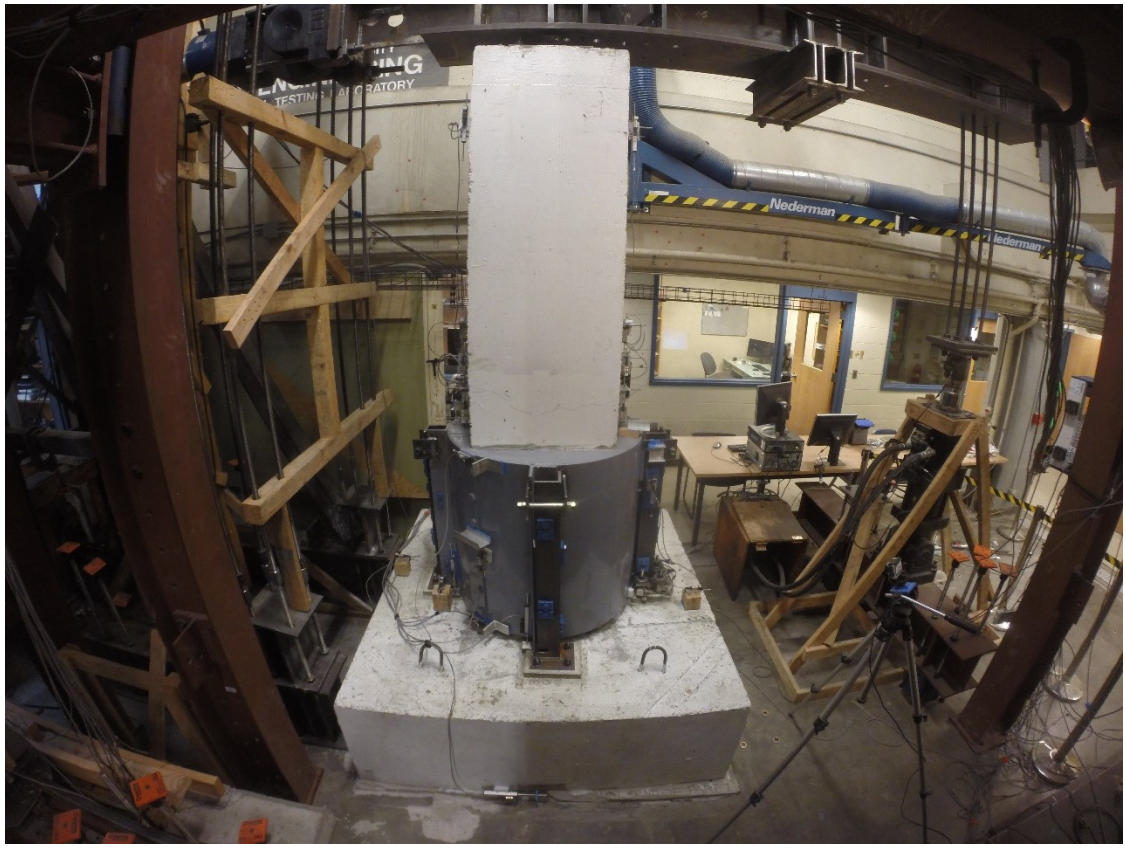

Figure 5.11: Test 4 @ initial state

5.2 MEASURED DATA

The following subsections include load-displacement responses for all four tests. The load-displacement response for the repaired column is plotted in black and the as-built load-displacement response is plotted in blue. Under positive displacements (push cycles), the axial load increased to a maximum of +240 kips. Under negative displacements or pull cycles, the axial load decreased to a minimum of +160 kips.

5.2.1 Test 1

The lateral load-displacement response for test 1 is shown in Figure 5.12. The peak lateral load from the as-built column was 44.9 kips and the target peak lateral load was 46.4 kips. The peak lateral load measured from the repaired test was 40.2 kips, 13.3% less than target. The hysteresis shows self-centering behavior. On the return cycles, as the lateral displacement is returned to zero, the lateral load approaches zero. This behavior is a result of the location and magnitude of the axial force, working to restore the column to its original position.

There are two negative displacement cycles on the repaired-column test that are different from the rest. These cycles occurred when the axial load actuator stroked out and axial load was lost. Following these two cycles, the test-setup was adjusted, and the test continued. These cycles can be observed in the hysteresis on Figure 5.12 where the load decreases to zero (0) at a

displacement of approximately -2.75 inches and does not follow the typical self-centering behavior of the hysteresis.

The repaired column shows less strength degradation than the as-built column. At the maximum displacement of 5.4 inches, the as-built column lateral load has degraded to approximately 77% of its peak while the repaired column maintains approximately 85% of its peak lateral load.

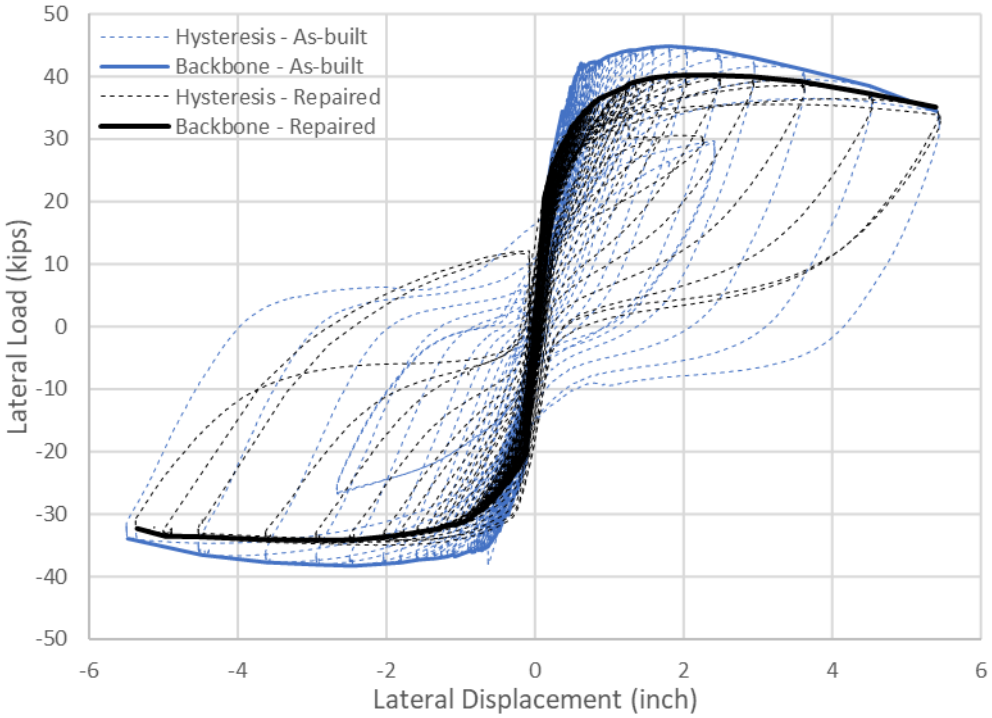

Figure 5.12: Test 1 Hysteresis

5.2.2 Test 2

The second specimen was repaired for Test 2 and the conventional ACI lateral loading protocol was used for the as-built column test and the repaired column test. The repair was oriented with the hold-downs at each face of the column and the hold-down caps were installed. The lateral load-displacement response for Test 2 is shown in Figure 5.13. The as-built column had a peak horizontal load of 40.3 kips, and the expected lateral load based on the static analysis is 48.9 kips. The measured peak lateral load for the repaired column was 31.6 kips, 35% less than expected and 21% less than as-built. Test 2 showed greater strength degradation than Test 1. At the final cycle displacement of 5.4 inches, the strength degradation was 25% compared to 15% in Test 1.

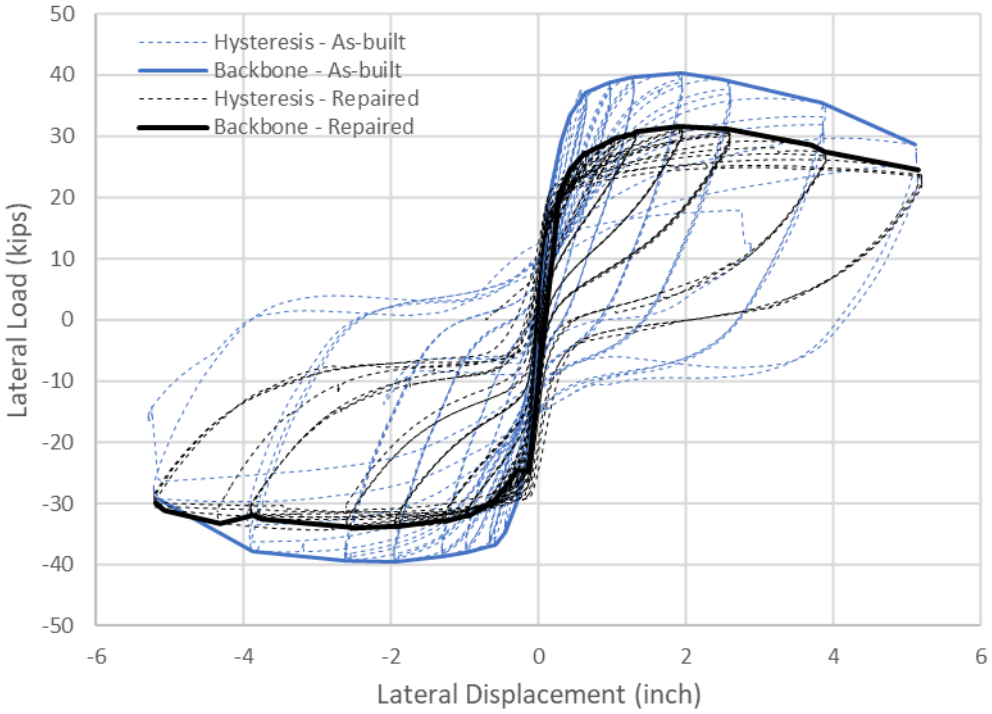

Figure 5.13: Test 2 Hysteresis

5.2.3 Test 3

After Test 2, new UFPs were installed, and the specimen was used again for Test 3. The UFPs matched the geometry of those in Test 2. Therefore, the as-built peak horizontal load and expected repaired peak horizontal load are the same as Test 2, 40.3 kips and 48.9 kips, respectively. The differences between Test 2 and Test 3 are the addition of the hold-down rollers and the cyclic history of the specimen. The lateral load-displacement response for Test 3 is shown in Figure 5.14. The measured peak lateral load for the repaired column was 30.5 kips, 37% less than expected based on the static approach and 24% less than as-built.

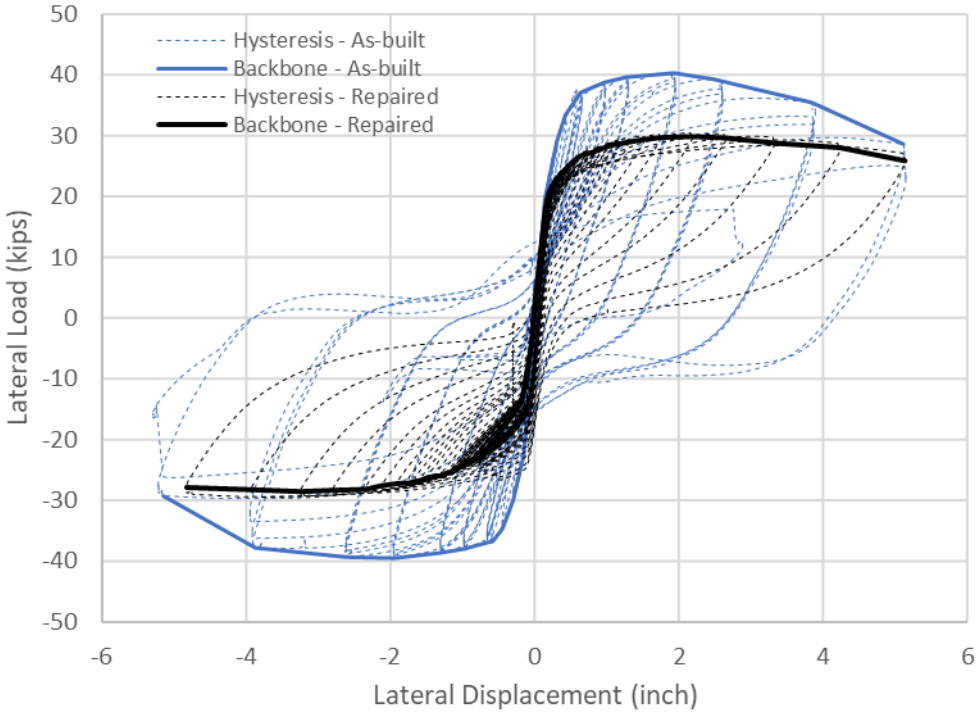

Figure 5.14: Test 3 Hysteresis

5.2.4 Test 4

The repair for Test 4 utilized the same specimen from Test 2 and Test 3; however, Test 4 was designed to increased lateral capacity. The UFP thickness was increased by 1/8th inch, which results in an expected hold-down force, of 53 kips, 62% greater than the previous three tests. The lateral load-displacement response for test 4 is shown in Figure 5.15. The peak lateral load measured from the repaired test was 38.6 kips, up from 30.5 kips in the previous test.

The increase in hold-down strength reduced the self-centering behavior that was observed in the previous tests. The hysteresis shows that on the return cycles, as the lateral displacement is returned to zero, the lateral load does not return to zero. This behavior is a result of increased hold-down strength and the plastic deformation. The axial force is not enough to restore the hold-downs to their original position.

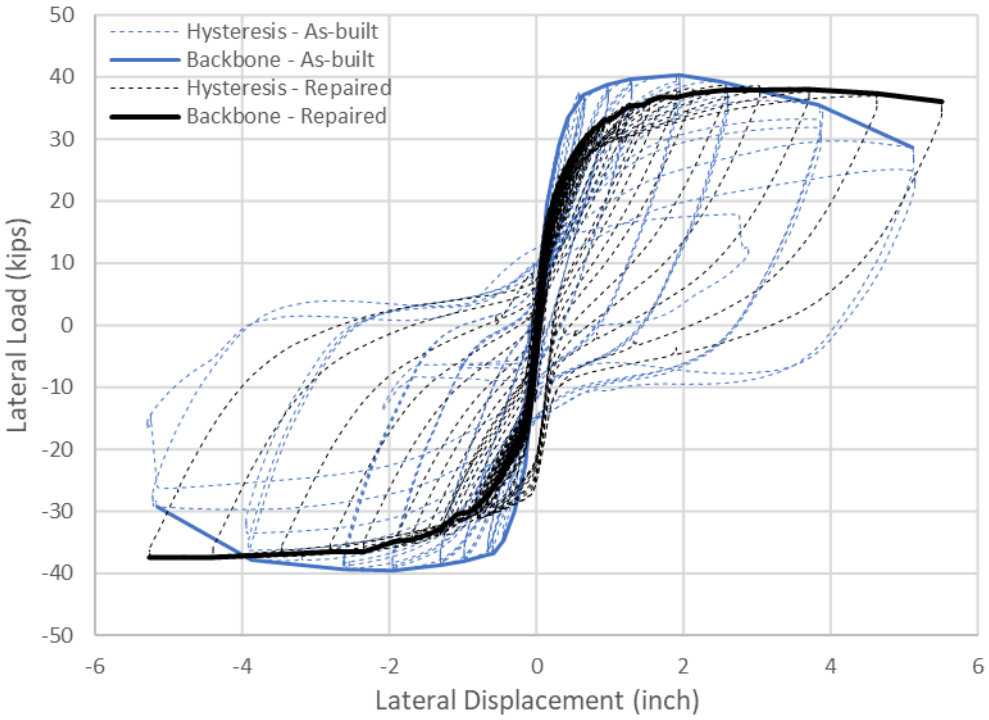

Figure 5.15: Test 4 Hysteresis

5.3 CURVATURE PROFILE

Average displacement for a particular segment of 3 inches and 6 inches height were measured with LVDT's and was later used to compute the average rotation of the segment. Average column curvature for these segments were then approximated by dividing the rotation with the height of the individual segment. Figure 5.16 presents the average curvature profile along the length of the column starting from the top of the shell. The vertical axis represents the column height (inches) starting at 37 inch (top of the steel shell) and the horizontal axis represents average curvature (rad/in). The average column curvature for the pre-yield and post-yield loading cycles were plotted separately in order to compare the results with the analytical yield curvature for the as-built column. In addition, the pull and push cycles of loading were plotted separately to compare the results under different axial loading. The bottom 3-inch segment (from 37 to 40 inches) on top of the shell experienced the maximum average curvature for all the specimens tested. It is noted that the LVDT measuring the displacement in the bottom 3-inch segment (from 37 to 40 inches) was placed on the face of the grout casted within the steel jacket. Hence, any slip between the grout and the existing column interface was also recorded by the LVDT measuring the displacement. There was no additional LVDT measuring the slip between the existing column and the grout and hence any slip component was not separated from the measured curvature. Physical observation during the test showed no significant slip between the two interfaces.

The primary objective of the repair methodology was to restore the column strength through accumulating inelastic deformation in the sacrificial replaceable fuses while protecting the column from any damage. Hence, the average column-curvature profile can be used as an

important criterion to estimate the inelastic deformation in the column section. The efficacy of the repair method in terms of limiting column damage can then be compared for different test specimens.

The pre-yield curvature profiles for tests 2, 3 and 4 show a linear profile under pull cycles of loading. The push cycles of loading experienced somewhat erratic curvature profile where the average curvature increases linearly until the second segment (40 to 46 inches) and the least curvature was recorded for that segment. Finally, the bottom segment (37 to 40 inches) was recorded to have the maximum average curvature. This indicates a double curvature bending behavior of the column section under the push cycles of loading. A similar trend in curvature profile for push cycles of loading was also observed for post-yield curvature profile. The behavior was most notable for test 1 where the second segment (40 to 46 inches) showed negligible average curvature. Nonlinear distribution of the average curvature was observed for the post-yield push and pull cycles of loading. Comparing the results between different test specimens, test 3 was found to have the least average-curvature for both the pre-yield and post-yield loading cycles. The specimen for test 3 showed an elastic curvature profile until the final loading cycles at displacement ductility 6 and 8 where the average curvature for the bottom segment (37 to 40 inches) exceeded the analytical yield curvature. However, it should be noted that the test 3 achieved the lowest peak lateral load capacity. The maximum peak lateral load capacity was obtained for test 1 followed by test 4 and test 2. Test 1 experienced the highest average curvature followed by test 4 and test 2. This can initially be attributed to the higher demand imposed on the column sections resulting from higher peak lateral capacity achieved.

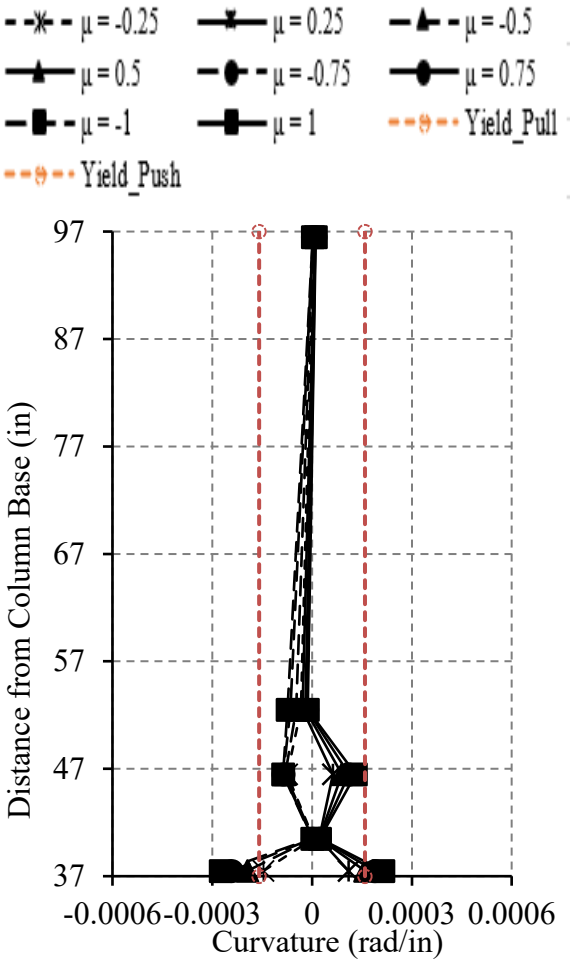

(a) Test 1-Pre Yield

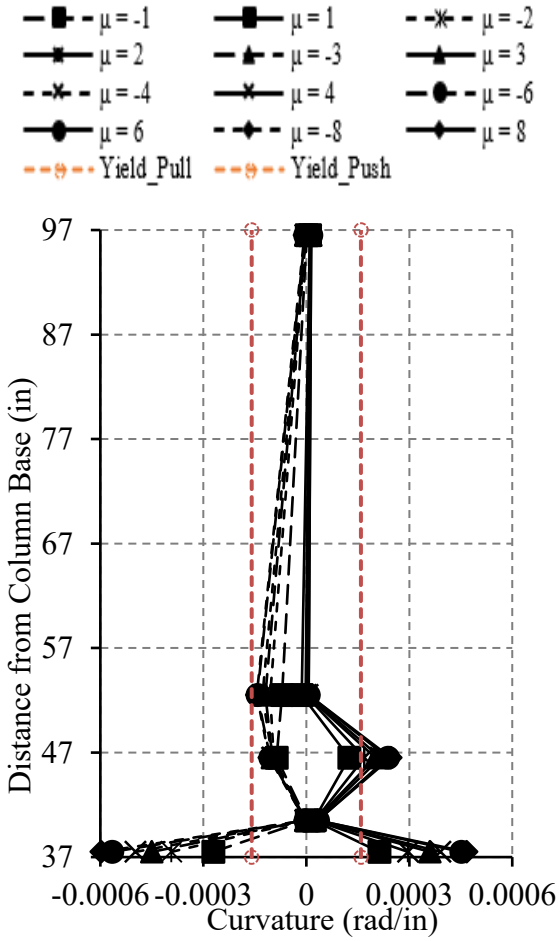

(b) Test 1-Post Yield

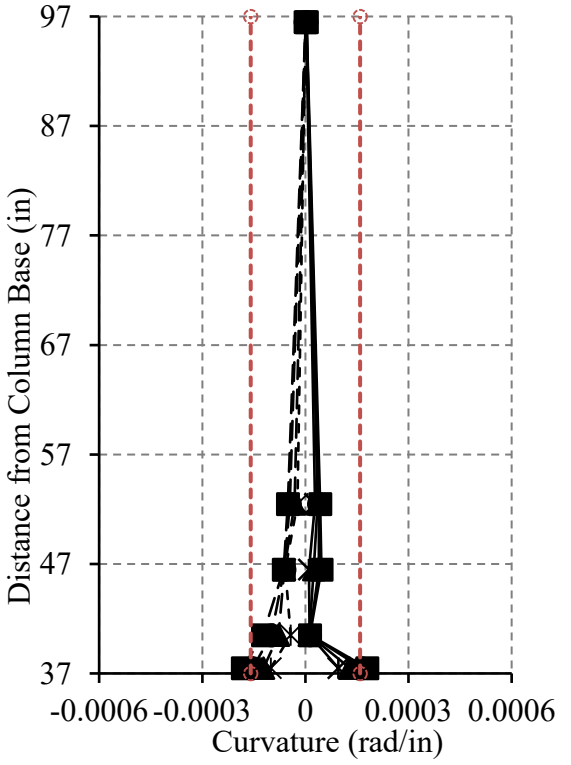

(c) Test 2-Pre Yield

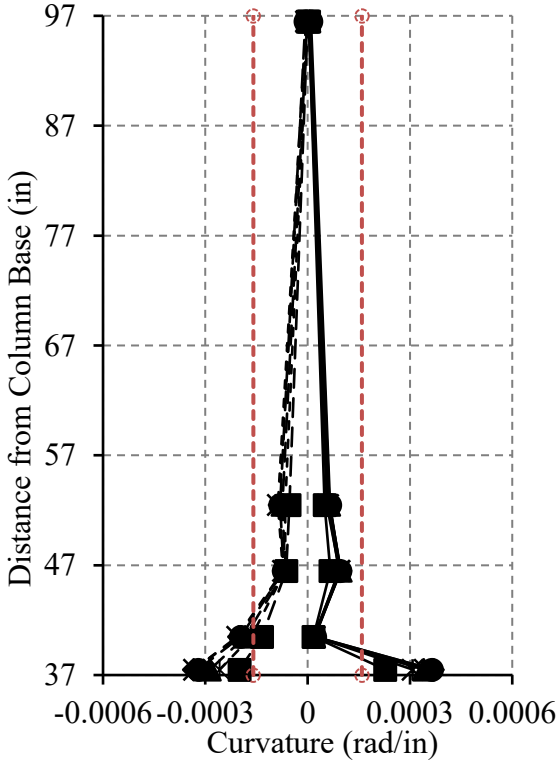

(d) Test 2-Post Yield

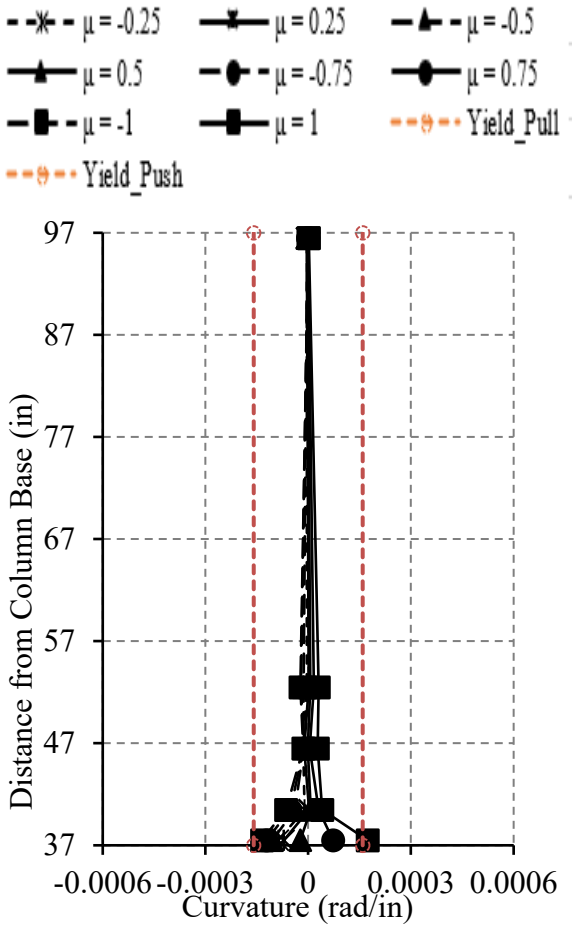

(e) Test 3-Pre Yield

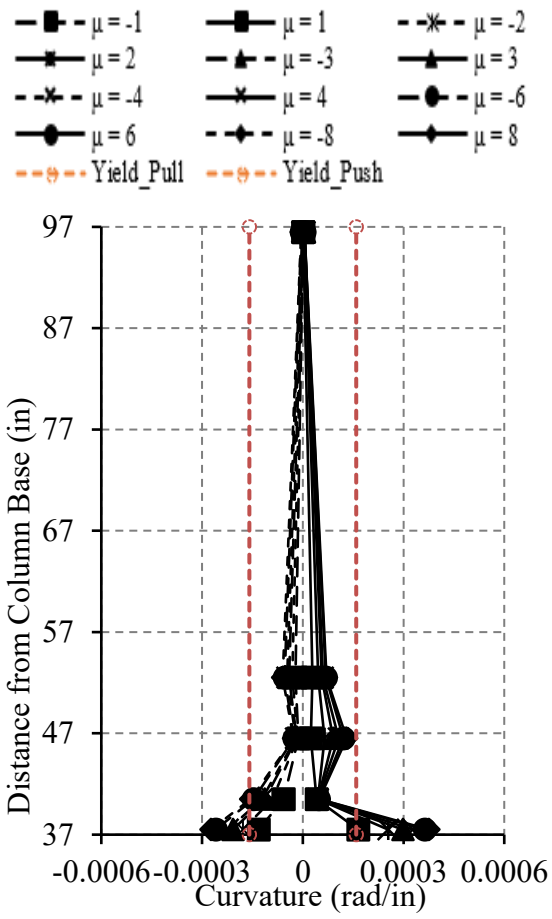

(f) Test 3-Post Yield

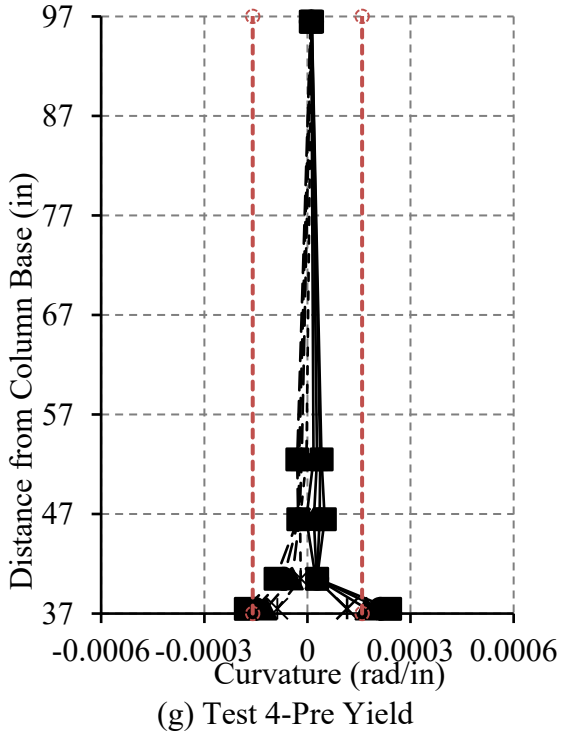

(g) Test 4-Pre Yield

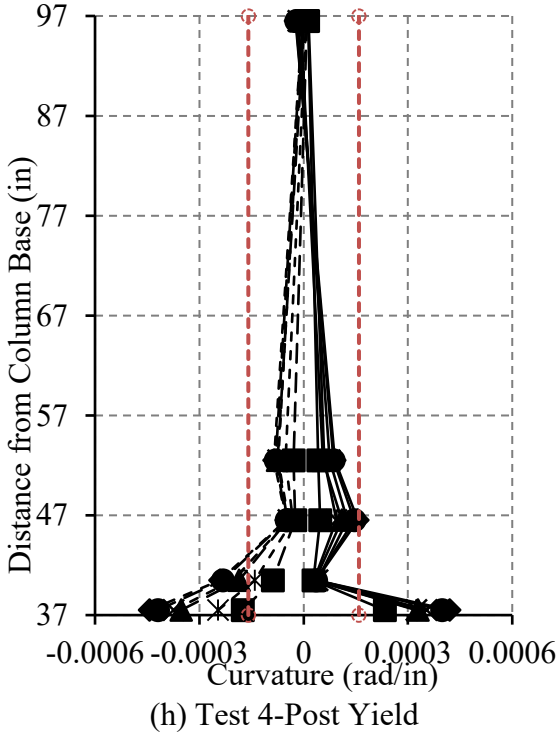

(h) Test 4-Post Yield

Figure 5.16: Pre-yield and post-yield curvature profile for (a-b) Test 1, (c-d) Test 2, (e-f) Test 3 and, (g-h) Test 4

5.4 STIFFNESS DEGRADATION

Secant stiffness (K_{sec}) at each displacement ductility cycle normalized against yield stiffness (K_y) is presented herein as the stiffness degradation parameter. The secant stiffness was calculated as the ratio of the force over displacement for the first cycle at each displacement ductility level, whereas the yield stiffness corresponds to the secant stiffness at the effective yield displacement level. Figure 5.17 shows stiffness degradation plotted against displacement ductility for both the pull and push cycle for all the four repair specimens.

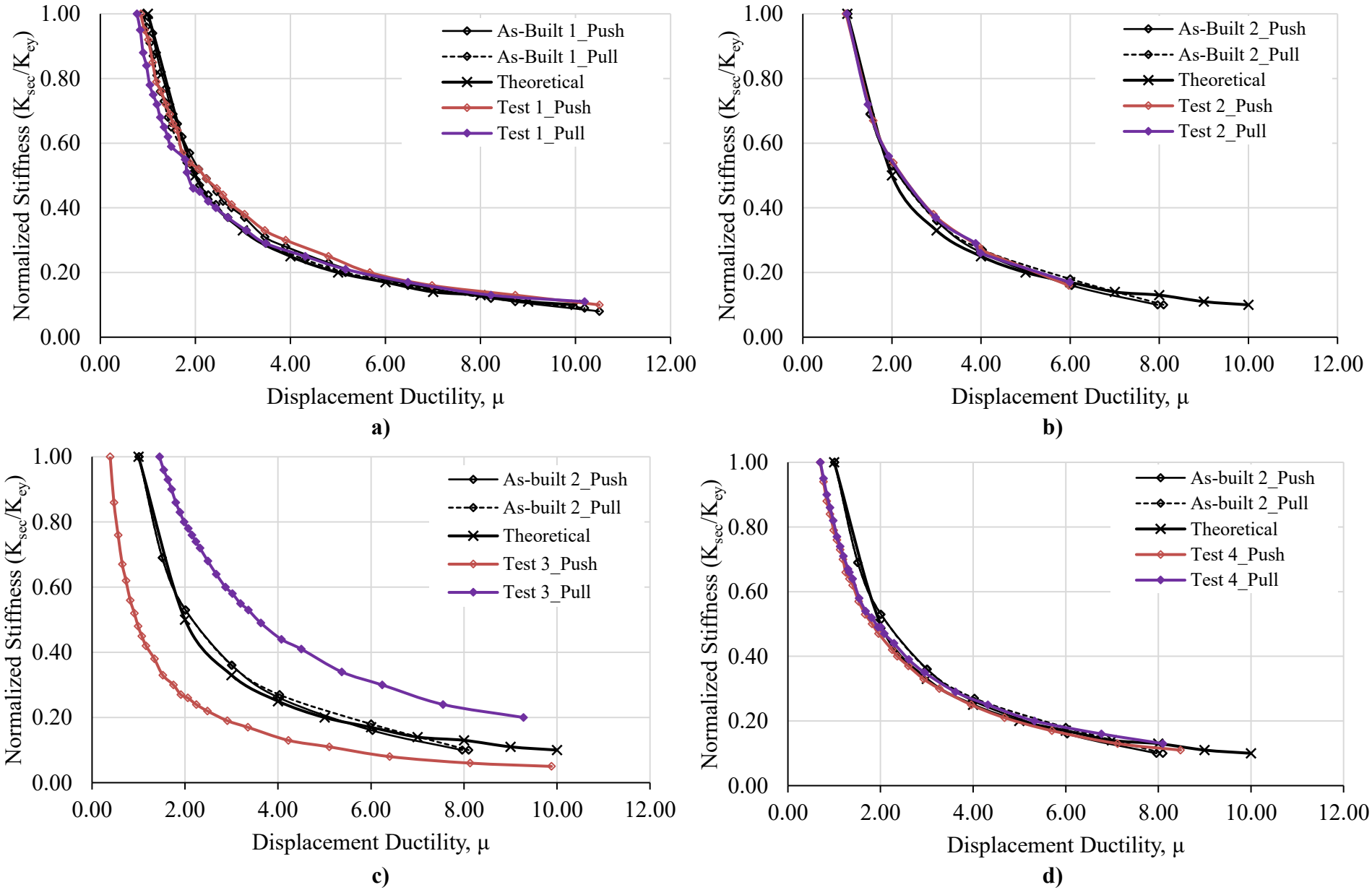

Figure 5.17: Stiffness degradation for the as-built and repaired column (a) Test 1, (b) Test 2, (c) Test 3 and, (d) Test 4

All the four specimens showed similar stiffness degradations for push and pull cycles of loading. The pull cycle of loading for all the repaired specimens resulted in comparably lower stiffness degradation compared to the push cycle of loading. This can be attributed to the higher axial load associated with the push cycle of loading for the tested specimens. Gulkan and Sozen (1974) proposed a relationship between displacement ductility and secant stiffness, as shown in Equation 5-1. This relationship, which is shown as the theoretical curve in Figure 5.17, was found to agree well with the stiffness degradation for all tested specimens except test 3. Test 3 was found to have significantly different stiffness degradation for push and pull cycles of loading. The initial cycles at low displacement ductility demand were observed to have the most damage and the difference reduced for higher displacement ductility cycles.

$$\left(\frac{K_{sec}}{K_y}\right)_{\text{Theoretical}} = \frac{1}{\mu} \leq 1 \qquad \textbf{(5-1)}$$

5.5 DISCUSSION

The experimental program provided encouraging evidence to support the feasibility, adequacy, and benefits of the proposed repair methodology. This discussion correlates visual observations and measured data to evaluate the overall success of the design objectives. The objectives were to develop a practical post-earthquake repair methodology that (1) could be rapidly implemented following the CSZ earthquake, (2) incorporate low damage earthquake resilience for future shaking, (3) achieve restored or controlled strength. The following three subsections individually address the success of these objectives.

5.5.1 Rapid and Economic Deployment

This methodology could potentially be adopted, and necessary parts prepared prior to a major earthquake. The parts and components such as steel jackets, hold-downs, and UFPs, could be pre-manufactured and stockpiled for rapid access when needed. In that case, the time or labor of installation is the most important factor when evaluating the feasibility of rapid application.

The process of implementing and re-implementing the proposed repair methodology in the laboratory demonstrated the feasibility of rapid application and provided insight for efficient constructability. The proposed repair methodology was implemented on two damaged column specimens. The first specimen was repaired and tested once. The second specimen was repaired and tested three times by re-implementing the existing repair. Upon each successive implementation or re-implementation, the installation process became quicker. The first implementation was difficult due to fabrication tolerances. Some of the bolt holes in the UFPs did not align with the holes in the exterior hold-down leg. This was mainly due to slightly misshaped UFPs. Bending consistent geometries proved difficult but improved with experience. The addition of oversized holes and plate washers on the second repair greatly reduced the time and difficulty of installing the UFPs and hold-downs. With practice and refinement, the proposed repair methodology can be both feasible and rapid.

Residual displacement is one of the key issues that needs to be addressed while repairing the column after an earthquake. The proposed repair method can be installed on a column having residual displacement. However, if the components (i.e., hold downs, UFPs etc.) are prefabricated then the installation process could be complicated due to alignment issues resulting from the geometry of the leaned column and tolerance problems for hole dimension. Hence, it is recommended to align the column in upright position before installing the repair components. In the laboratory experimentation, vertical alignments of the column were ensured before repair. Recentering of the column can be achieved easily for the proposed repair method as the rebar continuity is eliminated prior to the installation of the hold-down components. Furthermore, shoring of the bridge bent would be needed to reflect the observed damage and stability prior to any repair work. If the bridge deemed stable enough then a decision can be made to repair one column at a time without shoring.

5.5.2 Enhanced Resilience

Visual observations suggest that this repair methodology successfully met the design objective of isolating inelastic deformations and damage to the easily replaceable ductile fuse hold-downs. Thus, enhancing resilience for future aftershocks and earthquakes. Visual observations from all four tests revealed very little damage to the original column and the footing remained completely undamaged throughout all four tests.

Conventional repair methods will shift damage to the area above the repair in future seismic events. The four tests showed that the proposed methodology does not shift damage to the area above the repair. There were small flexural cracks above the repaired zone in all four tests. These cracks were initiated during the as-built test and were lengthened during testing of the repaired column. Throughout all four tests, there were no residual gaps in the flexural cracks. The second specimen was repaired and tested three times and still, the zone above the repair showed no increase in damage. These observations suggest that inelastic strains did not occur and that the design objective was met.

5.5.3 Restored or Controlled Strength

The lateral load displacement plots in Figure 5.12 through Figure 5.15 show similar behavior and strength between the as-built column and the repaired column however, the repaired columns consistently underperformed the expected repair capacity in terms of lateral strength. This suggests that the proposed repair methodology is capable of achieving restored or controlled strength, but that the design methodology needs refinement. This section will quantify the success of achieving restored or controlled strength and then present suggestions for a refined design process.

Key metrics were calculated and compared to the as-built columns. These key metrics are effective stiffness, peak horizontal load, displacement at peak horizontal load and horizontal load degradation at final cycle and are tabulated in Table 5.1. While the design methodology directly aims to control strength, it is also important to consider stiffness. Effective initial stiffness was calculated by taking the load divided by displacement at the first peak or target displacement per the loading protocol. The average effective stiffness from all peaks at the first target displacement is reported in Table 5.1. The effective initial stiffness for Test 1 was within 2% of

the as-built column. For the other tests, the effective initial stiffness varied by as much as 32% greater than as-built and 13% less than as-built.

Horizontal load at final cycle was calculated by taking the percent difference between peak horizontal load and horizontal load at the final cycle, which occurred at approximately 5.4 inches of displacement at the top of the column. All four tests showed that the repaired columns had a significant reduction in horizontal load degradation at final cycle. The as-built columns degraded an average of 26% while the repaired columns degraded an average of just 15% at final cycle. This suggests a reduction in degradation could be an added benefit of the low-damage repair methodology. The repaired columns remain undamaged whereas the as-built column experiences significant damage in the plastic hinge region such as concrete spalling, concrete crushing, rebar yielding and rebar buckling leading to strength degradation.

It is also important to compare the strength degradation between the four repaired tests. The average horizontal load degradation of the first two tests is 20% while the average over the last two tests is only 10%. This difference could be because of hold-down leg separation that is discussed in section 5.1.0 and pictured in Figure 5.3. The addition of the hold-down rollers, which were added after Test 2 and described in section 5.1.3, prevent hold-down leg separation. In Test 2, the hold-down legs separated by as much as ¾ inch, while in Test 3 the hold-down rollers limit separation of the legs to 1/4 inch. The maximum hold-down force is inversely proportional to the distance between legs and a ¾-inch separation results in an 18.7% reduction in theoretical hold-down force. It is also possible that hold-down leg separation effects can be observed in the measured data by comparing Test 2 and Test 3. The UFP geometry remained constant between these two tests. However, the displacement at peak horizontal load is 1.908 inches in Test 2 and 2.492 inches in Test 3. Monitoring separation with instrumentation while testing would help to better understand the effects of hold-down leg separation. The difference in displacement at peak horizontal load along with the difference in horizontal load degradation at final cycle, suggests that the hold-down rollers were successful in preserving hold-down force by retaining the outer leg of the hold-down through cyclic loading.

Table 5.1: Results Comparison

Test	Effective Stiffness, k (kips/inch)	Peak Horz. Load (kips)	Displacement at Peak Horz. Load (in.)	Horz. Load Degradation at Final Cycle (%)
As-built 1	164	44.9	1.80	23
Test 1	166	40.2	2.01	15
As-built 2	144	40.3	1.94	29
Test 2	190	31.6	1.91	25
Test 3	130	30.5	2.49	13
Test 4	122	38.6	2.49	7

The design process and selection of UFP geometry was based on the static design process explained in methodology section. Based on the assumptions and simplifications of the static design process, the expected peak horizontal load was predicted to overestimate the lateral strength. All four tests confirmed this prediction. The measured peak horizontal load in Test 1

was 13% less than the static design process predicted. The difference was larger in the next three tests: 35% in Test 2, 37% in Test 3, and 37% in Test 4.

The assumptions from the static design method are (1) the rocking point is at the edge of the column, (2) column curvature is negligible, and (3) the maximum expected hold-down forces are acting about the column in its undeformed state. When the rocking point is assumed to be a single point at the column edge, the compressive force or reaction in the concrete is assumed to act directly through the overturning point and have no effect on the overturning moment. In reality, the rocking point is located some distance inward from the column edge and might be described better as a neutral axis, where there is a compression block between the neutral axis and the column edge. In this case, the compression force does not act directly through the neutral axis and actually contributes to resisting overturning forces.

The hold-down resisting forces are also impacted by the location of the rocking point or neutral axis. If we consider the simple static analysis from methodology section, but vary the rocking point location, we can plot the effects it has on expected peak horizontal load. In Figure 5.18, the x-axis represents the location of the rocking point or neutral axis with respect to the column edge. At x = 0 inches, the plot shows the expected peak horizontal load assuming rocking occurs at the column edge. As that distance increases, the summation of lever arms between the hold-downs and the neutral axis decreases. The distance between the axial load and neutral axis also decreases. This results in a decrease in overturning moments and thus a decrease in expected peak horizontal load. Figure 5.18 also shows that this effects corner orientation and face orientation differently. As the rocking point moves inward from the column edge, the expected peak lateral load decreases faster for face orientation than for corner orientation. This is solely due to the position of hold-downs relative to the neutral axis.

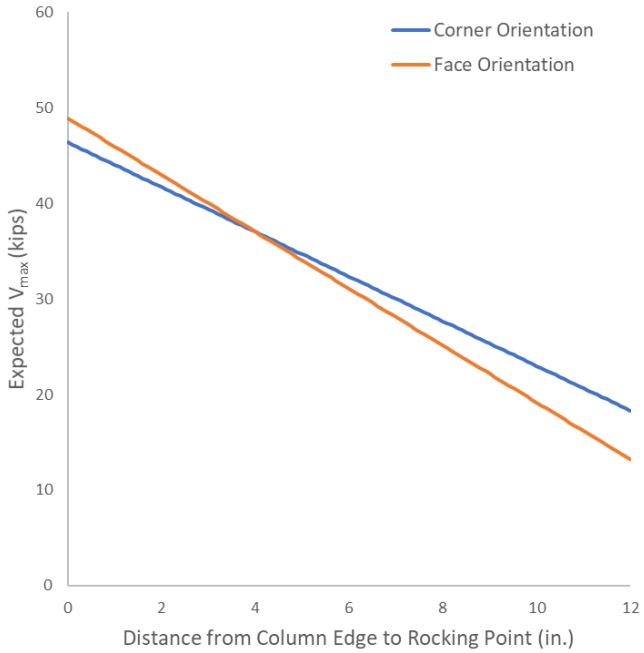

Figure 5.18: Effects of rocking point assumption

To remove this assumption from the design methodology, the actual neutral axis was calculated from the measured data. During testing, each hold-down was equipped with a LVDT to monitor vertical displacement. If we assume the principals of rigid body motion apply to the repair jacket, the four hold-down LVDTs can be used to calculate the actual neutral axis on the rotating column. Figure 5.19 shows the results of this calculation from Test 1. The dots represent the neutral axis distance from column edge at peak displacements, yellow dots are on push cycles when the axial load is increased, and grey dots are on pull cycles, when the axial load is decreased. As you would expect, the neutral axis is near the middle of the column at very small displacements, and it moves toward the edge as the column is pushed further. As column displacements become large, the neutral axis approaches a horizontal asymptote around three to four inches from the column edge.

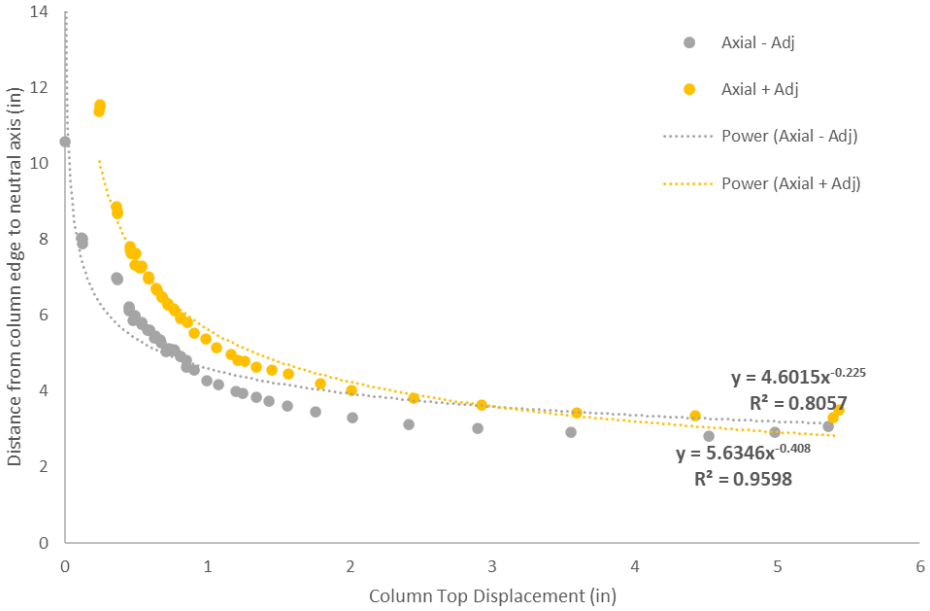

Figure 5.19: rocking point distance to edge of column, corner orientation

The actual rocking point and its effects on peak lateral load can be accounted for if the pushover analysis method from methodology section is used. This method also accounts for assumption (3) which states that the maximum expected hold-down forces are acting about the column in its undeformed state. In reality, the hold-downs exert no force on the column in its undeformed state. The hold-downs do not engage until the column has started rocking and there is vertical displacement at the hold-downs. The pushover analysis method assumes rigid body motion of the repaired column and calculates the hold-down force based on a bi-linear force-displacement relationship of the UFPs. The pushover analysis method also accounts for p-delta effects by reducing the lever arm between the axial load and the neutral axis and the column is displaced laterally. Figure 5.20 shows the results of the pushover analysis overlaid on top of the lateral load-displacement response from Test 1. The red line is a pushover analysis that assumes rocking occurs at the edge of the column, as described in methodology section. The yellow line is a pushover analysis that is modified to account for the actual measured rocking points from Figure 5.19. These methods of analysis appear to predict the systems behavior more accurately

than the static design method. For this repair, the static method predicted a peak horizontal load of 46 kips while the push over analysis predicted a peak horizontal load of 43 kips before accounting for the actual rocking point and 37 kips after accounting for the actual rocking point. The measured peak lateral load from this test was 40 kips.

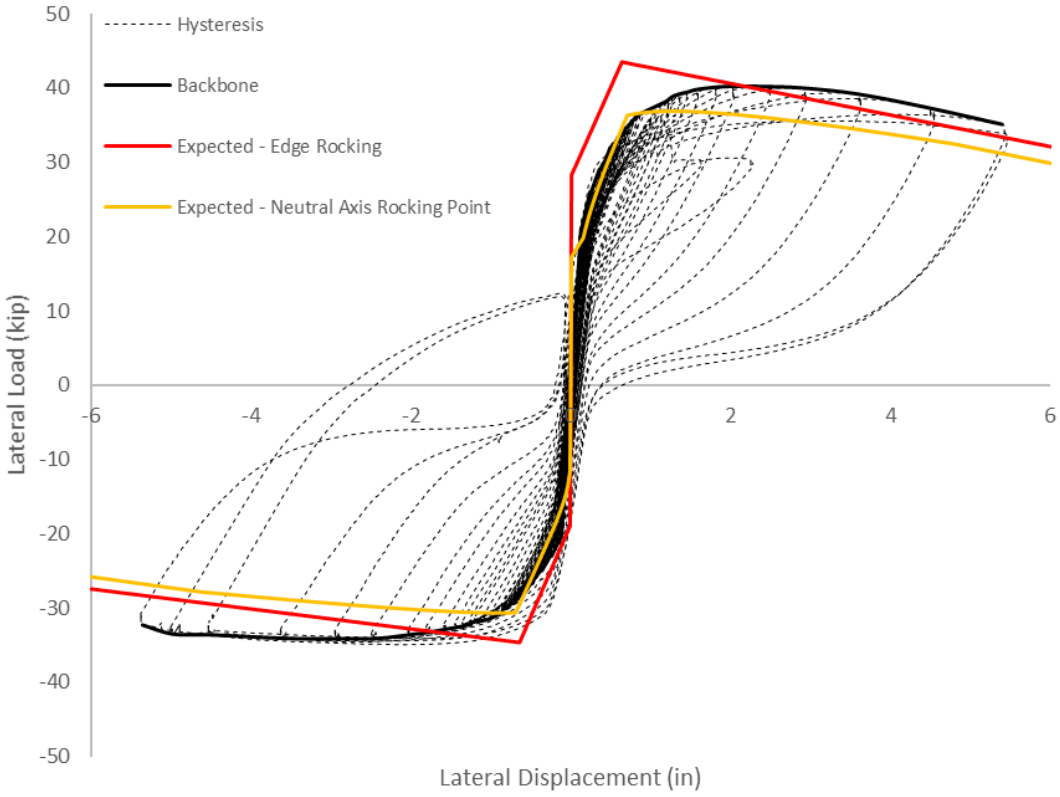

Figure 5.20: Refined design methodology

6.0 DESIGN PARAMETERS AND ANALYTICAL RESPONSE PREDICTION

6.1 INTRODUCTION

This chapter outlines an analytical response prediction method for the current repair method and investigates individual parameters of the analytical equations based on measured data from the experimental testing. Section 6.2 of this chapter discuss the proposed analytical response prediction method. The iterative section analysis procedure was used to develop the analytical response prediction for the repaired columns. The total column lateral displacement was divided into two main components i.e., column top displacement resulting from hold-down rotation and the contribution of flexural deformation along the length of the repaired column. Each of these two components were measured with displacement transducers during the experimental testing and were evaluated for the justification of the initially developed analytical equations. Section 6.3 of this chapter presents the findings of experimentally evaluated data and compares the result with proposed analytical method. Finally, the chapter concludes with proposed modification to the analytical equations, or co-efficient of equations based on the experimental data evaluation and are presented in Section 6.4.

6.2 ANALYTICAL RESPONSE PREDICTION

One of the main objectives of the current research undertaking was to validate the design of the rapid repair methodology through experimental testing. The design principal adopted for the repair method was to minimize the damage in the substructure while restoring the strength and stiffness of the as-built column after an earthquake event. The simplified preliminary design procedure as outlined in Chapter 3 can be used to determine the initial design parameters e.g., collar details, hold-down arrangements, UFP properties etc. However, a more refined method is necessary to predict the load-deformation response of the repaired column more accurately and hence to ensure similar strength and stiffness parameters as compared to the as-built column. An iterative moment-rotation analysis procedure was used to predict the load-deformation response of the repaired column. The procedure was first developed by Pampanin et al. (2001) and was used to design precast concrete frames with ductile fuses. The procedure was modified to meet the current repair arrangement and is outlined step-by-step in the following section.

Step-1: Load-Displacement Response of As-Built Column

The analytical response prediction procedure starts with the analysis of the as-built column to determine the capacity of the column in its as-built condition. A moment-curvature analysis of the column cross section can be used to predict the overall moment-rotation response of the as-built column. The load-displacement behavior can therefore be predicted from the obtained moment-rotation response of the column. However, a more refined non-linear pushover analysis can also be performed to predict the load displacement behavior of the as-built column. The

following analysis procedure predicts the deformation response of the repair arrangement. It is based on the predicted as-built load-deformation response.

Step-2: Total Connection Rotation

The total rotation at the column connection can be approximated from the lateral column top displacement and the height of the column using Equation 6-1.

$$\Theta_T = \frac{\Delta_T}{H_C} \tag{6-1}$$

where:

Δ_T = Column top displacement

H_C = Height of the column

Step-3: Flexural Rotation

The total rotation calculated using Equation 6-1 can be divided into two components i.e., the flexural component resulting from the flexural deformation of the column and the connection rotation at the column-footing interface resulting from gap opening as shown in Figure 6.1. The flexural rotation can then be approximated using Equation 6-2 with the moment at the desired location and considering an appropriate rotational stiffness for the flexural component of the column deformation.

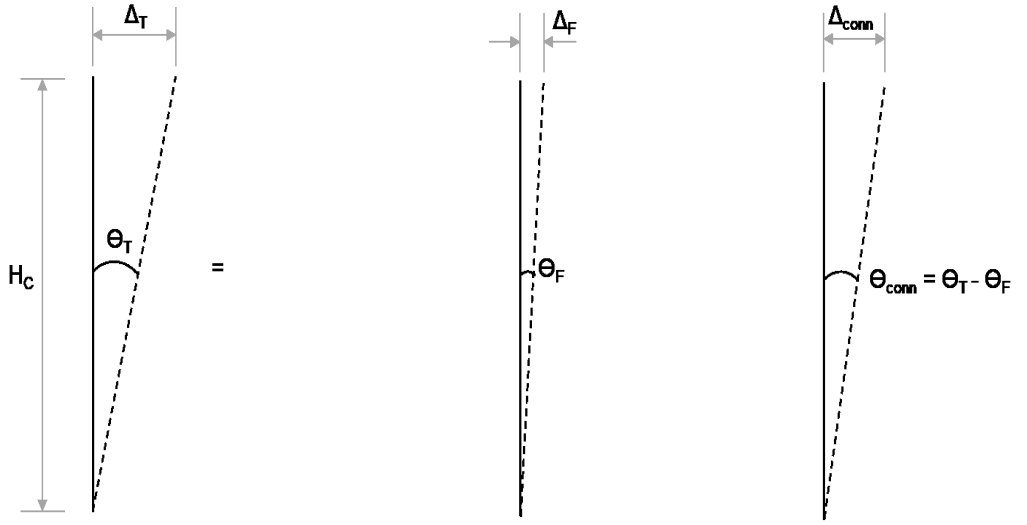

Figure 6.1: Distribution of total rotation into flexural and connection rotation component.

$$\Theta_F = \frac{M_F}{K_C}$$

(6-2)

where:

M_F = Flexural moment resulting from column top displacement = $H_F * K_C$

H_F = Height of the column where flexural deformation is expected = $H_C - H_R$

H_R = Height of rigid portion of the column jacketed with steel shell (collar and the gap height)

K_C = Column rotational stiffness = $3 * E_C * I_C / H_C$ (Considering a pin connection at the base)

Step-4: Connection Rotation

The connection rotation at the column-footing interface can then be calculated using Equation 6-3 below.

$$\Theta_{Conn} = \Theta_T - \Theta_F$$

(6-3)

The imposed connection rotation as calculated from Equation 6-3 can then be used to compute the neutral axis depth following an iterative procedure. Connection moment capacity can finally be achieved using subsequent computations following sectional analysis and section equilibrium concept.

Step-5: Determine Neutral Axis Depth, c (Iterative Procedure)

The determination of neutral axis depth is an iterative process that starts with the assumption of an initial value of neutral axis depth c. The first approximation can be started as one quarter of the cross-sectional depth of the column as shown in Equation 6-4.

$$C = 1/4 * h$$

(6-4)

where:

h = Column cross sectional depth.

Step-5a: Dissipaters Displacement's

The dissipaters' displacement resulting from the imposed connection rotation can be calculated as the function of the deformed geometry of the column and the neutral axis depth and using

Equation 6-5 through Equation 6-7. The deformed geometry of the connection under imposed rotation is shown in Figure 6.2 and the nomenclature used in following equations.

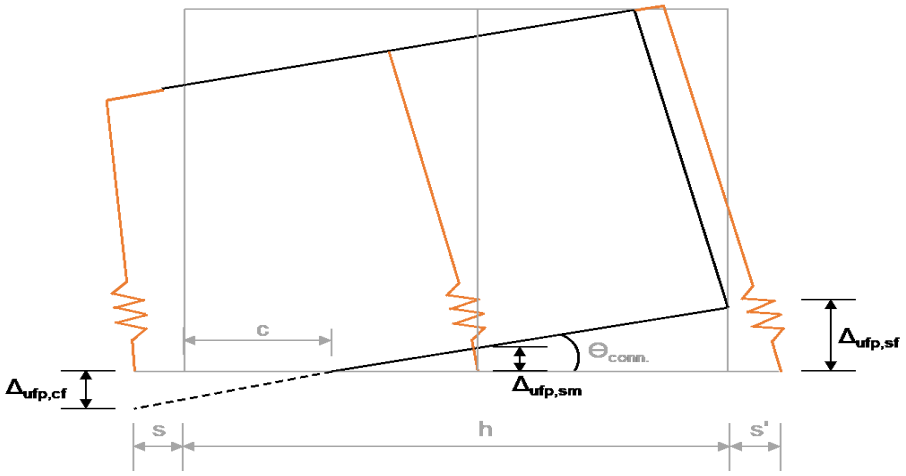

Figure 6.2: Deformed geometry of the column and the hold-downs

Displacement of the tension dissipaters at the column face under tension,

$$\Delta_{ufp,sf} = \Theta_{Conn}*(h+s'-c) \quad \textbf{(6-5)}$$

Displacement of the tension dissipaters at the middle of the column section,

$$\Delta_{ufp,sm} = \Theta_{Conn}*(h/2-c) \quad \textbf{(6-6)}$$

Displacement of the compression dissipaters at the extreme face of the column under compression,

$$\Delta_{ufp,cf} = \Theta_{Conn}*(s+c) \quad \textbf{(6-7)}$$

Step-5b: Dissipaters Force's

Figure 6.3 presents the section equilibrium and the forces in each component at the connection. Forces in each of the dissipaters can be computed using the force displacement behavior of individual UFPs. The force-displacement behavior of the UFPs can be modeled using the Ramberg-Osgood steel model following Baird et al. (2014) and as outlined in Equation 6-8.

$$\Delta_{ufp} = \frac{F}{K_o}\left[1 + \left\{\frac{F}{F_y}^{(r-1)}\right\}\right] \quad \textbf{(6-8)}$$

where:

F_y = Effective yield displacement of the UFP dissipaters

K_o = Initial stiffness

r = Ramberg-Osgood factor

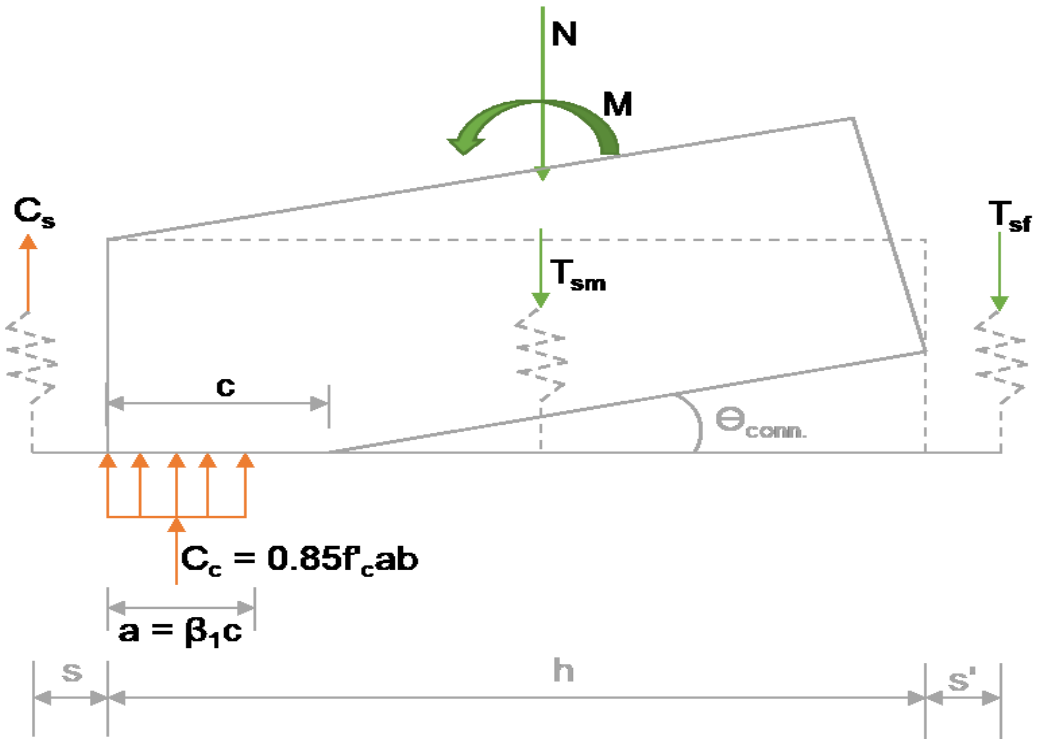

Figure 6.3: Section equilibrium at column-footing interface.

Step-5c: Section Equilibrium

Once the dissipaters' forces are known, the concrete compression resultant (C_C) can be calculated using the strain compatibility at the section and applying the principal of monolithic beam analogy theorem for a rocking element. According to the monolithic beam analogy, the displacement of the rocking element at the column-footing interface can be assumed to be the same as the monolithic beam element. Finally, the concrete compressive force can be computed using Equation 6-9.

$$C_C = N + T_{sf} + (2*T_{sm}) - C_s \quad \textbf{(6-9)}$$

where:

N = Axial load acting on the column

Step-5d: Determination of Neutral Axis Depth, c

A new value of neutral axis depth can finally be determined using the Whitney's stress block assumption for concrete compressive resultant using Equation 6-10.

$$\mathbf{c} = \frac{C_C}{0.85 f_c^{'} \beta_1 b} \tag{6-10}$$

where:

$a = \beta_1 c$ where β_1 is the ratio of depth of rectangular stress block to the depth of the neutral axis and

$f_c^{'}$ is the concrete compressive strength for the existing bridge column.

If the initially assumed value of c is equal to the newly obtained neutral axis depth, then the c value can be used for further calculation. Otherwise, iteration with a new value must be adopted and the steps 5a through 5d should be followed for convergence.

Step-6: Connection Moment Capacity

The connection moment capacity can finally be calculated using the neutral axis depth c. Summing moment at a/2 distance for the section –

$$\mathbf{M_{Conn} = [C_s*(s+a/2)] + [N*(h-a)/2] + 2*[T_{sm}*(h-a)/2] + [T_{sf}*(h+s'-a/2)]} \tag{6-11}$$

Finally, the lateral force can be calculated using Equation 6-12.

$$\mathbf{F = M_{Conn}/H_C} \tag{6-12}$$

The iterative procedure can be implemented repeatedly to achieve the final load-deformation response of the repaired column.

Subsequent sections discuss the efficacy of the outlined analytical response prediction method based on the evaluation of experimentally obtained data and modifications to the equations will be proposed to capture the displacement components more accurately.

6.3 MEASURED DISPLACEMENT COMPONENTS

Displacement data measured with the LVDT's were used to investigate the contribution of column flexural deformation and the hold down rotation into the total column top displacement. Flexural deformation of the column above the shell was determined from average column rotation measured with a series of LVDT's mounted on curvature rods for different segments

along the height of the column. The measured data was compared with the analytically predicted flexural moment-rotation hysteresis for the hold-down arrangement. The hold-down displacement was also measured with displacement transducers. The data measured was then used to determine the column rotation resulting from the hold-down displacement.

6.3.1 Load-deformation response

The load-deformation response of the repaired column for the push and pull cycles of loading is plotted in Figure 6.4 and Figure 6.5, respectively. The column top displacement measured with an independent string potentiometer is plotted against the lateral load measured with the built-in load cell of the lateral actuator. The column displacement presented here was corrected for any contribution of foundation uplift and the lateral load was corrected for the component of the axial load resulting from secondary P-Δ effect.

A spring analogy, as stated earlier in Section 6.2, was used to determine the component of column top displacement resulting from hold-down rotation and the flexural deformation of the column section beyond the elastic shell height. Hold-down rotation was calculated based on the measured data of the north and south hold-down displacement and using the stated Equation 6-13. Flexural deformation of the column above the shell was determined from average column rotation measured with the series of LVDT's mounted on curvature rods for different segments along the height of the column. Finally, the cumulative displacement resulting from column flexural deformation and the hold-down rotation were calculated through algebraic summation of these two components.

$$\boldsymbol{HD_{Rotation} = \frac{S_{HD} - N_{HD}}{D_{HD}}} \qquad \textbf{(6-13)}$$

Figure 6.4 presents the backbone envelope displacement for all the four tested specimens in the push cycle of loading along with the measured displacement components for the tests. Results showed a good agreement between the column top displacement measured with an independent string potentiometer and the cumulative displacement calculated from the individual displacement components calculated from measured LVDT readings. The flexural deformation component for the column showed a linear increase in displacement with the increase in lateral load. A constant slope representing the rotational stiffness of the flexural spring can be used to predict the flexural deformation response of the column. Further investigation into the flexural deformation response of the column is discussed in section. It can also be observed that the column top displacement resulting from the rotation of the hold-down is significantly higher than the flexural deformation. This can be attributed to the accumulation of plastic deformation in the UFPs and hence accounting for majority of the column top displacement resulting from hold-down rotation. In addition, the linear flexural deformation component showed that the remainder of the column section behaves essentially elastically.

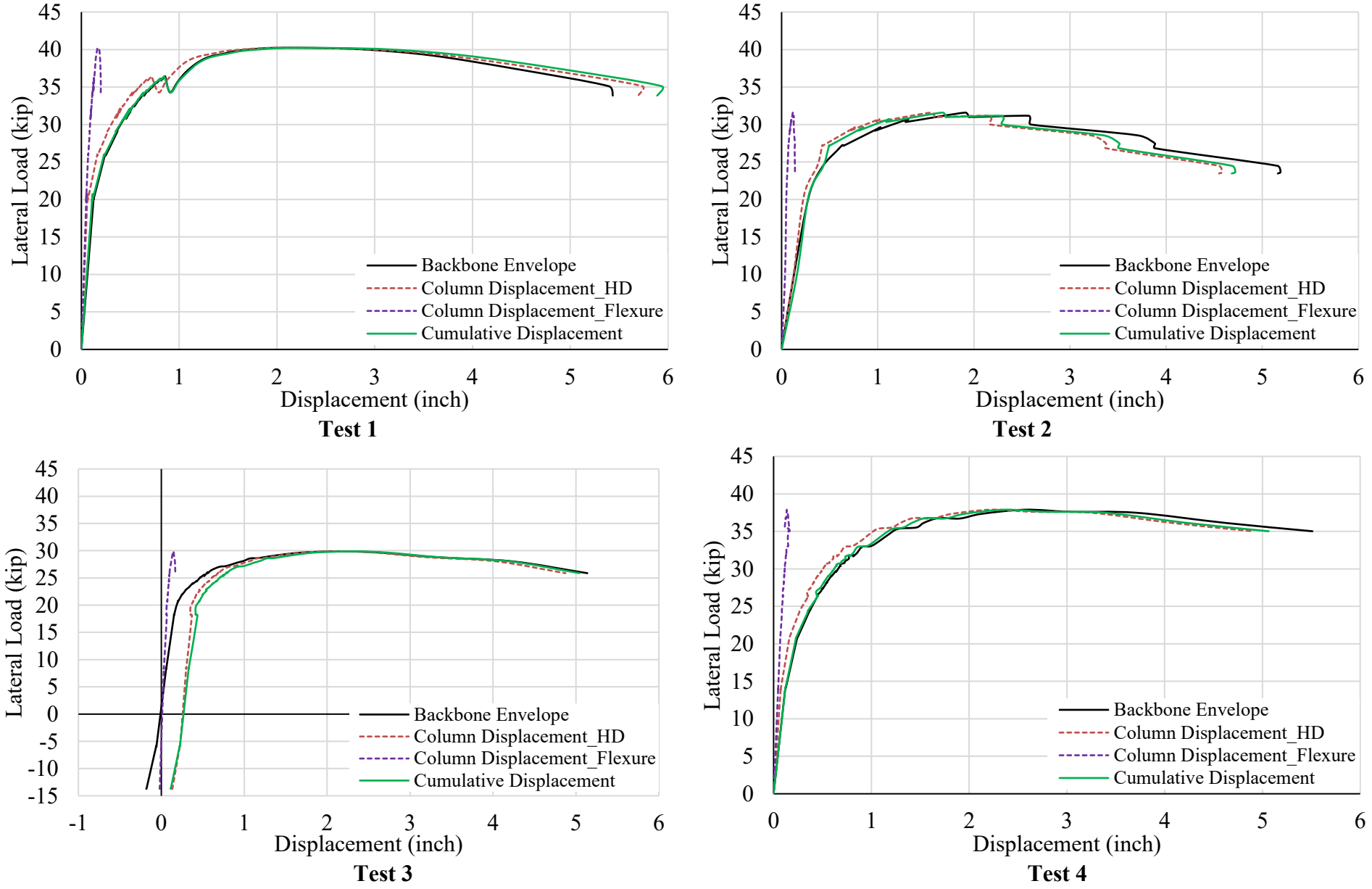

Figure 6.4: Contribution of flexural deformation and hold-down rotation into column top displacement for push cycle.

Figure 6.5 presents the backbone envelope displacement for tested specimens in the pull cycle of loading along with the measured displacement components. Similar trend in pull cycles of loading were also observed where the cumulative displacement calculated from the independent displacement component reasonably capture the total column top displacement measured independently. In addition, most of the displacement for the pull cycle of loading is resulting from the hold-down rotation. The column top displacement resulting from flexural deformation of the column was again found to be accounting for only a minor portion of the total column top displacement and increases linearly with the increase of lateral load. Hence, the efficacy of the repair method to limit damage in the column region can be experimentally verified for both the push and pull cycles of loading.

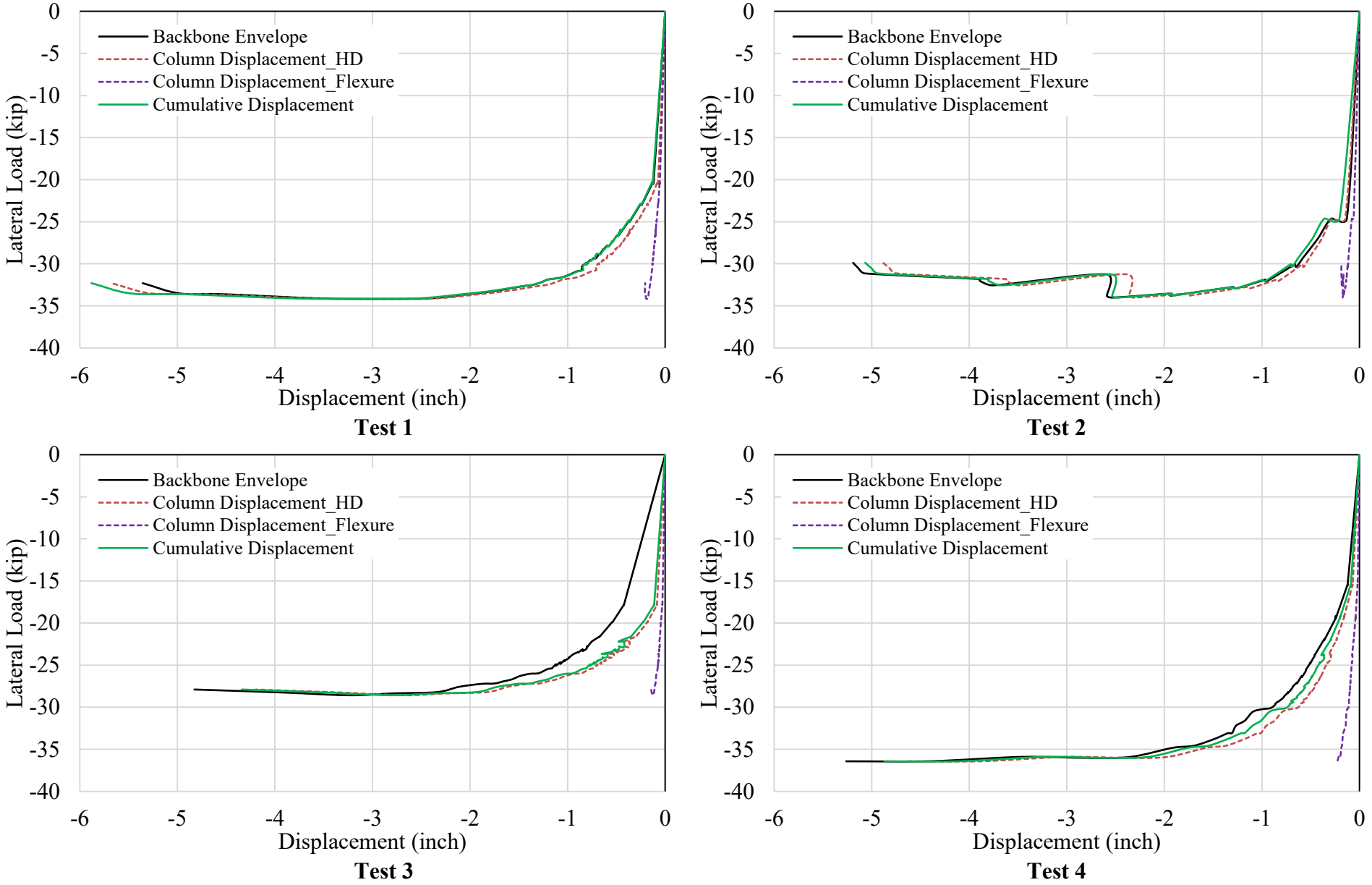

Figure 6.5: Contribution of flexural deformation and hold-down rotation into column top displacement for pull cycle.

Further investigation into the push and pull cycles of loading for test 4 was conducted to compare the effect of axial load variation on the displacement components. It was found that the column top displacement resulting from hold-down rotation for both the push and pull cycles of loading accounts for 88% of the total displacement at the maximum ductility cycle. Whereas the column top displacement resulting from the flexural deformation accounts for 3% in the push cycle and 4.5% in the pull cycle at the maximum ductility loading cycle. While the maximum ductility loading cycle accounts for the maximum variation in axial loading for push and pull cycles, the effect on displacement components is negligible. Similar results were obtained for the rest of the tested specimens where the effect of axial load variation has no significant impact on the efficacy of the repair method to limit damage in the column. Figure 6.6 and Figure 6.7 show the distribution of column top displacement resulting from different displacement components i.e., flexure and hold-down rotation as a percentage of the total column top displacement for individual loading cycles in the push and pull direction, respectively. In addition, the difference between the column top displacement measured independently and the calculated column top displacement resulting from individually measured components are shown in red color. Ideally, the difference should be zero if the column top displacement is resulting only from the contribution of the hold-down displacement and flexural deformation. However, shear deformation and any slip due to the lateral loading was not measured and was not accounted in the calculated cumulative top displacement. Hence, the difference in each loading cycle accounts for other sources of column displacement that was not directly measured during the experimentation. However, the difference was significantly lower for all the test specimens except test 3.

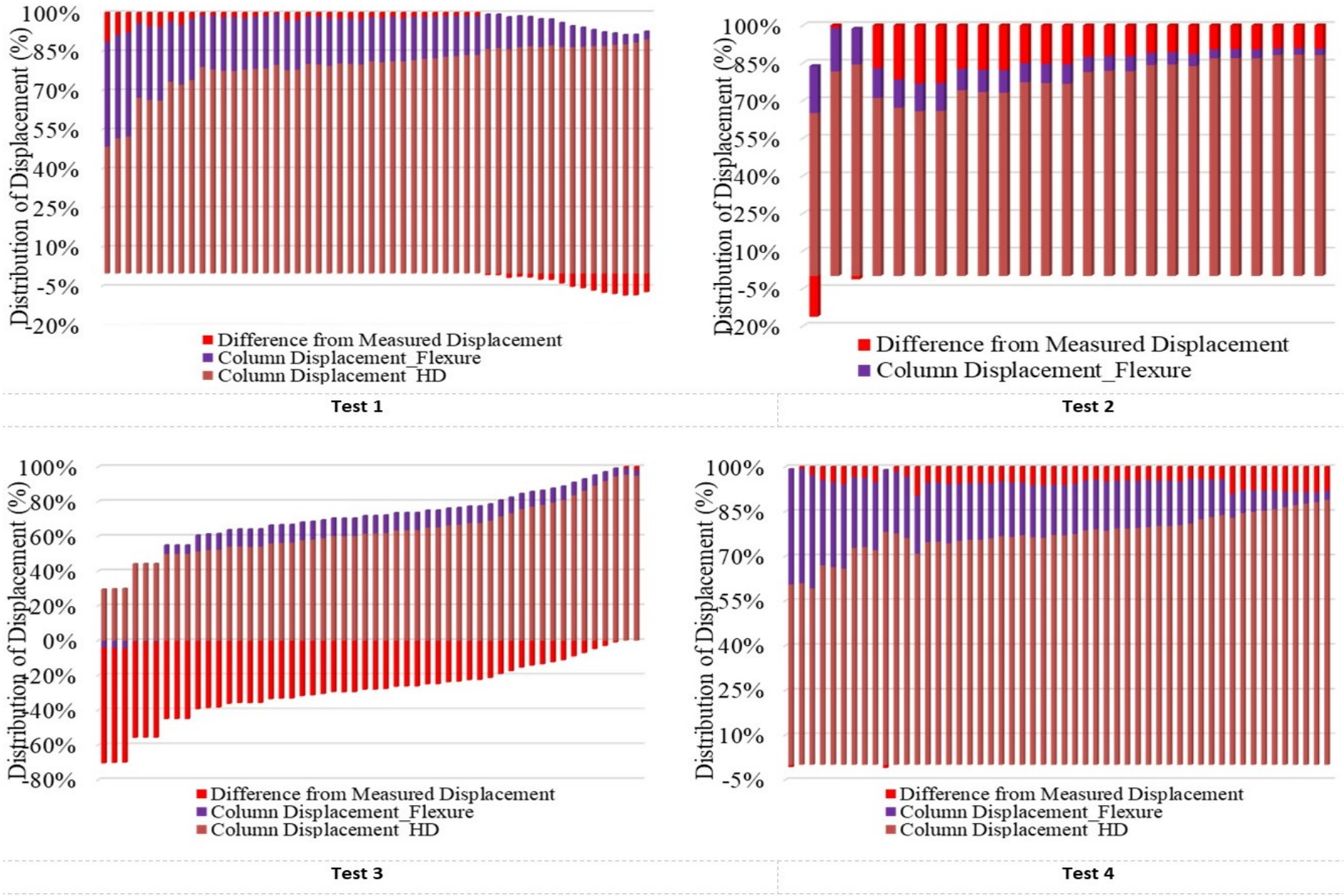

Figure 6.6: Distribution of displacement components for push cycles of loading

The majority of the column displacement resulted from the hold-down rotation. However, the impact of hold-down rotation was more pronounced in the higher ductility cycles where more than 85% of the total column top displacement was due to the hold-down rotation. This can be attributed to the yielding of UFPs in the hold-down and the accumulation of plastic deformation within the fuse elements. The column top displacement resulting from the flexural deformation accounts for almost 1/3 of the total displacement for the initial loading cycles and gradually decreases during the final loading cycles at higher displacement ductility. It can also be observed that the pull cycles of loading experienced less flexural deformation than the push cycles of loading. It is noted that the pull cycles of loading were associated with lower axial load compared to the push cycles of loading.

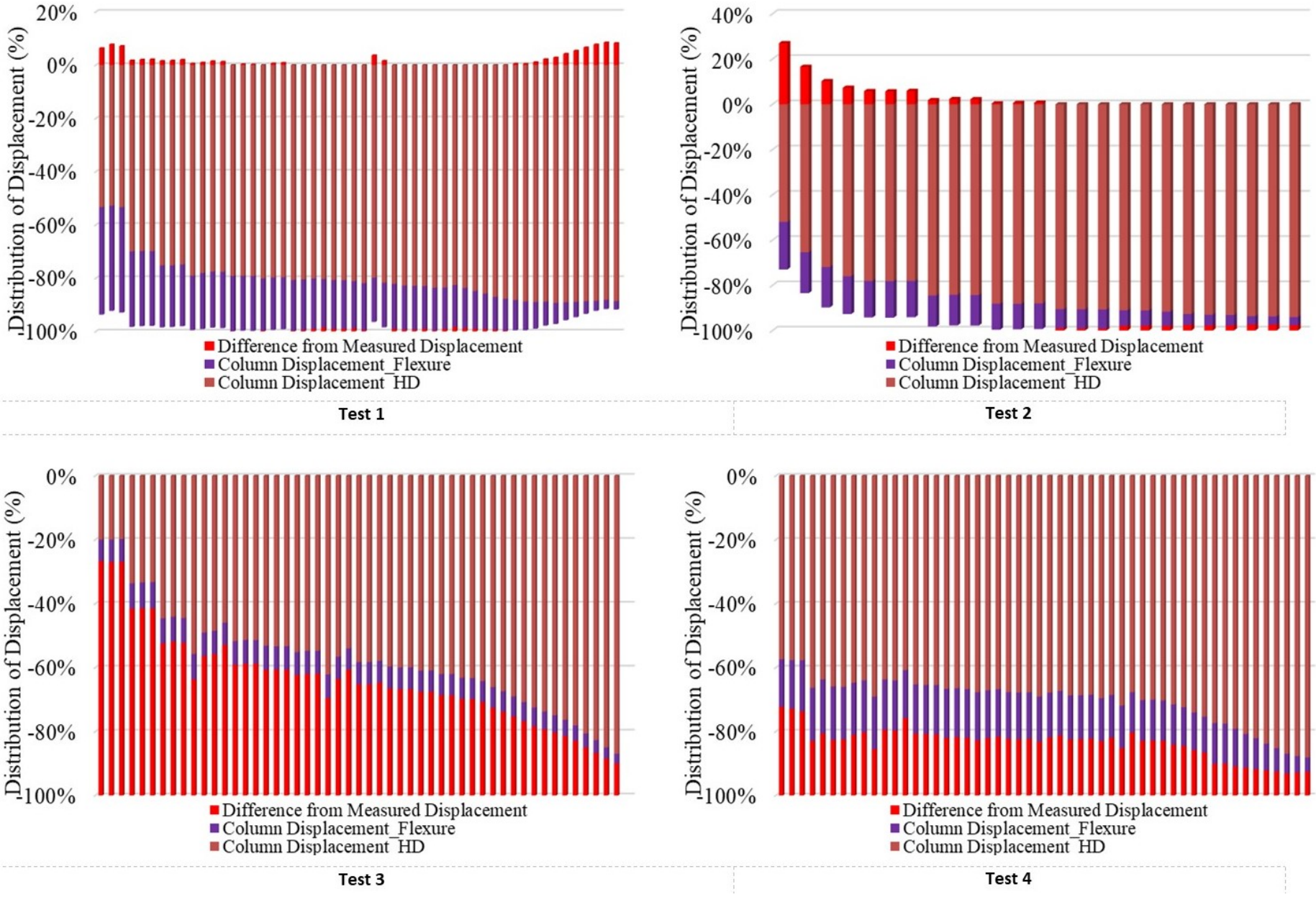

Figure 6.7: Distribution of displacement components for pull cycles of loading.

6.3.2 Hold-Down Displacement

Experimentally measured and the analytically predicted hold-down displacement is plotted against the lateral load and is presented in Figure 6.9 for the push cycles of loading and Figure 6.10 for the pull cycles of loading. An analogous spring model was used to predict the hold-down displacement response for the tested specimen.

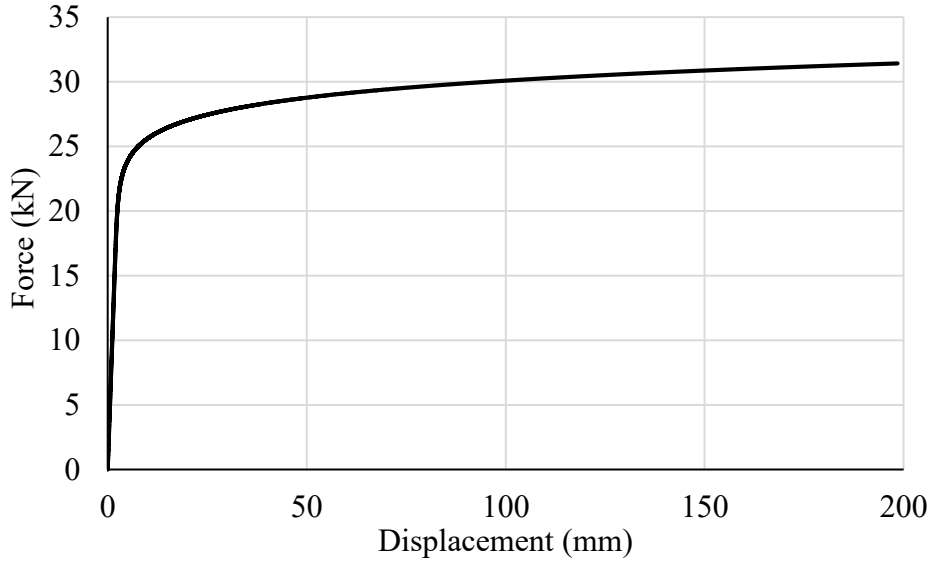

Figure 6.8: UFP hysteresis response adopted from Baird et al. (2014)

Measured hold-down response agrees well with the analytical prediction and shows that the analogous spring model can be efficiently used to predict the overall response of the hold-down displacement. However, it should be noted that the analytically predicted response is dictated by the adopted UFP hysteretic response and hence an accurate model of the UFP response would yield a closer prediction of the overall response. It can also be noted that the analytical prediction does not account for degradation in the higher ductility cycles due to the adopted hysteretic response of the UFPs as shown in Figure 6.8. The UFP hysteretic response was adopted after the recommendation of Baird et al. (2014). It is important to note that the UFPs used for the current experimental program are different in terms of how they were bent to U-shapes. The process of bending the steel plates can cause a difference in the response of the UFPs. Hence, the degradation could be a result of different load-deformation behavior of the UFPs. Furthermore, several other potential sources of degradation such as slip in the system at larger displacement cycles, strain penetration in the anchor rods, softening of steel at the reduced section of the hold-down leg (angle sections), deterioration of the concrete due to toe crushing, etc. can contribute to the degradation. Nevertheless, it should be stressed that the result shows a significant reduction in strength degradation for the repaired system as compared to the as-built column. The system reached significant ductility level without significant loss of strength and hence the small degradation in the overall system behavior can be disregarded.

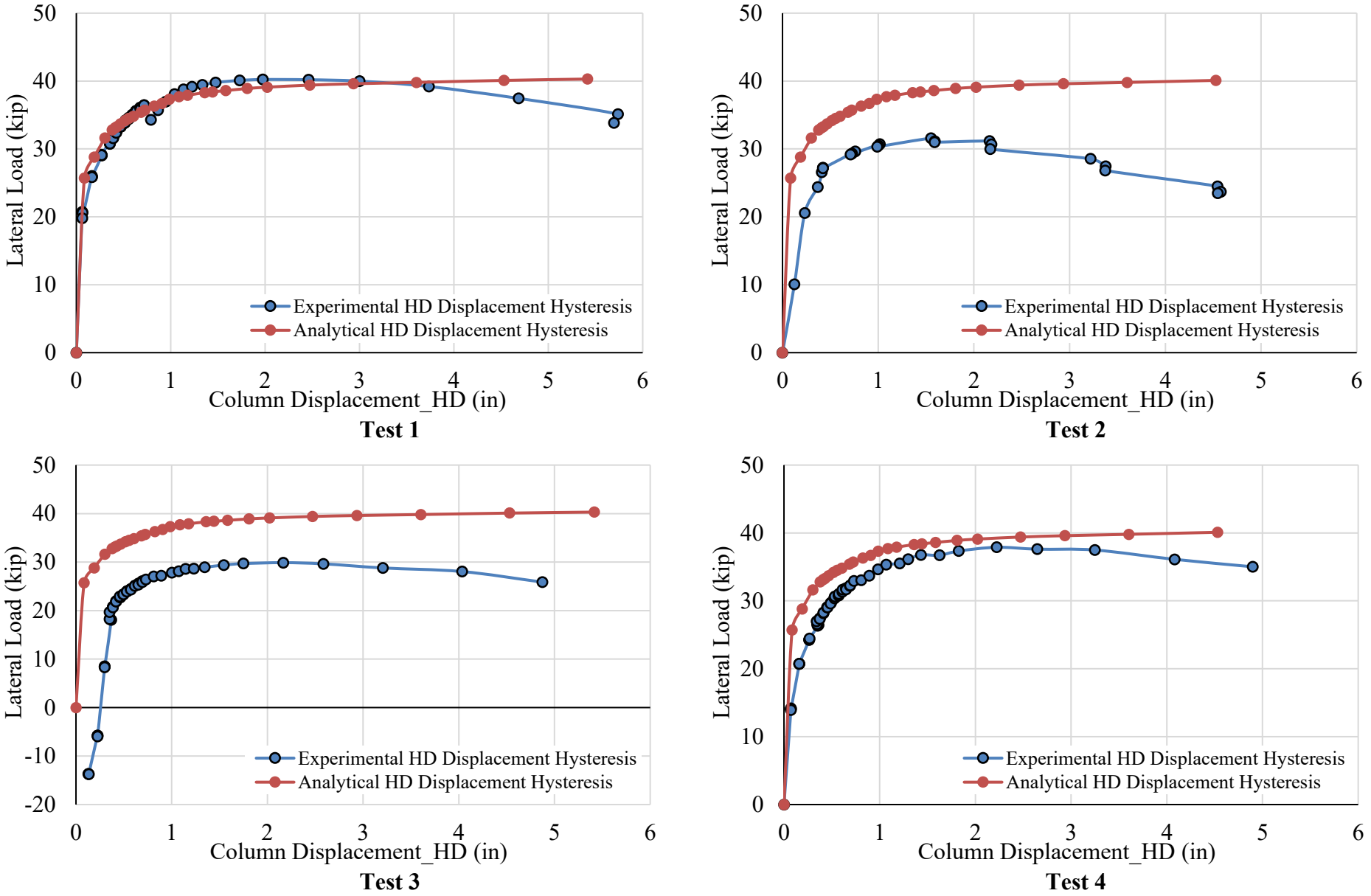

Figure 6.9: Envelope of hysteretic response of the hold-downs for push cycles of loading

The initial stiffness for the pull cycles of loading were well aligned with the analytically predicted initial stiffness. The analytical prediction closely captures the lateral load versus the column top displacement resulting from hold-down rotation for test 1 and test 2. For, test 3 the analytical equation overestimates the lateral versus hold-down component of column displacement whereas it underestimates the behavior for test 4. It is noted that both the specimens were tested under same loading protocol but with different UFP geometries. However, it should also be noted that the behavior presented here is an effective means of looking at the efficacy of the analytical response prediction, but the load presented in the vertical axes does not represent the hold-down forces. Rather, it represents the lateral load resisted by the column. Hence, a more refined analysis into the hysteretic response of the hold-down forces versus hold-down displacements would help investigate the efficacy of the adopted UFP model and any modification to the individual model parameter. For this report, the task was considered out of the scope and the adopted UFP model proposed by Baird et al. (2014) was considered to be accurate enough for the overall analytical response prediction.

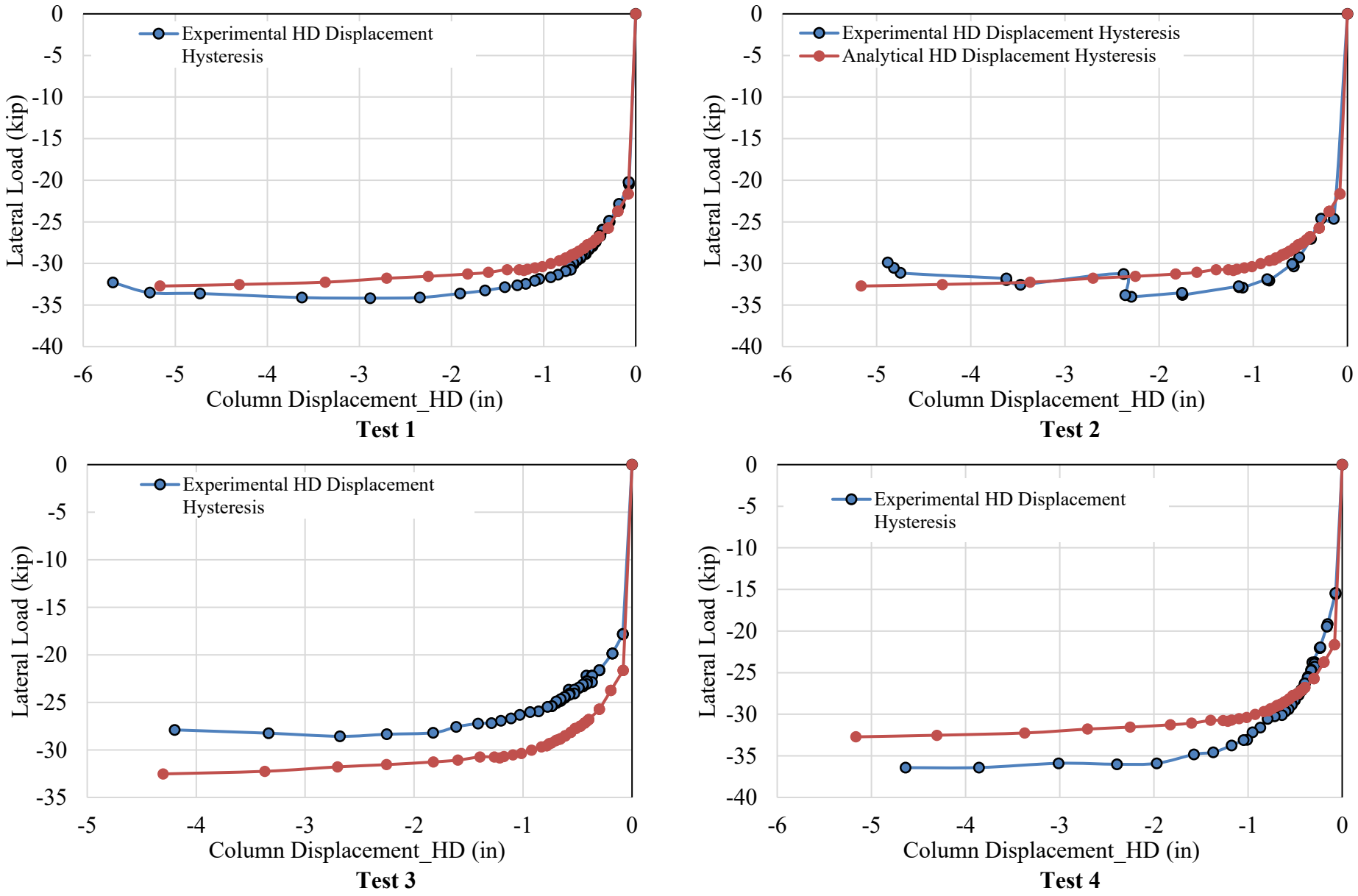

Figure 6.10: Envelope of hysteretic response of the hold-downs for pull cycles of loading

6.3.3 Column Flexural Displacement

The flexural deformation component of the total column top displacement was further investigated to determine the rotational spring constant of the assumed spring model. Figure 6.11 and Figure 6.12 shows the measured flexural displacement response plotted against the lateral load for push and pull loading cycles, respectively. The cluster of data in the higher displacement cycles indicates the decrease in flexural deformation of column and indicate the accumulation of plastic displacement in the replaceable U-shaped flexural plates (UFPs).

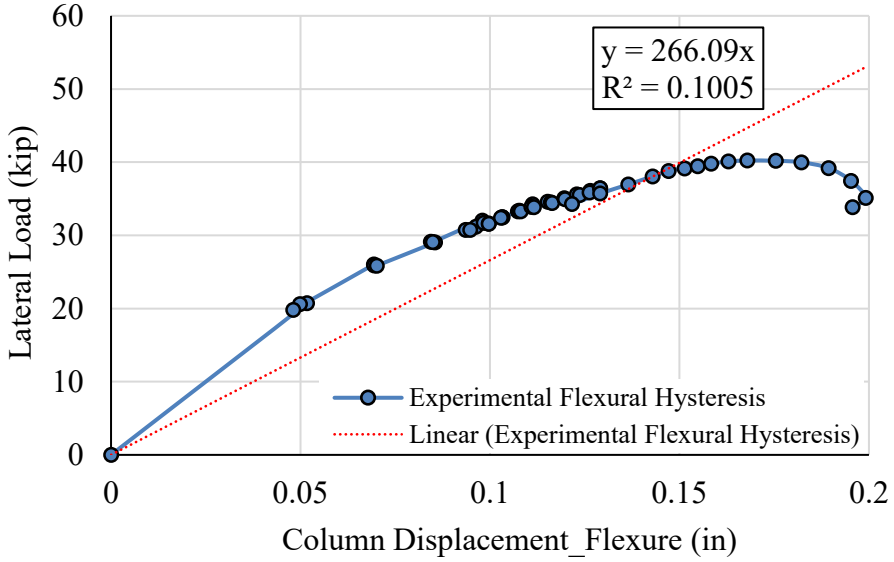

Test 1

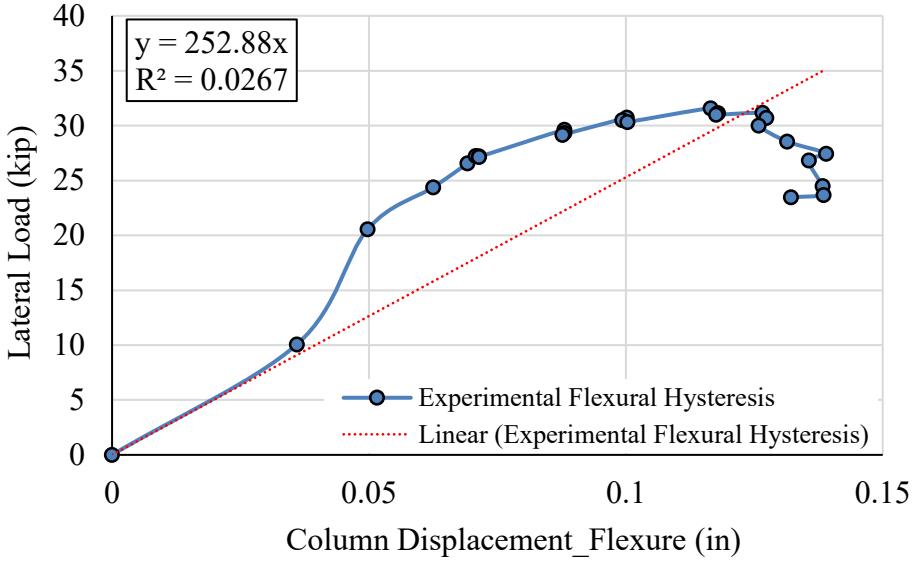

Test 2

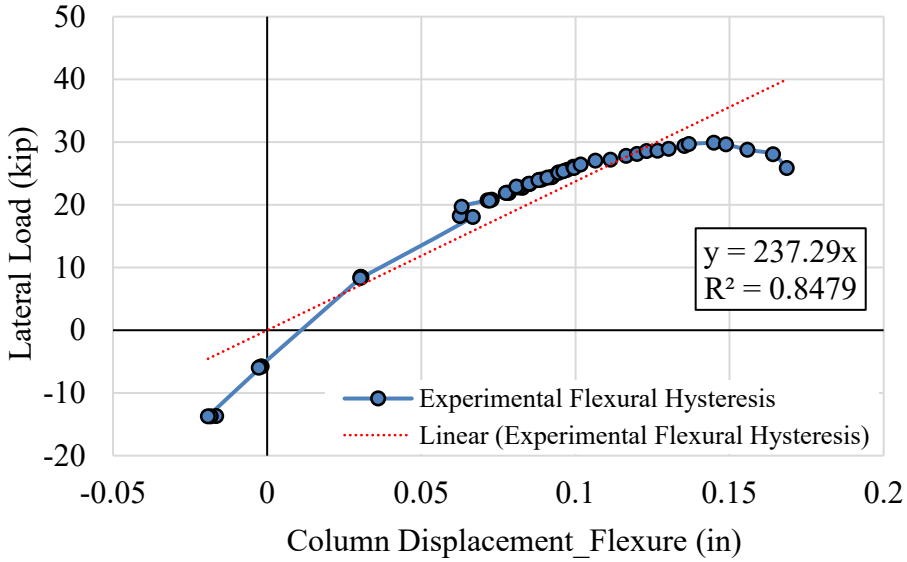

Test 3

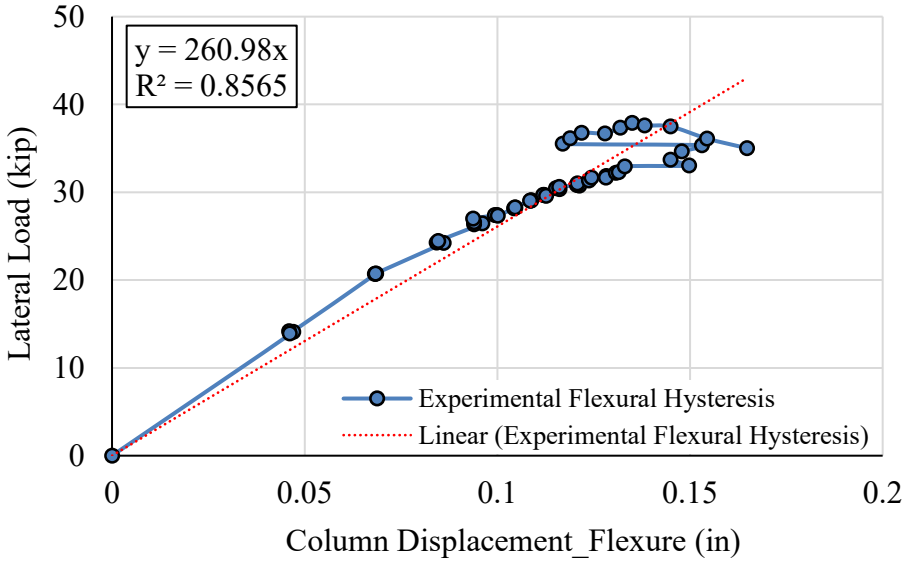

Test 4

Figure 6.11: Envelope of hysteretic response of flexural displacement for push cycles of loading

The lateral load versus column top displacement resulting from flexural deformation for the pull cycles of loading shows similar trend and can be approximated with a linear equation. However, the slope of the linear regression line for the pull cycles of loading was lower than the push cycles of loading and can be attributed to the lower axial load associated with the pull cycles of loading.

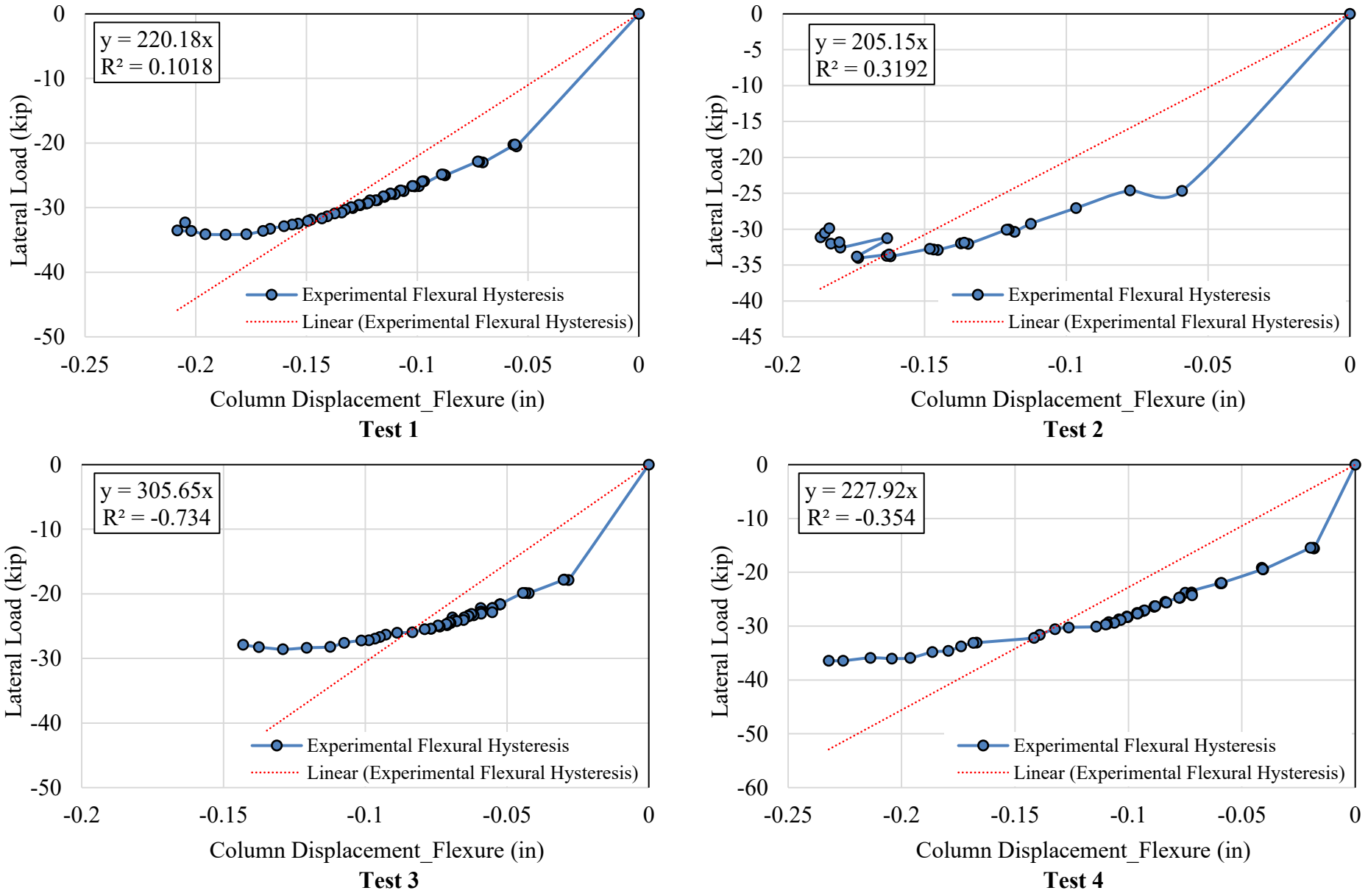

Figure 6.12: Envelope of hysteretic response of flexural displacement for pull cycles of loading.

A linear regression analysis shows that the flexural displacement of the column can be closely predicted with the linear line having a constant stiffness coefficient. The analytical equation to predict the column top displacement resulting from the flexural deformation of the column can be approximated using the linear equation presented with Equation 6-14 below.

$$F = K_r \Delta \quad \textbf{(6-14)}$$

where:

K_r = Stiffness for flexural dispalcement component (slope of the linear line in Figure 6.11 and Figure 6.12)

The stiffness coefficient, K_r for flexural displacement prediction for both the push and pull cycle of loading can be taken as the slope of the linear regression line and are presented in the Table 6.1.

Table 6.1: Flexural Stiffness Coefficient.

Specimen	Flexural Stiffness, K_r (kip/in)	
	Push Cycle	Pull Cycle
Test 1	266	220
Test 2	253	205
Test 3	237	305
Test 4	261	228
Mean	254	240
Average for Push and Pull	**247**	

The average stiffness coefficient approximated from the experimental data for the push cycle is 254 kip/in while the average coefficient for pull cycle is 240 kip/in. However, the average stiffness coefficient for both the push and pull cycles was found to be 247 kip/in.

6.3.4 Column Moment-Rotation

The moment-rotation response for the 37" to 40" segemnt (immediately on top of the shell height) is presnted in Figure 6.13 for the push cycles of loading. Experimentally measured response was compared with the analytically predicted behavior. The linear regression analysis used in the previous section was adequate to capture the overall flexural load-deformation response of the column. However, the computation of individual points in the moment-rotation plot using a single rotational stiffness coefficient leads to overestimation of the bending moment at higher displacement ductility cycles. By definition, the slope of the analytically predicted response is the rotational stiffness of the adopted analogous spring model (Section 6.2). Figure 6.13 shows that a linear equation with a single stiffness coefficient e.g. (3EI/H) is somewhat insufficient to predict the accurate moment-rotation resposne of the column section. Hence, a second order ploynominal equation was more adequate to capture the moment-rotation response. Figure 6.13 shows both the linear regression line and the ploynomial regression line for all the tests specimen in the push cycle.

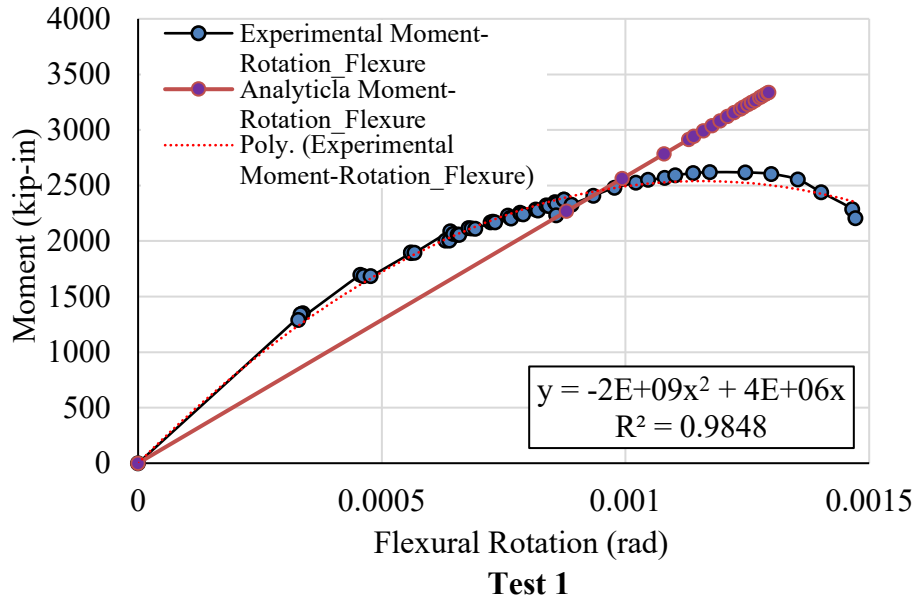

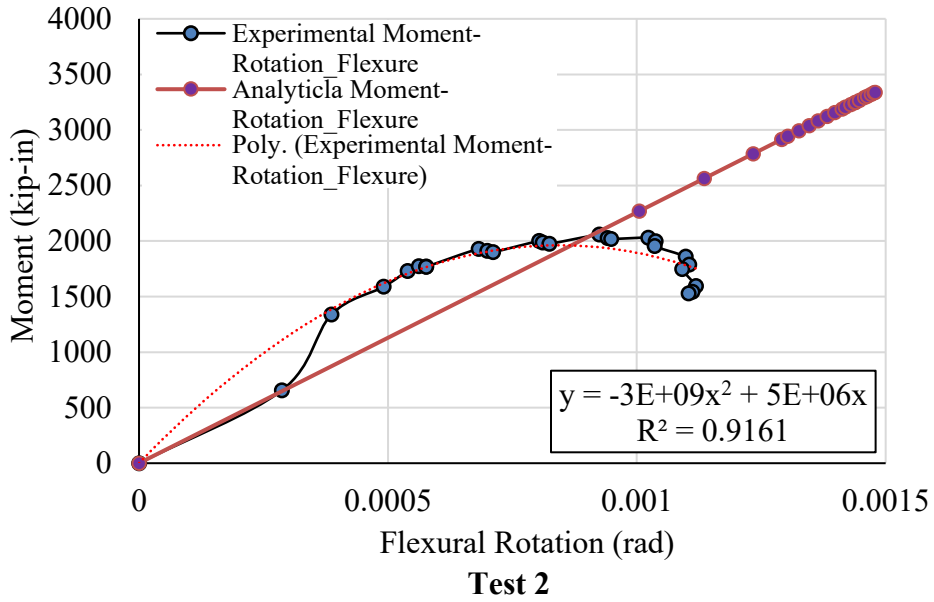

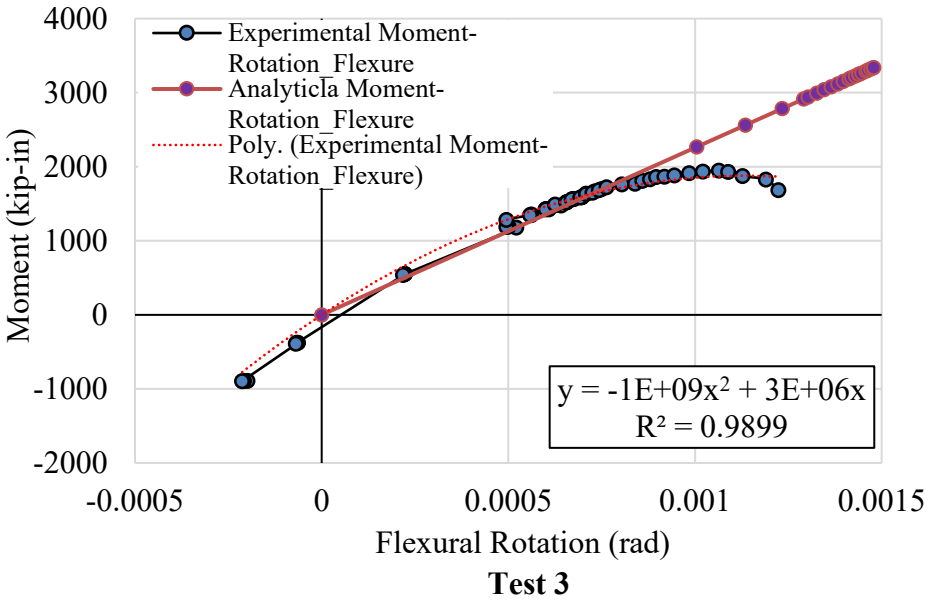

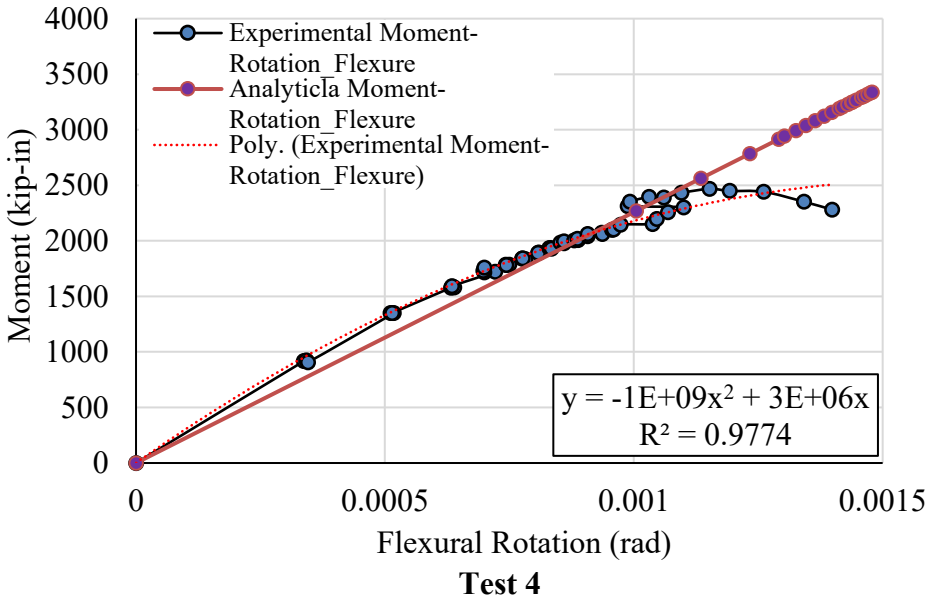

Figure 6.13: Flexural moment-rotation response for 37" to 40" segment for push cycles.

Figure 6.14 presents the moment-rotation response for the 37" to 40" segemnt in the pull cycles of loading. A similar trend for the pull cycle of loaidng was also found where the analytical equation represneting a signle rotational stiffness coefficient is somewhat inadequate to accurately capture the moment-rotation response. However, it should be noted that the accuracy of the linear regression line in predicting the moment-rotation response during the initial cycles is more accurate for pull cycles of loading than the push cycles. The push cycles of loading completely overestimates the initial loading cycles.

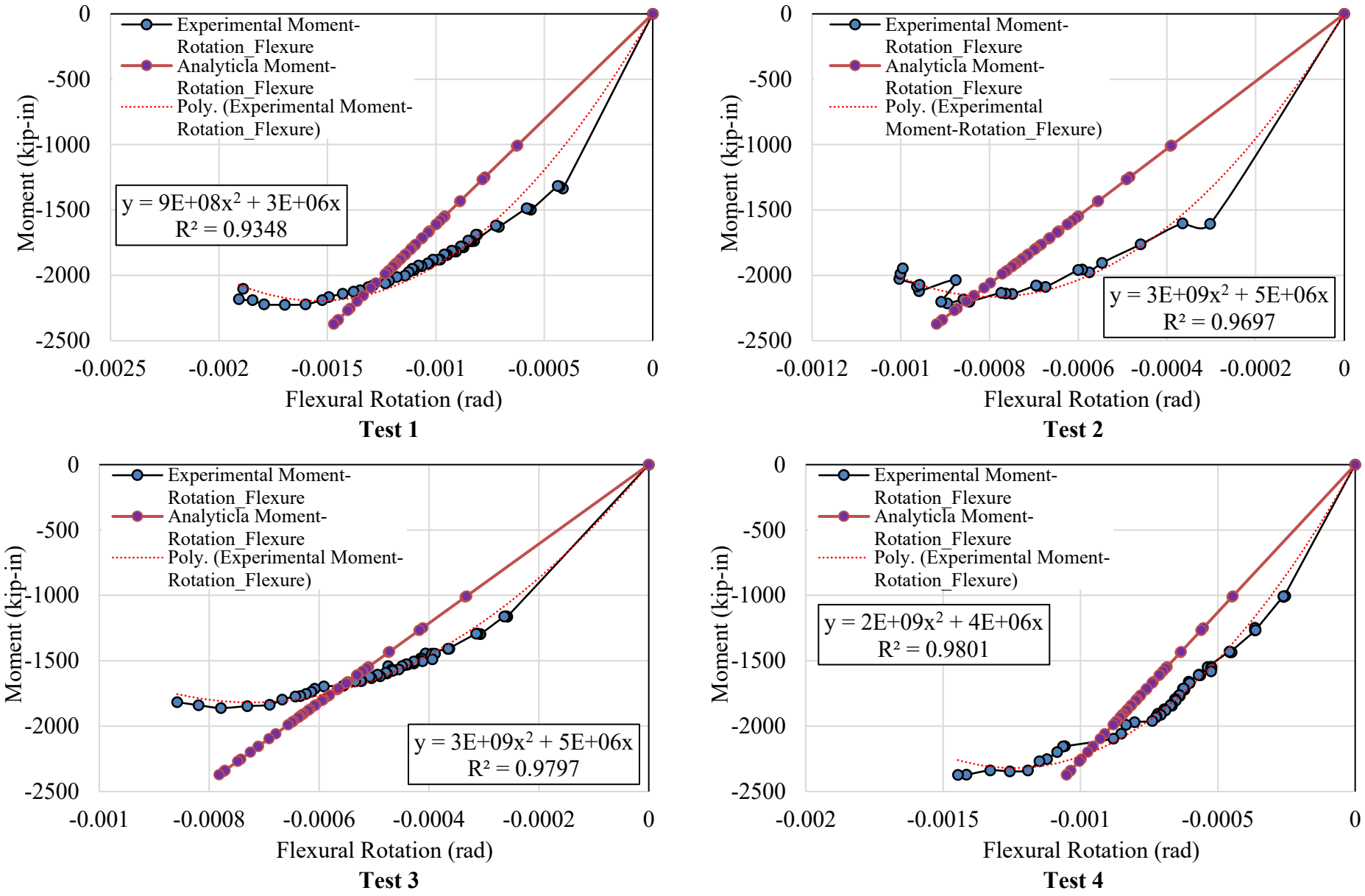

Figure 6.14: Flexural moment-rotation response for 37" to 40" segment for pull cycles.

The experimental spring constant was derived from the measured response and is used to validated the initially assumed spring constant for the analogus spring model in the analytical response prediction. Although it was found that a second order polynomial equation could accurately predict the moment-rotation response of the column section, using such an equation would compromise the objective of developing a simple set of equations for response prediction. Hence, an alternative method of predicting the moment-rotation response with a linear equation having a single initial rotational stiffness coefficient was considered along with a stiffness degradation model. The experimentally obtained data were used to plot the degradation of the secant stiffness and plotted for the push and pull cycles of loading in Figure 6.15 and Figure 6.16, respectively.

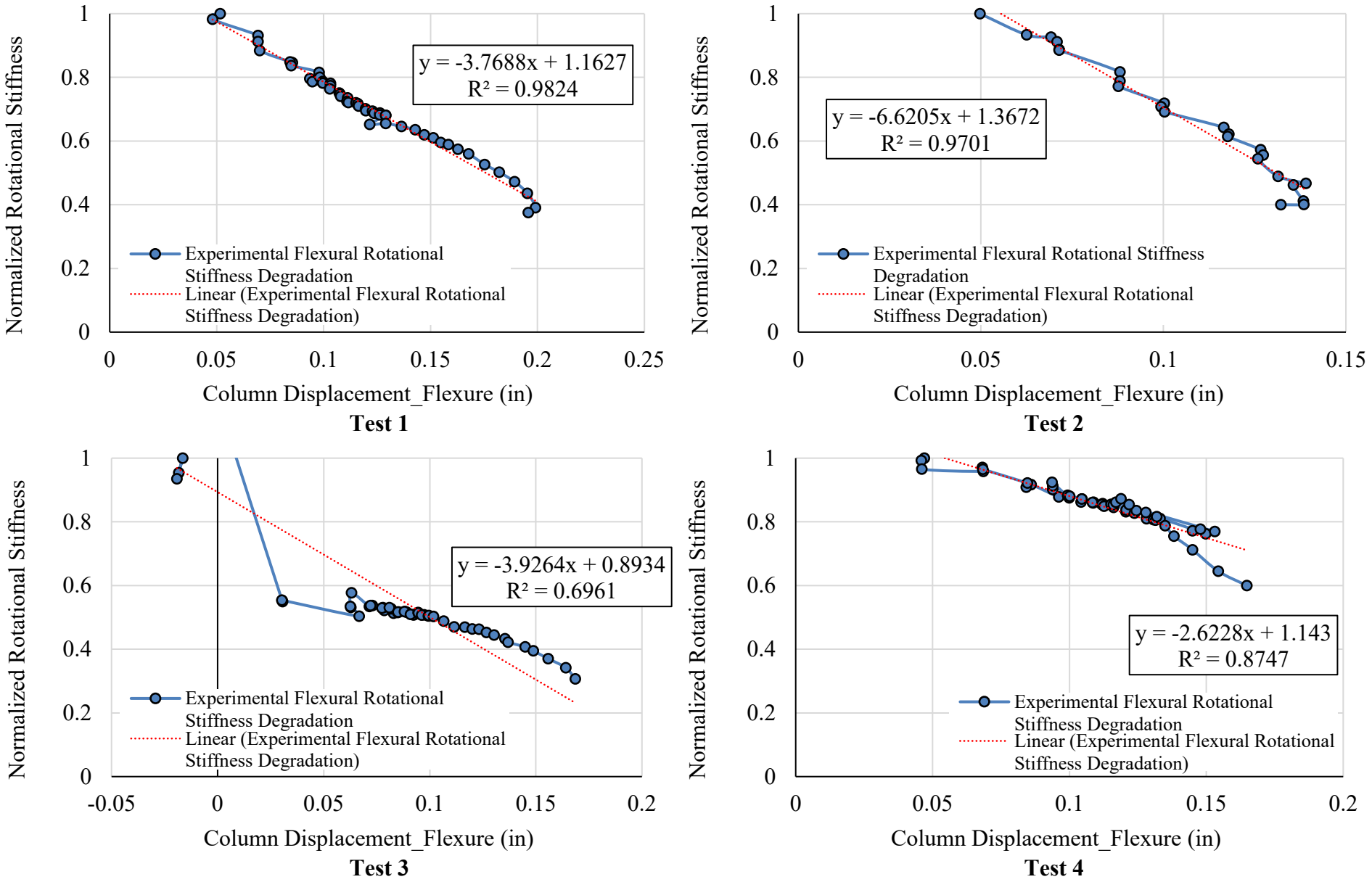

Figure 6.15: Degradation of rotational flexural stiffness for 37" to 40" segment for push cycles.

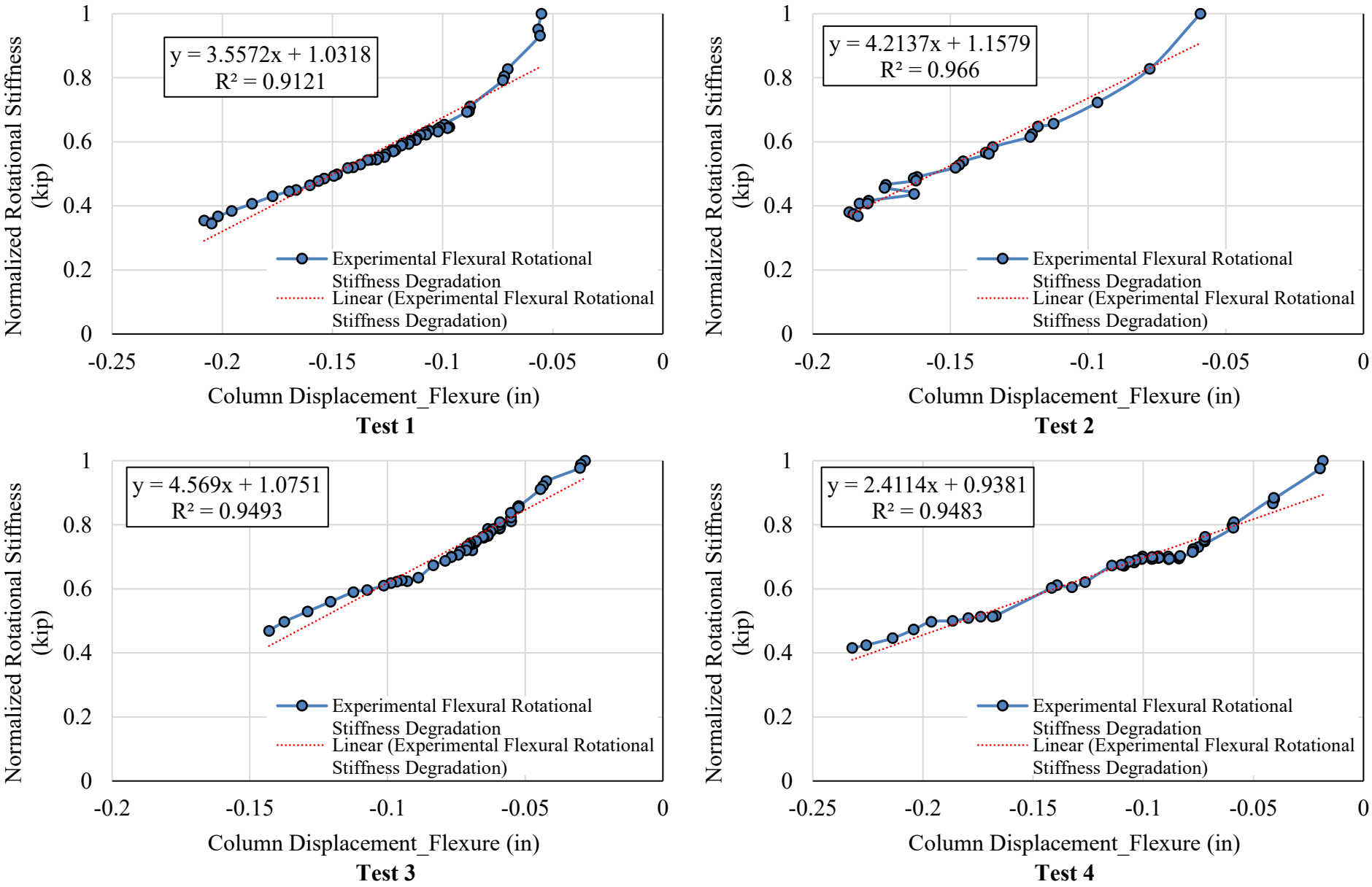

Figure 6.16: Degradation of rotational flexural stiffness for 37" to 40" segment for push cycles.

A linear regression line can be used to predict the rotational stiffness degradation of the column accurately. A linear equation presented here as Equation 6-15 can be used along with the initial rotational stiffness value.

$$K_{sec}/K_y = m\Theta + c \qquad \textbf{(6-15)}$$

where:

m is the slope of the regression line and

c is the constant.

The values of the slope and the constant for push and pull cycles for all the four specimens are listed in Table 6.2 along with the average values.

Table 6.2: Coefficient of the Linear Regression Line for Predicting Stiffness Degradation.

Specimen	Slope, m		Constant, c	
	Push Cycle	**Pull Cycle**	**Push Cycle**	**Pull Cycle**
Test 1	-3.77	-3.55	1.16	1.03
Test 2	-6.62	-4.21	1.37	1.16
Test 3	-3.92	-4.57	0.89	1.07
Test 4	-2.62	-2.41	1.14	0.93
Mean	-4.23	-3.69	1.14	1.05
Average for Push and Pull	**-3.96**		**1.10**	

7.0 CONCLUSIONS

The experiments validated the design goal of achieving restored or controlled strength, while isolating damage to replaceable ductile fuses and, in turn, enhancing the columns resilience to aftershocks or future seismic events. The experiments have shown the potential of this methodology to rapidly repair earthquake damaged columns with a relatively generic approach.

The key takeaways from the experiments are as follows:

- This study provided strong evidence to validate the design goal of achieving restored or controlled strength, however further testing and research is needed to predict the global behavior of the repair more accurately. This report presents three methodologies for predicting behavior: (1) the static method, (2) the pushover method, and (3) the pushover method adjusted with measured location of the neutral axis. The experimental results confirmed that static method consistently overpredicts the repaired peak lateral load. To achieve restored or controlled strength, a more detailed design process such as the pushover analysis should be used to size the hold-downs.

- The weld failure in Test 1 led to a critical improvement of the hold-downs. Exterior hold-down legs, along with the connection to the foundation, should be designed for the combination of uplift from the UFPs and flexural forces from the lateral drift of the exterior hold-down leg. Neglecting to account for flexural forces will greatly underestimate demand at the baseplate and anchors. A reduced section plastic hinge at the base of the hold-down leg can effectively be used to limit flexural forces. The expected UFP force plus the maximum expected moment from the reduced section plastic hinge will then govern the design of the weld, the base plate, and the anchors.

- An additional benefit to the proposed repair methodology is reduced strength degradation at high drifts and during long duration cyclic loading. The experimental results from all four of the repair tests showed a significant reduction in strength degradation from the as-built state. Strength degradation can be additionally reduced with the application of hold-down rollers, which work to prevent hold-down leg separation.

- The experimental program demonstrated the feasibility of the proposed repair methodology to be rapidly implemented. The components should be fabricated with adequate tolerances for constructability. Oversized hole and plate washers on the exterior hold-down leg greatly reduced the installation time. Prior to the CSZ earthquake, the proposed repair methodology should be pre-manufactured and inventoried for rapid access in the aftermath of an earthquake. Earthquake preparation should include training and practice for workers to implement the repair methodology.

- In conclusion, this study successfully demonstrated the development of a resilient repair methodology for earthquake damaged bridge columns that can be rapidly implemented following a damaging earthquake.

The current research program experimentally validated the feasibility of the proposed resilient repair method in restoring the lateral strength of earthquake damaged reinforced concrete bridge column. This repair method can be rapidly implemented for a damaged column that would be easily accessible after an earthquake event. However, the practicality and effectiveness of the repair method needs to be further investigated for a column buried under deep fill or submerged in water. Following is some of the recommendations for future studies addressing the issues.

- The proposed repair method uses replaceable hold-downs made of regular steel plates and angle sections. Such a setup is susceptible to corrosion when exposed to atmospheric conditions and the corrosion can be greatly enhanced under direct exposure to moisture. Hence, a preventive measure against corrosion should be considered while designing the components of the repair method. Further research can be conducted to find a suitable solution for corrosion prevention of the hold-down components to ensure long-term functionality of the repair method. The Steel Bridge Design Handbook (Kogler 2015) provides a list of alternative methods that can be considered as a preventive measure against corrosion. Furthermore, suitability of smart materials that are resilient against corrosion such as stainless steel, shape memory alloy (SMA) etc. can be considered as an alternative to regular steel. However, economic viability of such an alternative should be critically investigated.

- Toe concrete crushing of the column within the gap between the steel collar and the footing was observed during the experimental test of the repaired column. The crushing was not significant and does not have a significant impact on the response of the repaired system. However, the long-term performance of the repaired system must be ensured for resiliency and hence the integrity of the column concrete in the gap region must be ensured. Further research investigating different alternatives to prevent the toe crushing of the column should be considered.

- Self-centering behavior of the proposed repair method depended solely on the gravity load of the bridges. The current experimental program used an axial load ratio of 7% and 9% for pull and push cycles, respectively. Self-centering behavior was observed under these axial-load conditions but the behavior of a bridge substructure with significantly lower axial load level should be investigated. Especially, the ability of the repair method to provide self-centering behavior with lower axial load level should be scrutinized. Use of an un-bonded, post-tensioned system along with the axial load can be investigated to establish a pronounced self-centering behavior of the repair method.

- Development of a finite element modeling technique to predict the seismic response of the repaired system can be undertaken as future research endeavor. Furthermore, the global behavior of concrete bridges with replaceable hold-downs needs to be scrutinized. Transfer of load between the superstructure and the substructure should be further investigated and the component response should be examined.

8.0 REFERENCES

ACI Committee 318. (2014). B*uilding code requirements for structural concrete and commentary* (Standard No. ACI 318-14). Farmington Hills, Michigan: ACI Concrete.

ACI Committee 374. (2013). G*uide for testing reinforced concrete structural elements under slowly applied simulated seismic loads* (Standard No. ACI 374-1-05). Farmington Hills, Michigan: ACI Concrete.

Baird, A., Smith, T., Palermo, A., & Pampanin, S. (2014). Experimental and numerical study of U-shape flexural plate (UFP) dissipators. In *Towards integrated seismic Design: New Zealand society for earthquake Engineering technical conference And AGM: Conference handbook and book of abstracts: 21-23 March 2014, aotea CENTRE, AUCKLAND* (pp. 1–9). Wellington; New Zealand Society for Earthquake Engineering.

Buckle, I., Friedland, I., Mander, J., Martin, G., Nutt, R., & Power, M. (2006). *Seismic retrofitting manual for highway structures: Part 1—Bridges* (Report No. FHWA-HRT-06-032). McLean, VA: Federal Highway Administration. Retrieved from https://www.fhwa.dot.gov/publications/research/infrastructure/bridge/06032/06032.pdf

Chancellor, N., Eatherton, M., Roke, D., & Akbaş, T. (2014). Self-Centering seismic lateral force resisting systems: High performance structures for the City of Tomorrow. *Buildings*, *4*(3), 520–548. https://doi.org/10.3390/buildings4030520

Eatherton, M. R., Ma, X., Krawinkler, H., Mar, D., Billington, S., Hajjar, J. F., & Deierlein, G. G. (2014). Design concepts for controlled rocking of self-centering steel-braced frames. *Journal of Structural Engineering*, *140*(11), 04014082. https://doi.org/10.1061/(asce)st.1943-541x.0001047

Goldfinger, C., Nelson, C. H., Morey, A. E., Johnson, J. E., Patton, J. R., Karabanov, E., . . . Vallier, T. (2012). *Turbidite event history—Methods and implications for Holocene paleoseismicity of the Cascadia subduction zone* (U.S. Geological Survey Professional Paper 1661-F). Reston: Virginia: U.S. Department of the Interior. Retrieved from http://pubs.usgs.gov/pp/pp1661/f

Gulkan, P., & Sozen, M. A. (1974). Inelastic response of reinforced concrete structures to earthquakes. *Journal of the American Concrete Institute*, *71*(12), 604–610.

He, R., Yang, Y., & Sneed, L. H. (2015). Seismic repair of reinforced concrete bridge columns: Review of research findings. *Journal of Bridge Engineering*, *20*(12), 04015015. https://doi.org/10.1061/(asce)be.1943-5592.0000760

Kelly, J. M., Skinner, R. I., & Heine, A. J. (1972). Mechanisms of energy absorption in special devices for use in earthquake resistant structures. *Bulletin of the New Zealand Society for Earthquake Engineering*, *5*(3), 63–88. https://doi.org/10.5459/bnzsee.5.3.63-88

Kogler, R. (2015). *Steel bridge design handbook: Corrosion protection of steel bridge* (Report No. FHWA-HIF-16-002 - Vol. 19). Washington, D.C.: Office of Bridges and Structures, Federal Highway Administration (FHWA). Retrieved from https://www.fhwa.dot.gov/bridge/steel/pubs/hif16002/volume19.pdf

Lehman, D. E., Elkin, S. J., Nacamuli, A. M., & Moehle, J. P. (2001). Repair of earthquake-damaged bridge columns. *ACI Structural Journal*, *98*(2), 233–242. https://doi.org/10.14359/10192

Mashal, M., Palermo, A., & Chegini, Z. (2014). Quasi-static cyclic tests of half-scale fully precast bridge bents incorporating emulative and posttensioned low damage solutions. In *2nd European Conference on Earthquake Engineering and Seismology 2014 (2ND ECEES): Istanbul, Turkey, 25-29 August 2014*. Red Hook, NY: Curran Associates.

Murtuz, A. K. M. G., Dusicka, P., and Schumacher, T. (2020). *Seismic performance design criteria for bridge bent plastic hinge regions* (Report No. FHWA-OR-RD-21-04). Salem, OR: Oregon Dept. of Transportation. Retrieved from https://www.oregon.gov/odot/Programs/ResearchDocuments/SPR802BentPlasticHinge.pdf

Palermo, A., & Pampanin, S. (2005). Application of hybrid concept for an improved seismic ductile design of bridges. In *Planning and engineering for performance in Earthquakes: Conference 2005 technical papers*. Wellington, NZ: New Zealand Society for Earthquake Engineering.

Palnikov, I. S. (2017). *Design and experimental investigation of 500kV current transformer seismic retrofit utilizing structure rocking and supplemental damping with self-centering* (Published master's thesis). Oregon / Portland State University. doi:10.15760/etd.5557

Pampanin, S., Marriott, D., Palermo, A., & New Zealand Concrete Society. (2010). *PRESSS design handbook*. Auckland, N.Z.: New Zealand Concrete Society.

Pampanin, S., Priestley, M. J., & Sritharan, S. (2001). Analytical modeling of the seismic behavior of precast concrete frames designed with ductile connections. *Journal of Earthquake Engineering*, *5*(3), 329–367. https://doi.org/10.1080/13632460109350397

Priestley, M. J., & Park, R. (1987). Strength and ductility of concrete bridge columns under seismic loading. *ACI Structural Journal*, *84*(1), 61–76. https://doi.org/10.14359/2800

Priestley, M. J. N., Seible, F., & Calvi, G. M. (1996). *Seismic design and retrofit of bridges* (1st ed.). Hoboken, NJ: Wiley-Interscience.

Smith, A. (2019). *Test setup design and cyclic evaluation of rocking CLT wall and floor restoring force lateral system* (Master's thesis, Oregon / Portland State University, 2019). Portland. doi:10.15760/CCEMP.46

Stanton, J., Eberhard, M., Sanders, D., Thonstad, T., Schaefe, J., Kennedy, B., . . . Mantawy, I. (2014). *A pre-tensioned, rocking bridge bent for ABC in seismic regions*. Network for Earthquake Engineering Simulation (NEES). https://doi.org/10.4231/D36688K3G

Zhao, X., Wu, Y. F., Leung, A., & Lam, H. F. (2011). Plastic hinge length in reinforced concrete flexural members. *Procedia Engineering*, *14*, 1266–1274. https://doi.org/10.1016/j.proeng.2011.07.159

APPENDIX – A: HOLD DOWN DETAILS

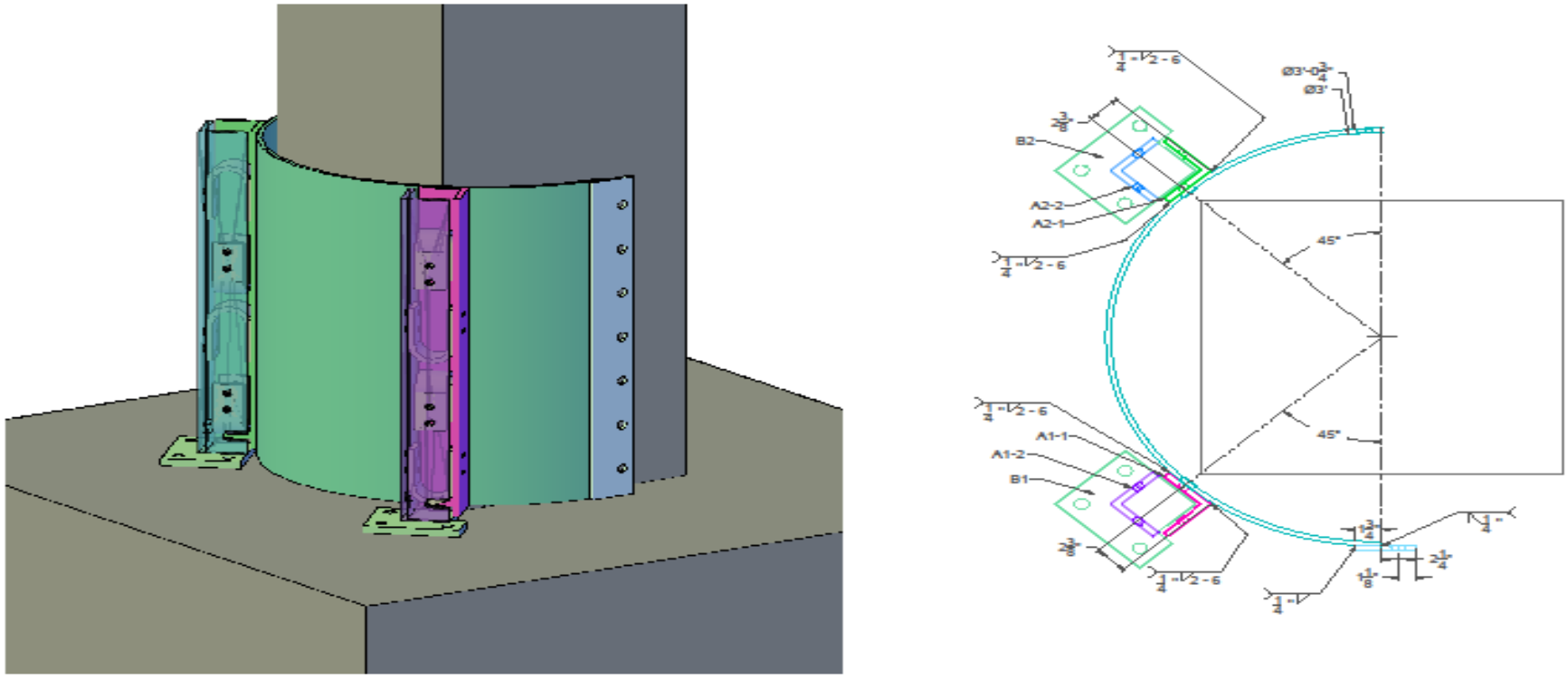

Figure A-1: Design detail of the steel collar

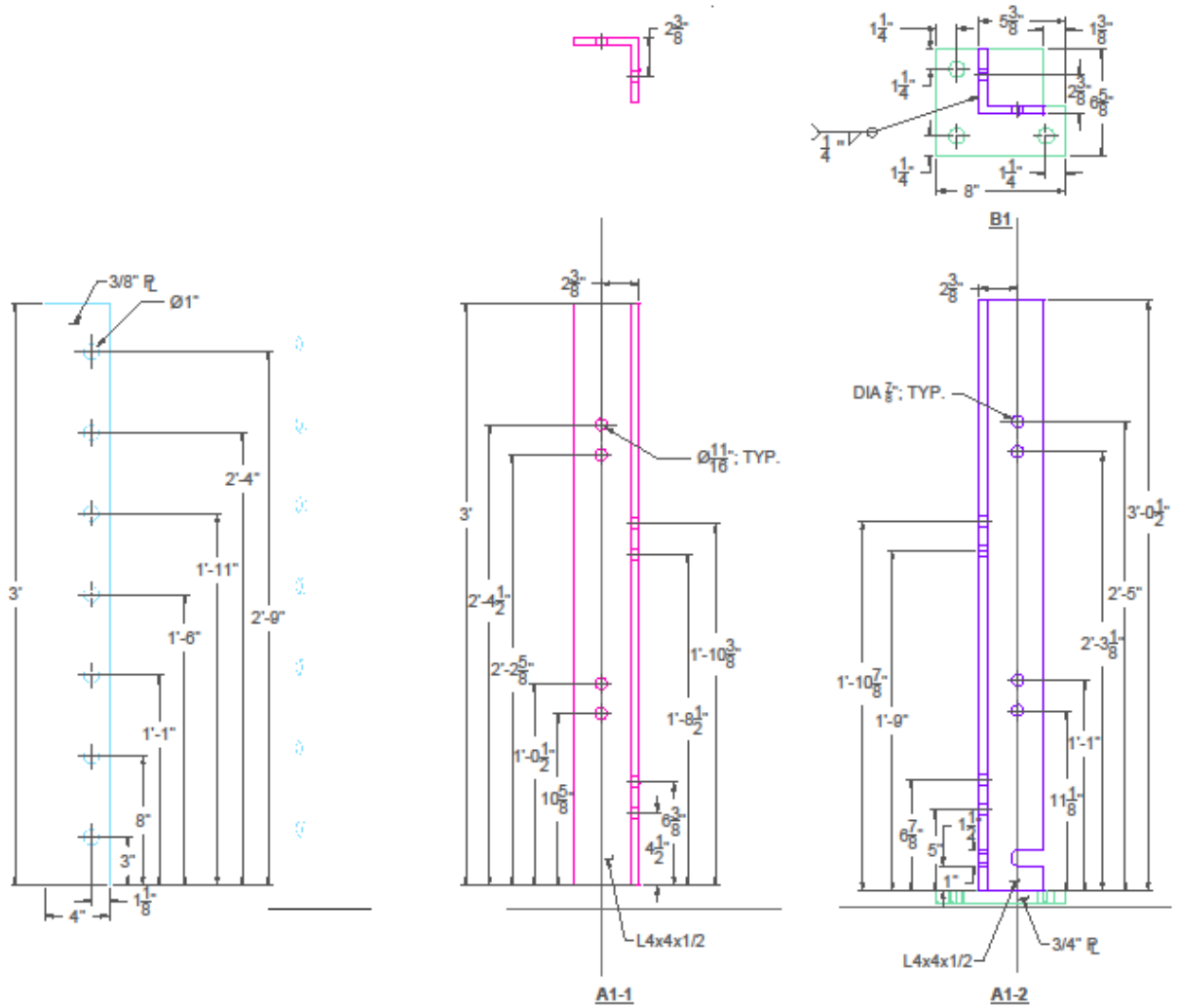

Figure A-2: Dimensional detail of the hold-down angle sections A1-1 and A1-2

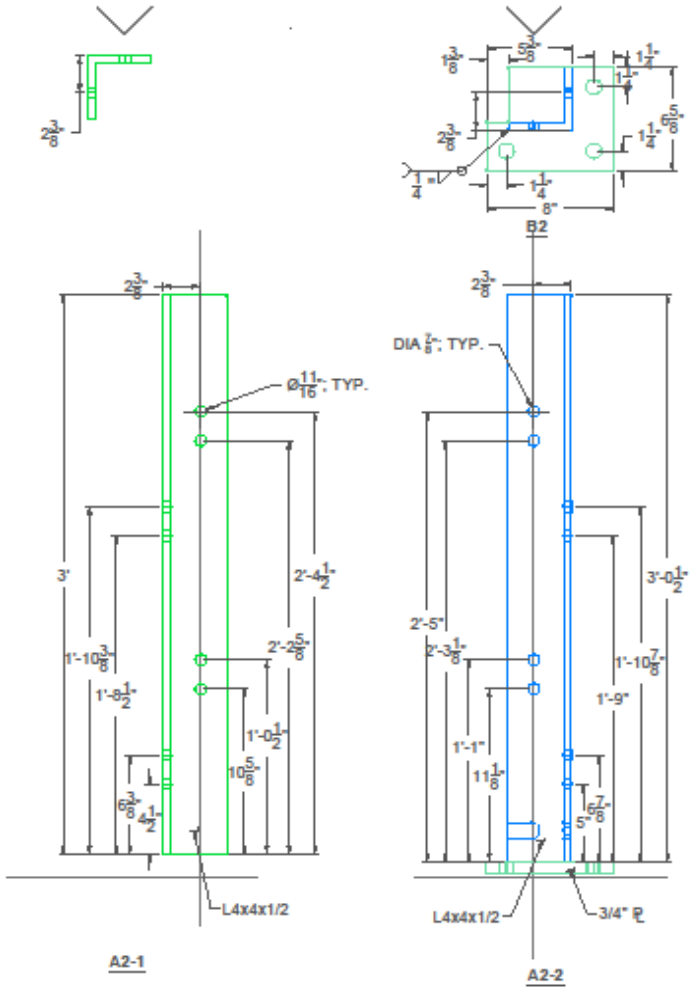

Figure A-3: Dimensional detail of the hold-down angle sections A2-1 and A2-2.

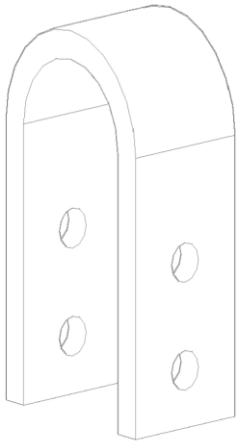

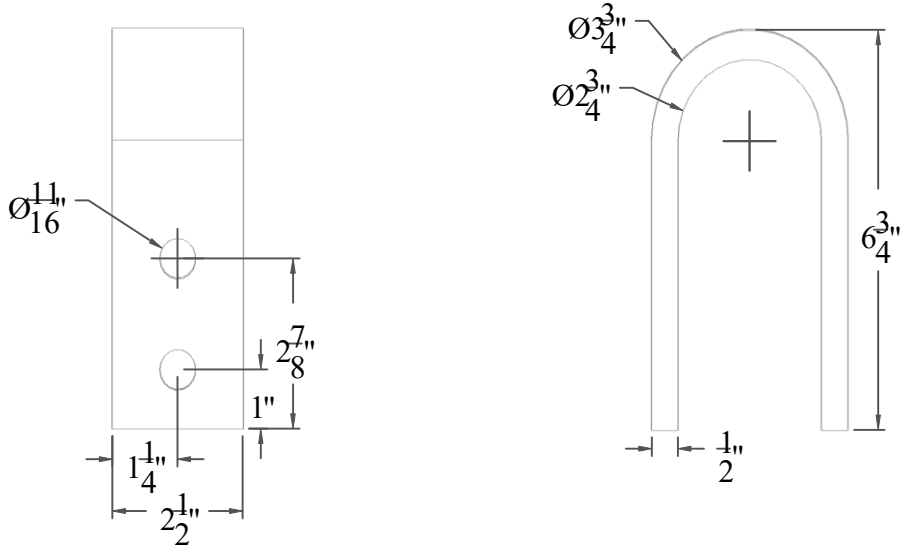

Figure A-4: UFP detail.